THE IMPACT OF EXTREME BLOCKING ON MELTING EVENTS OF THE

NORTHWESTERN GREENLAND ICE SHEET

by

KATRINA DUCRE

(Under the Direction of Thomas L. Mote)

**ABSTRACT** 

For several decades, the Greenland ice sheet has been rapidly and continuously melting,

causing changes in surface mass balance and destabilizing large parts of the ice sheet. However,

melting across the ice sheet is not evenly distributed as shown by the acceleration of surface melt

in the northwest, especially during periods of anomalously slow-moving high-pressure systems

known as atmospheric blocks. As blocking events are predicted to become more frequent and

intense, it is imperative to understand how blocking has changed from the past to help

understand how they could change in the future. The key findings are that extreme blocking has

more reliably contributed to mass loss in northwestern Greenland especially since the latter half

of the 2010s, and that recent mass loss is of a greater magnitude due to an increase in runoff,

temperatures, and positive sensible heat flux, as well as a decrease in snowfall, greater rainfall,

and a resulting reduction in surface albedo.

INDEX WORDS: Greenland, Surface Mass Balance, Atmospheric Blocking

# THE IMPACT OF EXTREME BLOCKING ON MELTING EVENTS OF THE NORTHWESTERN GREENLAND ICE SHEET

by

# KATRINA DUCRE BACHELOR OF SCIENCE, UNIVERSITY OF GEORGIA, 2022

A Thesis Submitted to the Graduate Faculty of The University of Georgia in Partial Fulfillment of the Requirements for the Degree

MASTER OF SCIENCE
ATHENS, GEORGIA
August 2025

@ 2025

Katrina Ducre

All Rights Reserved

# THE IMPACT OF EXTREME BLOCKING ON MELTING EVENTS OF THE NORTHWESTERN GREENLAND ICE SHEET

by

# KATRINA DUCRE

Major Professor: Thomas Mote

Committee: Andrew Grundstein Patricia Yager

Electronic Version Approved: Ron Walcott Vice Provost for Graduate Education and Dean of the Graduate School The University of Georgia August 2025

#### ACKNOWLEDGEMENTS

I'd like to begin by thanking my major professor Dr. Tom Mote who was constantly encouraging and pushing me to be a better scientist and student. I also want to thank my committee members Dr. Andrew Grundstein and Dr. Patricia Yager, Dr. John Knox and Dr. Jonathon Preece of the UGA Atmospheric Sciences department, and Dr. Gina Henderson and Dr. Jennifer Guerard of the United States Naval Academy for their feedback and additional assistance. This thesis was supported by a sub-award to the University of Georgia from Strategic Environmental Research and Development Program (SERDP) project RC-18-1658, "Downscaling of Global to Local Scale Climate Change Impacts Around Pituffik (Formerly Thule) Space Base, Greenland", awarded to Dr. Gina R. Henderson at the United States Naval Academy.

I would like to thank my friends and family who supported me through the most difficult accomplishment of my entire life. Without them cheering me on, there was absolutely no way I would have been able to complete my master's. Specifically, I would like to thank Mackenzie, Melissa, Meghna, Alison, Alana, Brielle, Annie, and Tina as well as my brothers Tim and Ben and the kind people at the National Water Center.

Finally, I would like to thank my parents most of all as none of this would have been possible without them. Their unconditional love and support are the reason I was able to flourish and persevere during the best and worst of times and their unwavering support for my education is a privilege I realize is not afforded to everyone. Therefore, none of this would have been possible without them and this accomplishment is as much for them as it is for me. I hope I will continue to make them proud!

# TABLE OF CONTENTS

ACKN	NOWLEDGEMENTS	iv
LIST	OF TABLES	vi
LIST	OF FIGURES	ix
CHAF	PTER	
1.	INTRODUCTION AND LITERATURE REVIEW	1
2.	DATA AND METHODOLOGY	15
3.	RESULTS	20
4.	DISCUSSION	71
5.	CONCLUSION	83
REFE	RENCES	88

# LIST OF TABLES

Table 3.1 Average surface mass balance of extreme blocking events averaged by decade23
Table 3.2: Average latent heat flux and sensible heat flux of Basin 8 during JJA extreme blocking events by decade
Table 3.3: This table shows the average snowfall (mm w.e. day <sup>-1</sup> ) and rainfall (mm w.e. day <sup>-1</sup> ) of Basin 8 during JJA extreme blocking events by decade
Table 3.4: This table shows the average runoff (mm w.e. day <sup>-1</sup> ) and sublimation (mm w.e. day <sup>-1</sup> ) of Basin 8 during JJA extreme blocking events by decade
Table 3.5: This table shows the average shortwave and longwave upwelling and downwelling radiation in (W m <sup>-2</sup> ) of Basin 8 during JJA extreme blocking events by decade33
Table 3.6: Surface mass balance (mm w.e. day <sup>-1</sup> ), average integrated water vapor transport (kg m <sup>-1</sup> s <sup>-1</sup> ), surface atmospheric temperature (°C), surface skin temperature (°C), latent heat flux and sensible heat flux (W m <sup>-2</sup> ) averaged for spatially and temporally over Basin 8 for a blocking event during 1–6 June 1997.
Table 3.7: Cloud optical depth (COD), upper- middle- and lower-cloud coverage percentages averaged for spatially and temporally over Basin 8 for a blocking event during 1–6 June 199743
Table 3.8: Downwelling shortwave radiation (SWD), downwelling longwave radiation (LWD), upwelling shortwave radiation (SWU), upwelling longwave radiation (LWU, all W m <sup>-2</sup> ) and albedo averaged for spatially and temporally over Basin 8 for a blocking event during 1–6 June 1997
Table 3.9: Snowfall (SF), rainfall (RF), runoff (RU), sublimation (SU), melt (ME) and firn refreezing (RZ) (W m <sup>-2</sup> ) averaged spatially and temporally over Basin 8 for a blocking event during 1–6 June 1997.

Table 3.10: Tables showing various atmospheric and surface variables, averaged spatially and	
temporally over Basin 8 for a blocking event during 15–20 August 20145	2
Table 3.11: Cloud optical depth (COD), upper- middle- and lower-cloud coverage percentages	
averaged for spatially and temporally over Basin 8 for a blocking event during 15-20 August	
20145	2
Table 3.12: Downwelling shortwave radiation (SWD), downwelling longwave radiation (LWD),	
upwelling shortwave radiation (SWU), upwelling longwave radiation (LWU, all W m <sup>-2</sup> ) and	,
albedo averaged for spatially and temporally over Basin 8 for a blocking event during 15–20	
August 20145	2
Table 3.13: Snowfall (SF), rainfall (RF), runoff (RU), sublimation (SU), melt (ME) and firn	
refreezing (RZ) (W m <sup>-2</sup> ) averaged spatially and temporally over Basin 8 for a blocking event	
during 15–20 August 20145	3
Table 2.14. Tables aboveing various atmospheric and surface variables assured anoticity and	
Table 3.14: Tables showing various atmospheric and surface variables, averaged spatially and	
temporally over Basin 8 for a blocking event during 5–10 July 19946	1
Table 3.15: Cloud optical depth (COD), upper- middle- and lower-cloud coverage percentages	
averaged for spatially and temporally over Basin 8 for a blocking event during 5-10 July	
19946	1
Table 3.16: Downwelling shortwave radiation (SWD), downwelling longwave radiation (LWD),	,
upwelling shortwave radiation (SWU), upwelling longwave radiation (LWU, all W m <sup>-2</sup> ) and	
albedo averaged for spatially and temporally over Basin 8 for a blocking event during 5–10 July	r
1994	
1//	' 1
Table 3.17: Snowfall (SF), rainfall (RF), runoff (RU), sublimation (SU), melt (ME) and firm	
refreezing (RZ) (W m <sup>-2</sup> ) averaged spatially and temporally over Basin 8 for a blocking event	
during 5–10 July 19946	2
Table 3.18: Tables showing various atmospheric and surface variables, averaged spatially and	
temporally over Basin 8 for a blocking event during 29 July – 3 August 2019	6

Table 3.19: Cloud optical depth (COD), upper- middle- and lower-cloud coverage percen	tages
averaged for spatially and temporally over Basin 8 for a blocking event during 29 July -	3
August 2019	69
Table 3.20: Downwelling shortwave radiation (SWD), downwelling longwave radiation (	(LWD),
upwelling shortwave radiation (SWU), upwelling longwave radiation (LWU, all W m-2) a	and
albedo averaged for spatially and temporally over Basin 8 for a blocking event during 29	July – 3
August 2019	69
Table 3.21: Snowfall (SF), rainfall (RF), runoff (RU), sublimation (SU), melt (ME) and f	ĭrn
refreezing (RZ) (W m <sup>-2</sup> ) averaged spatially and temporally over Basin 8 for a blocking ev	ent
during 29 July – 3 August 2019	70

# LIST OF FIGURES

Figure 1.1: Contours are 500 hPa geopotential heights, shading shows integrated water vapor
transport (kg m <sup>-1</sup> s <sup>-1</sup> ), vectors are 700 hPa wind vectors (m s <sup>-1</sup> )6
Figure 1.2: Outline of Greenland's major ice drainage basins
Figure 3.1: Histogram of Greenland Blocking Index values from JJA 1990–202321
Figure 3.2: Timeseries of average JJA surface mass balance on days of extreme blocking during 1990–2023 from MAR
Figure 3.3: Average surface mass balance and latent feat Flux of Basin 8 during JJA extreme blocking episodes from 1990–2023.
Figure 3.4: Average surface mass balance (mm w.e. day <sup>-1</sup> ) (bars) and sensible heat flux (W m <sup>-2</sup> ) (line) of Basin 8 during JJA extreme blocking episodes from 1990–2023
Figure 3.5: Average surface mass balance (mm w.e. day <sup>-1</sup> ) (bars) and snowfall (mm w.e. day <sup>-1</sup> ) (line) of Basin 8 during JJA extreme blocking episodes from 1990–2023
Figure 3.6: Average surface mass balance (mm w.e. day <sup>-1</sup> ) (bars) and rainfall (mm w.e. day <sup>-1</sup> ) (line) of Basin 8 during JJA extreme blocking episodes from 1990–2023
Figure 3.7: Average surface mass balance (mm w.e. day <sup>-1</sup> ) (bars) and runoff (mm w.e. day <sup>-1</sup> ) (line) of Basin 8 during JJA extreme blocking episodes from 1990–202331
Figure 3.8: Average surface mass balance (mm w.e. day <sup>-1</sup> ) (bars) and sublimation (mm w.e. day <sup>-1</sup> ) (line) of Basin 8 during JJA extreme blocking episodes from 1990–2023
Figure 3.9: Average surface mass balance (mm w.e. day <sup>-1</sup> ) (bars) and upwelling shortwave radiation (W m <sup>-2</sup> ) (line) of Basin 8 during JJA extreme blocking episodes from 1990–202333
Figure 3.10: Average surface mass balance (mm w.e. day <sup>-1</sup> ) (bars) and downwelling shortwave Radiation (W m <sup>-2</sup> ) (line) of Basin 8 during JJA extreme blocking episodes from 1990–202334

Figure 3.11: Average surface mass balance (mm w.e. day <sup>-1</sup> ) (bars) and upwelling longwave
radiation (W m-2) (line) of Basin 8 during JJA extreme blocking episodes from 1990-202335
Figure 3.12: Average surface mass balance (mm w.e. day <sup>-1</sup> ) (bars) and downwelling longwave
radiation (W m <sup>-2</sup> ) (line) of Basin 8 during JJA extreme blocking episodes from 1990–202335
Figure 3.13: Average surface mass balance (mm w.e. day <sup>-1</sup> ) for the extreme blocking event
during 1–6 June 1997
Figure 3.14: Average integrated water vapor transport (kg m <sup>-1</sup> s <sup>-1</sup> ), 700 hPa wind vectors (m s <sup>-1</sup> ),
and 500 hPa geopotential heights for the extreme blocking event during 1-6 June 199739
Figure 3.15: Total cloud coverage for the extreme blocking event during 1–6 June 199740
Figure 3.16: Cloud optical depth for the extreme blocking event during 1–6 June 199741
Figure 3.17: Cloud base height (m) for the extreme blocking event during 1–6 June 199742
Figure 3.18: Average surface mass balance (mm w.e. day <sup>-1</sup> ) for the extreme blocking event
during 15–20 August 2014
Figure 3.19: Average integrated water vapor transport (kg m <sup>-1</sup> s <sup>-1</sup> ), 700 hPa wind vectors (m s <sup>-1</sup> ),
and 500 hPa geopotential heights for the extreme blocking event during 15-20 August 201448
Figure 3.20: Total cloud coverage percentage for the extreme blocking event during 15–20
August 201449
Figure 3.21: Cloud optical depth for the extreme blocking event during 15–20 August 201450
Figure 3.22: Cloud base height (m) for the extreme blocking event during 15–20 August 2014. 51
Figure 3.23: Average surface mass balance (mm w.e. day <sup>-1</sup> ) for the extreme blocking event
during 5–10 July 199456
Figure 2.24. Assessed interests 1 motors and the second (loss self-il). 700 l.D. min 1 motors (second il).
Figure 3.24: Average integrated water vapor transport (kg m <sup>-1</sup> s <sup>-1</sup> ), 700 hPa wind vectors (m s <sup>-1</sup> ),
and 500 hPa geopotential heights for the extreme blocking event during 5-10 July 199457
Figure 3.25: Total cloud coverage percentage for the extreme blocking event during 5–10 July
1994

Figure 3.26: Cloud optical depth for the extreme blocking event during 5–10 July 199459
Figure 3.27: Cloud base height (m) for the extreme blocking event during 5–10 July 199460
Figure 3.28: Average surface mass balance (mm w.e. day <sup>-1</sup> ) for the extreme blocking event during 29 July – 3 August 2019
Figure 3.29: Average integrated water vapor transport (kg m <sup>-1</sup> s <sup>-1</sup> ), 700 hPa wind vectors (m s <sup>-1</sup> ), and 500 hPa geopotential heights for the extreme blocking event during 29 July – 3 August
201965
Figure 3.30: Total cloud coverage percentage for the extreme blocking event during 29 July – 3  August 2019
Figure 3.31: Cloud optical depth for the extreme blocking event during 29 July – 3 August
201967
Figure 3.32: Cloud base height (m) for the extreme blocking event during 29 July – 3 August 2019

#### CHAPTER 1

#### INTRODUCTION AND LITERATURE REVIEW

#### 1.1 Introduction

For several decades, observations have shown that the Greenland ice sheet is melting at an accelerated pace (Chen et al., 2006; Rignot et al., 2011) and that rates of warming in the Arctic are approximately 2.5 times greater than the rest of the world (Previdi et al., 2021; Rantanen et al., 2022; Serreze et al., 2009). The overall mass balance of the ice sheet is a function of the surface mass balance (SMB) and dynamic losses, where the latter consists of solid ice discharge through marine- and land-terminating calving losses. Solid ice discharge is commonly seen as the collapsing of ice shelves on the edges of the sheet into the water below. Further, SMB is determined by the difference between accumulation and ablation and sublimation. While the ratios of accumulation to ablation have historically been near balance, the last several decades of aforementioned anomalous warming have tipped the scale of surface mass balance increasingly in favor of ablation variables, causing concern for rising sea levels from the shrinking ice sheet (Cazenave & Remy, 2011; Khan et al., 2015; Shepherd et al., 2012).

The current perception of climate change for the public is largely centered around the rising of surface temperatures globally. However, rising temperatures are only a part of a larger dynamic shift in the Earth's atmosphere that is further complicated through differential impacts across the globe due to changes in oceanic and atmospheric circulation. One such dynamic that is

causing great concern is atmospheric blocking, a center of anomalous high-pressure that dislodges from large-scale longwave patterns and remains quasi-stationary over a region for an extended period. Blocking events are especially significant over Greenland due to their documented impact on the SMB of the ice sheet. The unprecedented melt event that occurred during Summer 2012 was subsequently linked to intense blocking regimes (Hanna et al., 2014; McLeod & Mote, 2016; Tedesco et al., 2013), and even non-extreme blocking events have been linked to enhanced levels of melt (Hanna et al., 2013).

The relationship between atmospheric blocking and melt events is further complicated by outside influences from warm moisture transport, latent and sensible heat flux, and radiation terms as documented in prior studies (Barrett et al., 2020; Ettema et al., 2010; Mattingly et al., 2018; Van Den Broeke et al., 2011; Wouters et al., 2013). The effect of atmospheric blocking may be further enhanced through the transport of latent and sensible heat on the upstream side of the block through long filaments of enhanced water vapor transport via atmospheric rivers.

Atmospheric rivers are long, narrow bands of enhanced water vapor in the lower atmosphere, often facilitated by blocking events (Barrett et al., 2020; Henderson et al., 2021), and have been shown to affect the SMB of the GrIS (Mattingly et al., 2016, 2018, 2020).

Previously, literature has focused on the impacts of atmospheric blocking on Greenland as a whole without consideration for how the impact might differ across the ice sheet. A minority of studies focused on more regional effects of blocking and often conclude that the associated effects are not spatially homogenous across the entire ice sheet. In addition, the rate of mass loss in response to blocking events has changed over time, particularly in the northwest (Mouginot et al., 2019; Tedesco et al., 2016; Velicogna et al., 2014). Therefore, this thesis aims to examine the mechanisms of the most extreme blocking events, and how they have changed over time

in one specific area of northwestern Greenland. I plan to accomplish a more detailed understanding of how the SMB during extreme blocking events has changed over the last several decades in an area of the ice sheet signaling accelerated surface mass loss. In addition, this work aims to provide possible explanations for why this acceleration is happening and how conditions during blocking events differ in the present day compared to the 1990s.

The project uses model data that is particularly well-suited for resolving small-scale ice sheet processes. Summer extreme blocking days were selected from 1990–2023 and a set of key variables was extracted from within the boundaries of the major drainage Basin 8 in northwestern Greenland (Zwally et al., 2012). Average yearly values for these variables were compared to the SMB over the 30 years to provide greater context for accelerating surface mass loss. The findings presented here provide important insights into the impact of climate change on the Greenland ice sheet, especially if blocking becomes more frequent and more intense in response to a greenhouse-enhanced climate.

#### 1.2 Literature Review

# 1.2.1 Atmospheric Blocking

At its most broad description, atmospheric blocking is defined as a quasi-stationary anticyclonic system that interrupts the large-scale pattern of waves in the atmosphere (Barrett et al., 2020; Lupo, 2021; Nakamura & Huang, 2018; Rex, 1950; Schwierz et al., 2004; Tyrlis & Hoskins, 2008; Woollings et al., 2018). While all definitions include a duration component, the exact threshold is not widely agreed upon but is generally understood to be greater than five consecutive days. The most common metrics of blocking include the frequency of occurrence, duration of individual events, and intensity of blocking (Lupo, 2021), where there is a positive correlation between blocking duration and intensity (Lupo et al., 2019).

Since the mid-20<sup>th</sup> Century, atmospheric blocking events have been documented and discussed in scientific literature, but to this day the exact physical mechanisms that lead to blocking are still not widely understood, and have therefore spawned a variety of blocking indices to reflect a varied range of opinions and blocking types (Woollings et al., 2018). For example, Rex (1950) specified that blocks were anticyclones stationed upstream of a mid-latitude cyclone (Woollings et al., 2018), interrupting long Rossby waves and supporting easterly meridional flow (Hoskins et al., 1985), which is later largely associated with the Pelly-Hoskins Index for blocking (Pelly & Hoskins, 2003). On the other hand, omega blocking, where a large anticyclone is flanked by two low pressure systems both downstream and upstream of the anticyclonic ridge, has different blocking indices that are popularly utilized in research.

Wachowicz et al. (2021) examined multiple metrics for Greenland blocking and found that no single blocking metric is without its own drawbacks, and further exemplified the difficulties associated with standardizing blocking metrics across a single region, let alone multiple distinct regions.

While the exact dynamics that lead to atmospheric blocking are not fully understood, certain aspects of the formation of atmospheric blocks are more widely agreed upon, as have there been dedicated studies and reviews that sought to further understand blocking dynamics (Michel et al., 2021; Steinfeld & Pfahl, 2019; Woollings et al., 2018). Often, blocking dynamics are defined by an anticyclonic system formed from an air mass of low vorticity that is advected towards the poles due to a large-scale stationary ridge (Davini et al., 2012; Steinfeld & Pfahl, 2019; Woollings et al., 2018). These differences in blocking structure and location cast a challenge for current agreement on blocking events but also forecasting for future blocking in an ever-changing climate.

Blocking can be characterized by different patterns or types: an omega block, stationary ridge, cyclonic wave breaking pattern, anticyclonic wave breaking pattern, or rex/dipole block (Kautz et al., 2022; Lupo, 2021; Preece et al., 2022; Woollings et al., 2018). Omega blocks are identified as a high-pressure ridge that sits stationary between two low-pressure systems (e.g., Figure 1.1). A stationary ridge is an area where an anomalous, anticyclonic system moves very slowly relative to its surrounding areas (Woollings et al., 2018). Cyclonic and anticyclonic wave breaking represent ridges folding in either a clockwise or anti-clockwise configuration (Woollings et al., 2018). Rex or Dipole blocks occur when a high-pressure system sits poleward of a low-pressure system (Woollings et al., 2018).

As scientific interest has grown in the impacts of blocking over the past several years, many reviews have been published that further discuss and explain various facets of anticyclonic blocking in general (Lupo, 2021; Woollings et al., 2018), as well as region-specific (Henderson et al., 2021; Wazneh et al., 2021). As blocking events occur in various locations and climates, seasonality also affects blocking conditions differently. The frequency of blocking changes throughout the year, most commonly occurring in winter and spring and least commonly occurring during the summer (Barriopedro et al., 2006; Lupo, 2021). Blocking can enhance harsh winters by obstructing polar air and deflecting air masses toward the equator (Hoskins & Sardeshmukh, 1987; Woollings et al., 2018). Alternatively, blocking is also associated with decreased summer cloud cover and higher temperatures that amplify summer heatwaves and droughts (Black et al., 2004; Fang & Lu, 2020; Woollings et al., 2018).

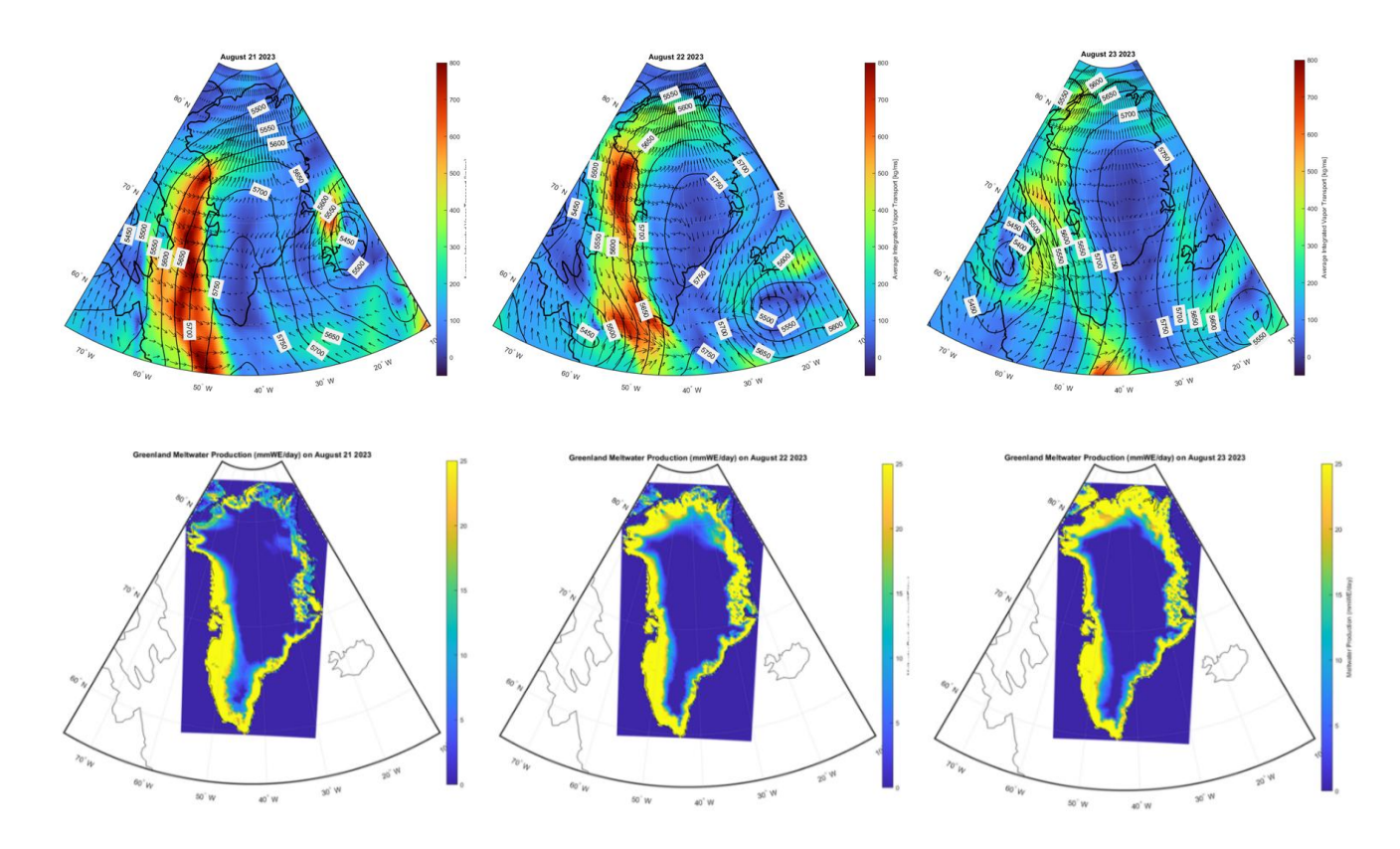


**Figure 1.1**: (Top Row) Contours are 500 hPa geopotential heights, shading shows integrated water vapor transport (kg m<sup>-1</sup>s<sup>-1</sup>), vectors are 700 hPa wind vectors (m s<sup>-1</sup>). (Bottom Row) Meltwater production (mm w.e. day<sup>-1</sup>). In August of 2023, an omega block formed and stationed over the interior of the Greenland ice sheet. In response, warm water vapor from the midlatitudes moved over the northwestern ice sheet over the course of a week. The above figures reflect a three-day period where anomalous meltwater production occurred in response to Greenland Blocking and water vapor intrusion.

Atmospheric circulation and the prevalence of atmospheric blocking has already responded to post-industrial climate change from anthropogenic causes, which is especially prominent and fast-paced in the Arctic (Previdi et al., 2021; Serreze et al., 2009). Blocking occurrences overall have increased in the 21<sup>st</sup> Century (Lupo, 2021). The period from 2007–2013 was found to have higher blocking frequency and duration compared to decades prior, and this pattern is especially prevalent during the spring and summer months (Hanna et al., 2022;

McLeod & Mote, 2015). Some metrics suggested an increase for winter and summer Greenland blocking events when accounting for a 5-year running mean (Wachowicz et al., 2021). In addition to increasing blocking frequency, the number of extreme blocking events has also increased, as has the magnitude of recent seasonal extremes (Barrett et al., 2020).

Models have difficulty resolving blocking characteristics like intensity, duration, and frequency (Lupo, 2021; Maddison et al., 2024; Matsueda, 2009; Tedesco & Fettweis, 2012) and recent research suggests that most climate models have failed to indicate the recent increasing trend in summertime atmospheric blocking over Greenland (Maddison et al., 2024). Many models also fail in adequately considering changes in ice topography (Helsen et al., 2012; Tedesco & Fettweis, 2012). As previously discussed, the formation of blocking conditions is not the same across the globe, leading to uncertainties in future model predictions. These uncertainties are apparent even for low-frequency modes of atmospheric circulation that are well understood (e.g. teleconnections) and have historically already shown a correlation with blocking, such as the North Atlantic Oscillation (NAO) (Hanna et al., 2015).

Previous studies suggest that blocking events over Greenland have often affected the SMB as well as the energy balance of the ice sheet, and that notable significant blocking events over Greenland have been linked to unprecedented ablation of the ice sheet. As there are many different types of blocking that occur, there are also differences in the temperature and SMB effects that blocking patterns have on various areas of the ice sheet (Sousa et al., 2018), such as studies that have shown discrepancies in melt conditions between northern and southern Greenland from past observations and future models (Tedesco et al., 2016; Tedesco & Fettweis, 2012). Past research suggests that in Greenland, omega blocks are primarily associated with intense melt events in the northern basins (Preece et al., 2022), especially during the

summertime, where blocking events largely influence the acceleration of ice mass loss of the Greenland ice sheet (Hanna et al., 2016; McLeod & Mote, 2015). However, blocking types are not exclusively associated with regional melting events. The anomalously warm summer of 2012 saw unprecedented surface mass loss throughout the coast and far inland in response to an omega block (Hanna et al., 2013; Nghiem et al., 2012).

### 1.2.2 Surface Mass Balance

In its simplest terms, the balance between the accumulation and ablation of Greenland's surface ice is known as surface mass balance (SMB). Accumulation, or variables that increase SMB, consists of snowfall and deposition, while ablation terms, those that decrease SMB, include runoff and sublimation. Rainfall is a complicated process that adds mass to the firn but also adds latent heat that contributes to ablation.

Runoff tends to be the dominant component of surface ablation and is composed of meltwater produced from melting surface ice as well as non-percolating rainfall. Not all meltwater contributes to runoff, as some meltwater is retained in the firn and refreezes. However, once the pore space in the firn is sufficiently filled, runoff begins. The buffering capacity of the firn to retain meltwater is a function of the firn density. As the firn densifies due to increased melt, the buffering capacity in future years is reduced. It possibly contributes to an impermeable surface layer, potentially increasing runoff in future years, even if the climate remains static (Amory et al., 2024; Braithwaite et al., 1994; Harper et al., 2012; Pfeffer et al., 1991).

#### 1.2.2.1. Radiation

The surface energy budget drives the processes that determine whether accumulation or ablation become the dominant term. The surface energy budget includes shortwave and

longwave radiation as well as sensible and latent heat and the energy storage into the firn. The surface radiation balance includes the flux of incoming and outgoing radiation from the Earth's surface and atmosphere and has been shown to have an impact on surface melt before (Ettema et al., 2010; Van Den Broeke et al., 2011). Incoming shortwave solar radiation passes through the Earth's atmosphere, where it is either reflected or scattered by clouds or other atmospheric hydrometeors, or absorbed by the atmosphere and the surface. Longwave radiation originates from the surface and makes its way back into the atmosphere, where it once again is either absorbed, reflected, or transmitted into space.

# 1.2.2.2 Cloud Radiation Budget

However, factors that complicate this process include numerous variables such as cloud coverage as well as the diurnal cycle. A clear, sunny day may have more shortwave radiation reaching the surface as there are fewer clouds. Alternatively, a cloudy night may have higher surface temperatures due to clouds blocking the transmission of radiation back into space. Various physical characteristics of clouds also impact the radiation budget. For instance, cloud optical thickness describes the optical depth between the top and bottom of a cloud. It is more difficult for radiation to pass through thick, puffy clouds than it is through thin, wispy ones. Cloud phase is also important, as clouds that are primarily composed of ice will be able to reflect more radiation than liquid-based ones. Cloud base height and temperature are components that affect cloud emissivity, as lower/warmer clouds will re-emit more infrared radiation than higher/cooler clouds. Prior studies have spoken on the importance of cloud radiative effects on Greenland's SMB (Bennartz et al., 2013; Ryan, 2024; Ryan et al., 2022; Van Tricht et al., 2016).

#### 1.2.2.3 Sensible and Latent Heat

Further complicating these dynamics are latent and sensible heat flux. Latent heat is the exchange of heat between water and the atmosphere as water transitions between its solid, liquid, and gas phases. Latent heat is released during the condensation of water vapor into liquid, such as during the formation of clouds, which impacts the surface energy budget as previously stated. Sensible heat is the exchange of heat that is not associated with the changing of phases. Both latent and sensible heat flux are shown to have a positive relationship with melt energy (Mattingly et al., 2020), meaning that higher heat flux is more likely to positively influence ablation terms than accumulation terms.

#### 1.2.3 Atmospheric Rivers

Large influxes of water vapor, latent heat, and sensible heat, as well as their subsequent impacts, can often be attributed to the movement of atmospheric rivers. Atmospheric rivers (AR), also known as warm moisture conveyor belts or tropospheric rivers, are long narrow streams of water vapor that occur in the lower atmosphere and are often accompanied by a strong low-level jet ahead of extratropical cyclones (Dacre et al., 2015; Gimeno et al., 2016; Newell et al., 1992; Ralph et al., 2017). In the Arctic, atmospheric rivers also play a limited positive role in SMB (Mattingly et al., 2018). Increased water vapor transport into Greenland's atmosphere supplies the critical moisture component for cloud formation, which is also associated with higher rates of frozen precipitation and accumulation. Increasing cloud coverage also helps prevent a fraction of shortwave solar radiation from reaching Earth's surface by limiting absorption, subsequent reemission, and therefore further surface warming. However, studies show that there has been a significant decrease in summertime cloud coverage that limits the positive effects of cloud coverage and contributes to the melt-albedo feedback loop (Hofer et al., 2017; Neff, 2018).

# 1.3 Project Motivation

Despite the growing body of work seeking to understand blocking scenarios and their impact on the SMB of Greenland's ice sheet, there is still much to learn about past, present, and future conditions that can – and already have – impacted the ice sheet. We already know that blocking, moisture transport, and the energy budget all work together to impact both small- and large-scale ablation of the ice sheet, but the scale and inconsistency with which these variables impact ablation differs spatially. This body of work aims to closely examine how the rate of melt in northwestern Greenland is affected by using high-resolution model output, in hopes that it will further our understanding of how Greenland's surface ice will change over time.

Atmospheric blocking events over the Greenland Ice Sheet (GrIS) are highly correlated with atmospheric rivers and subsequent melt events (Barrett et al., 2020; Mattingly et al., 2018; Neff, 2018; Wouters et al., 2013), as well as changes in cloud coverage, surface albedo, temperatures, shortwave and longwave radiation, and precipitation amounts that all further accelerate GrIS mass loss (Ettema et al., 2010; Mattingly et al., 2018, 2020; McLeod & Mote, 2015, 2016; Tedesco et al., 2016; Van Den Broeke et al., 2011; Woollings et al., 2018). Quasistationary blocking conditions over GrIS form a ridge that facilitates the movement of water vapor, sensible heat, and latent heat from the midlatitudes onto the ice sheet, which negatively impacts ice mass through various physical processes. The anticyclonic nature of blocking conditions is also linked to decreased cloud coverage that amplifies heatwaves and droughts, especially in the summertime (Black et al., 2004; Fang & Lu, 2020; Woollings et al., 2018).

Atmospheric blocking conditions over Greenland are shown to be increasing in frequency over the last several decades (Barrett et al., 2020; Lupo, 2021; Mattingly et al., 2016; McLeod & Mote, 2015). As previous research has indicated that atmospheric blocking enhances melt and

other forms of surface mass loss, it is important to continue studying these events in a world where a changing climate is impacting the intensity and frequency of such events in ways never seen before.

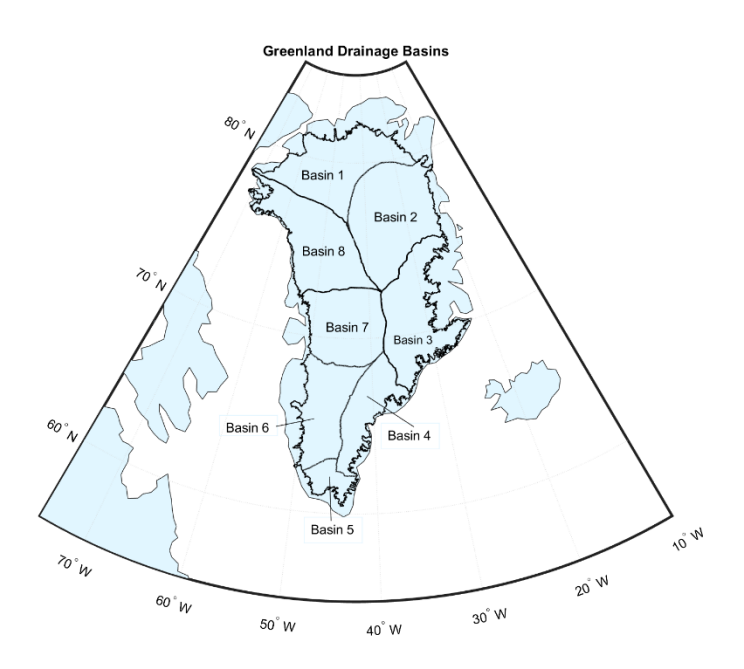


**Figure 1.2:** Outlines of Greenland's major ice drainage basins. Data is sourced from NASA's Cryospheric Sciences Laboratory (Zwally et al., 2012), and the graphic was created using MATLAB.

Historically, surface mass loss has varied over GrIS during periods of extreme blocking and periods not affected by extreme blocking. As previously mentioned, blocking events have far-reaching consequences for many atmospheric variables and surface conditions, including cloud coverage and latent heat flux. Since blocking conditions do not have a standard impact across the entire ice sheet, we would also see differences in surface and atmospheric variables.

Recent studies have also suggested that surface mass loss in northwestern Greenland, as seen in Figure 1.2 as Basin 8, contributes greatly to total GrIS mass loss and that regional mass loss is accelerating, particularly during blocking events (Mouginot et al., 2019; Tedesco et al., 2016; Velicogna et al., 2014). Further research on water vapor flux and surface energy budget during blocking periods could further our understanding of how blocking conditions accelerate surface mass loss in northwestern Greenland.

#### 1.4 Research Questions

This work focuses on the following questions related to the role of blocking on the SMB of the Greenland ice sheet, as well as case studies:

- 1. Greenland Blocking: How does surface mass loss over northwestern Greenland compare to other regions of the ice sheet on days experiencing extreme atmospheric blocking conditions?
- 2. **Surface Energy Balance:** How have surface energy balance components, such as latent and sensible heat flux, radiative fluxes, and accumulation and ablation terms, changed in northwestern Greenland during extreme blocking events between 1990 and 2023?

We hoped to use our analyses to further our understanding of atmospheric blocking events over northwestern Greenland. We sought to possibly explain the changes that have resulted in increased ice mass loss during recent extreme blocking events using various modes of analysis, such as statistics and time series. We also created case studies to further investigate how differences in surface and atmospheric variables changed the SMB of several extreme blocking events. As blocking episodes over Greenland are expected to become more frequent and intense,

the ice sheet is increasingly at risk for large-scale melt events. By studying the previous changes to extreme blocking episodes, it will give greater insight to scientists and affected communities and therefore greater planning and adaptability.

#### CHAPTER 2

#### DATA AND METHODOLOGY

Increased ablation of the Greenland ice sheet (GrIS) has negative consequences on SMB. In recent years, there has been a sheet-wide acceleration in ice loss through large-scale ice discharge and ablation processes. Large scale ablation events have been particularly prevalent during atmospheric blocking events over Greenland that help facilitate warm-moisture transport into the Arctic and affect surface energy budget variables, therefore having consequences on all portions of the sheet. By examining these blocking events and their relationship with the surface radiation and energy budget, we can better understand the differences in how GrIS reacts in response to changes in atmospheric conditions, particularly in areas like the northwest that have seen accelerated surface mass loss during blocking conditions.

This work is focused on understanding atmosphere-ice interactions that are quantified using SMB, the relationship between ablation and accumulation terms for the Greenland ice sheet. This chapter details the data and methods to address the research questions posed at the end of Chapter 1 around the impact of extreme atmospheric blocking events on the mass balance of the GrIS with a focus on northwestern Greenland.

# 2.1 Modèle Atmosphérique Régionale (MAR)

The main data source used in this study was Modèle Atmosphérique Régionale (MAR) (Gallée & Schayes, 1994) version 3.14.0 that was forced using ERA5-Renalaysis. MAR is a regional climate model (RCM) that is a coupled atmosphere-land model using a one-dimensional

scheme known as SISVAT (Soil Ice Snow Vegetation Atmosphere Transfer (Gallée and Schayes, 1994; Fettweis, 2022). SISVAT uses CROCUS, a numerical model that simulates snow and rain processes including refreezing, compaction, albedo, and meltwater production (Fettweis, 2022; Brun et al, 1989). SISVAT allows MAR to better account for the exchanges of energy between land ice, sea ice, and the atmosphere, making it ideal for polar research (Fettweis, et al., 2013; Fettweis et al., 2017). MAR has been extensively validated through field campaigns and passive remote sensing observations, as well as used in prior Greenland-based studies (Mattingly et al., 2018; Mattingly et al., 2020; Noël et al., 2014; Lambin et al., 2023; Fettweis et al., 2013; Fettweis et al., 2005; Leeson et al., 2018). Additionally, due to MAR being used as a downscaled model, providing higher spatial resolution that makes it favorable over global models to better understand impacts on the ice sheet (Franco et al., 2012).

This study utilized a MAR simulation with a spatial resolution of 15km. Temporal resolution of the MAR database is once daily from 1950 through 2023, but only years from 1990–2023 were used. Both SMB and surface energy budget variables from MAR were used in analysis for this study.

# 2.2 ERA5-Reanalysis

ERA5, the successor to ERA-Interim, is gridded data from the European Centre for Medium-Range Weather Forecasts (ECMWF) and provides data on atmospheric, land, and ocean variables at greater spatial and temporal resolutions. ERA5-Reanalysis is climate reanalysis data that includes the use of boundary conditions and radiative forcing. It is available on a global scale with the possibility of scaling to smaller regions and is advantageous to use temporally because of its availability at hourly intervals as well as daily and monthly averages. In addition, ERA5 is available over both single and multiple pressure levels, as well as potential temperature

levels (*Climate Reanalysis* | *Copernicus*, n.d.; Hersbach et al., 2020; Setchell, 2020). ERA5 benefits over previous ERA iterations by having a more refined and accurate method of resolving atmospheric physics (Bell et al., 2021). It also includes better and larger integration of historical observations using data assimilation techniques (*Climate Reanalysis* | *Copernicus*, n.d.; Hersbach et al., 2020; Setchell, 2020).

This study used ERA5-Reanalysis hourly data on single levels as well as hourly data on multiple levels that has been regridded to 0.25° by 0.25° (Copernicus Climate Change Service, 2018) over an area encompassing Greenland from 10°W-80° W and 50°N-90°N. Because of the seasonality of blocking events, only the meteorological summer consisting of June, July, and August was analyzed in this study. Future research could replicate these methods focusing on other seasons.

# 2.3 Atmospheric Blocking Analysis

Analysis of atmospheric blocking events will consist of Summer (June, July, August) for the years 1990–2023. The Greenland Blocking Index (GBI) is a common metric of geopotential heights used to identify and quantify Greenland blocking events (Hanna et al., 2016). The GBI consists of the average geopotential height at 500 hPA for the area encompassing the Greenland ice sheet, or 60-80° N and 20-80° W (Hanna et al., 2016). High, positive GBI values will indicate anomalous blocking events over Greenland. As this body of work is focused on extreme values of blocking and therefore does not need to account for the increasing trend in geopotential heights due to atmospheric warming, the original version of GBI was used.

To calculate GBI, geopotential at the 500 millibar level from ERA5-Reanalysis was divided by gravitational acceleration ( $g = 9.80665 \text{ m/s}^2$ ) to calculate geopotential heights and then spatially averaged over  $60-80^{\circ}$  N and  $20-80^{\circ}$  W°. GBI values for JJA are compiled over the

time span from 1990 to 2023 and ranked from highest to lowest. Following similar methodology to Mattingly (2020), the top 10% of GBI days are then categorized as "extreme" blocking days.

# 2.4 Surface Energy Balance Analysis

MAR data for net radiation, latent heat and sensible heat flux, as well as accumulation and ablation terms from the pre-selected extreme blocking events were further investigated. After masking the data to only include Basin 8, yearly averages for every variable were calculated and graphed alongside SMB to create a timeseries. Decadal averages were also used to conduct Analysis of Variance (ANOVA) testing and determine statistical significance ( $\alpha$  = 0.05) between the averages of each decade. Statistically significant values were noted with an asterisk. Cloud variables such as total cloud coverage and cloud optical depth, integrated water vapor, geopotential, and wind vectors from MAR and ERA5-Reanalysis data were utilized to create the case study maps in MATLAB. Case studies were selected by time and SMB to allow for a range of extreme blocking responses.

# 2.5 Ice/Land Masking

As this body of work hopes to distinguish the differences in SMB between each of Greenland's 8 major drainage basins (Figure 1.2), masking was utilized to distinguish between basin boundaries as well as oceans. The data used to create the outlines for Greenland's major drainage basins was acquired from NASA's Cryospheric Sciences Laboratory (Zwally et al., 2012) and further used to create a mask for each basin. Only gridded values that were at least 50% within the boundaries of the mask were considered part of a basin.

Utilizing timeseries and decadal averages allowed us to examine long-term trends, while our case studies provided us with further context as to what discerns extreme blocking events

that result in positive SMB from negative ones. In summary, this thesis methodology aimed to use multiple types of analyses and data to help create a more thorough understanding of extreme blocking events in northwestern Greenland.

#### CHAPTER 3

#### **RESULTS**

# 3.1 Greenland Blocking

This work aimed to examine the unique impacts of extreme blocking episodes on northwestern Greenland on both short and long timescales. In recent years, extreme blocking events have increasingly resulted in large surface mass loss, and these events are only expected to become more frequent in the future. Using downscaled, regional climate data from MAR and ERA5-Reanalysis, several time series encompassing extreme blocking days during summers from 1990 to 2023 were created. In addition, case studies from four different extreme blocking-related events were chosen based on the resulting SMB. Using case studies, I hoped to better understand why some events have led to negative mass balance while others to surface mass gain and how the effect of blocking on mass balance has changed across the past three decades.

Extreme blocking was defined using the top 10% of Greenland Blocking Index (GBI) days from 1990–2023, and an event was defined by sequential extreme blocking days  $\pm$  2 days to account for the latency effect of water vapor transport. Each day was temporally and spatially averaged within the boundaries of each basin to calculate the mean SMB for each event (Figure 3.1).

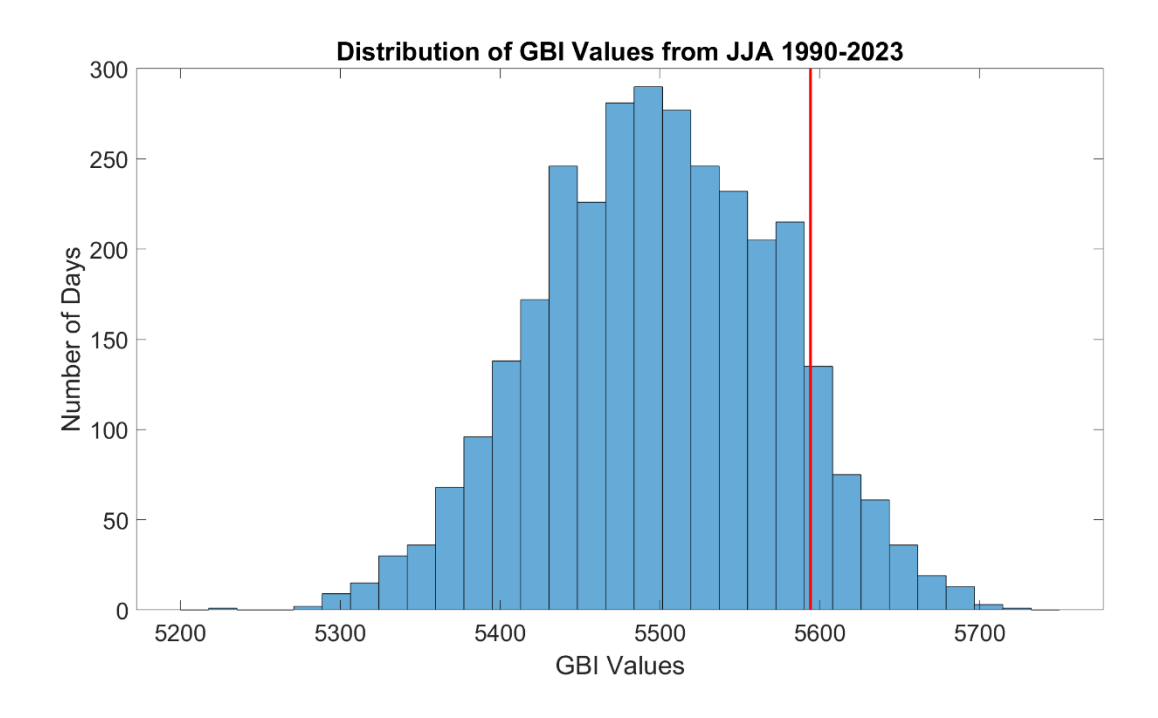


**Figure 3.1:** A histogram of all Greenland Blocking Index values from JJA 1990–2023. The red line shows the point where the GBI days begin to be considered 'extreme' by the definition presented here (>= 90%).

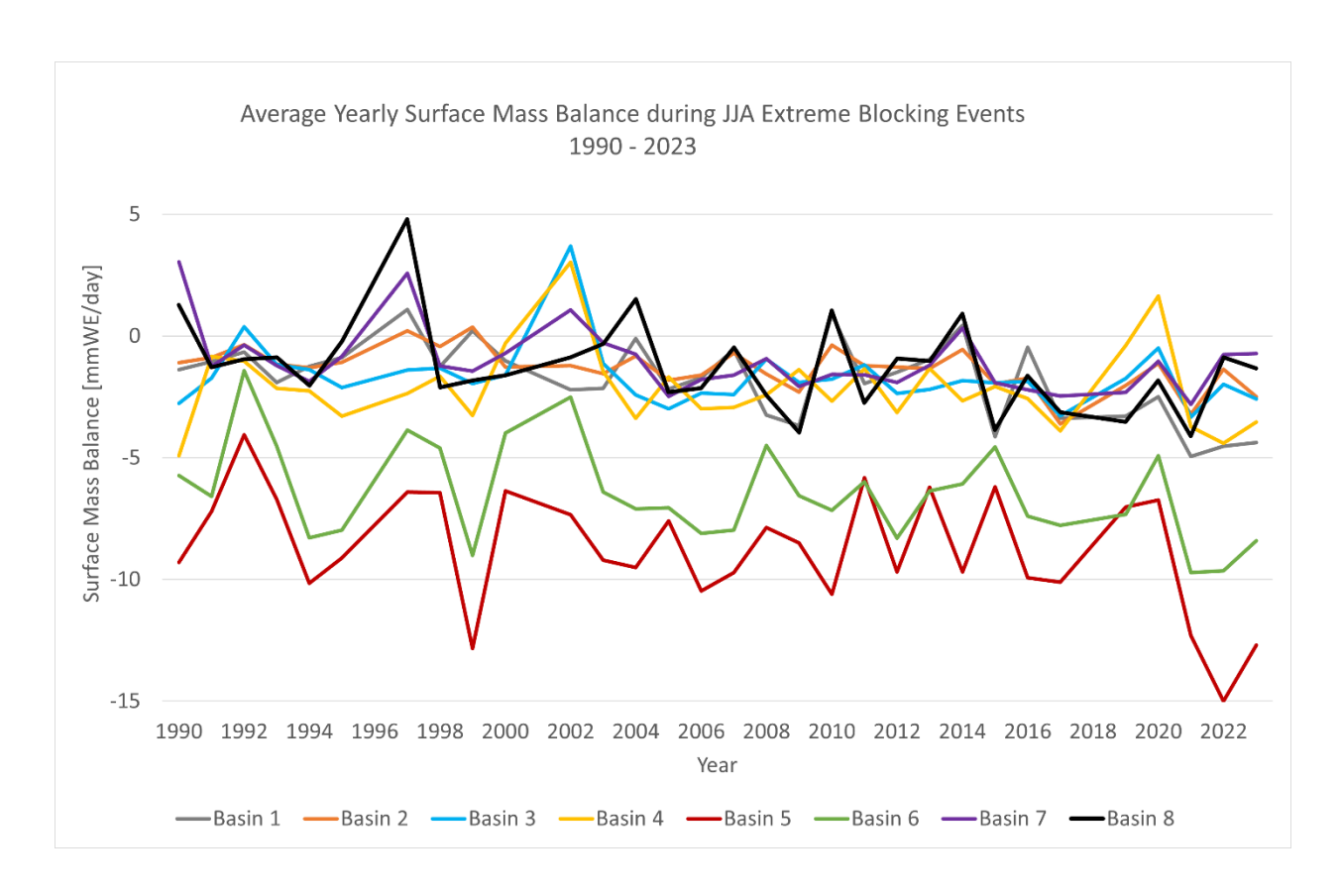


**Figure 3.2:** Timeseries of average JJA surface mass balance (mm w.e. day<sup>-1</sup>) on days of extreme blocking during 1990–2023 from MAR. Basin 8 in northwestern Greenland is highlighted in black and shows a general downward trend.

The average JJA SMB during extreme blocking events varied over the entire period (Figure 3.2; 1990–2023). This graph only encompasses "extreme" blocking events that occurred during meteorological summer (JJA) for this period. This study chose to focus on the most extreme blocking episodes as a changing climate is expected to make blocking episodes more frequent and intense. Therefore, the episodes that are now considered extreme may in the future become normalized. Atmospheric blocking already often results in large-scale melt events in the Arctic which is also warming faster than the rest of the planet. When this warming is coupled with more frequent and intense blocks, the resulting surface loss will be compounded.

Consequently, it is essential to further our understanding of blocking episodes in order to help communities prepare and adapt.

When examining the yearly trends of SMB during extreme blocking events, Basin 8 followed a trend similar to most other basins, with the exception of Basins 5 and 6 in the northeast. Figure 3.2 shows the temporal variability in extreme blocking effects, and it is important to note that not all years resulted in net negative SMB in Basin 8. In several years extreme blocking events had positive effects on SMB, with one example as recent as 2014. However, following 2014, extreme blocking events have only coincided with negative SMB values. The slight negative trend of the SMB time series in conjunction with several years of negative SMB values does suggest that extreme blocking events may be shifting to a greater tendency toward mass loss in Basin 8.

**Table 3.1:** Average surface mass balance (mm w.e. day<sup>-1</sup>) of extreme blocking events averaged by decade.

Decade	Basin 1	Basin 2	Basin 3	Basin 4	Basin 5	Basin 6	Basin 7	Basin 8
1990s	-1.116	-0.696	-1.429	-2.178	-7.751	-5.692	-0.734	-0.905
2000s	-1.873	-1.469	-1.841	-2.051	-9.109	-6.682	-1.353	-1.598
2010s	-2.294	-1.688	-2.121	-2.315	-8.627	-7.374	-1.912	-2.284
2020s	-2.487	-1.269	-1.448	-1.110	-7.553	-5.240	-1.056	-1.919

As prior studies have found that blocking episodes are becoming more intense and frequent (Lupo, 2021; McLeod & Mote, 2015, 2016), we further examined our data to see if this change is also evident in the subsequent impacts on SMB. When comparing the average SMB during extreme blocking events from past decades, a familiar pattern appeared for several basins.

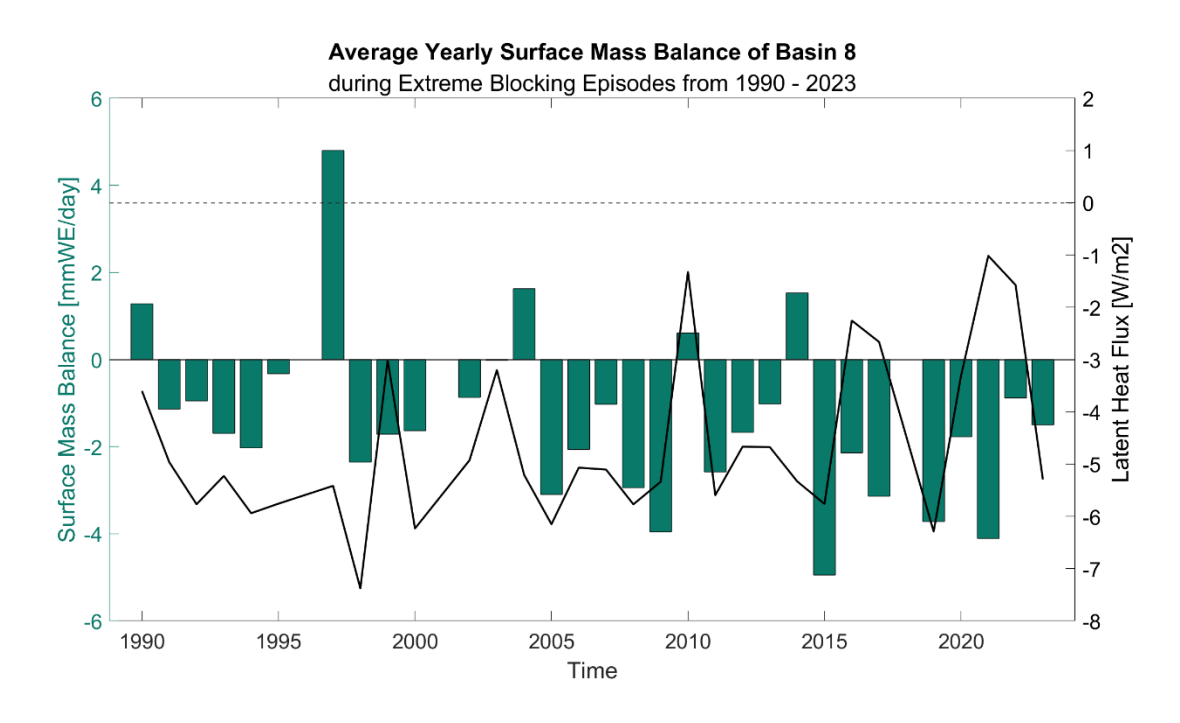
For many of the GrIS major ice drainage basins, including Basin 8, the magnitude of surface mass loss increased decade over decade, but then decreased in the 2020s (Table 3.1). When omitting Basins 5 and 6, which have always had higher mass loss than other basins, Basin 8 had the second highest average surface mass loss in the 2010s and 2020s. Considering this ice drainage basin had initially been the third lowest on average during the 1990s, this would mean that extreme blocking-related surface mass loss had clearly shown an acceleration. However, it should be noted that the data for the 2020s was limited to 3 years, so conclusions for this decade were not as robust as previous decades.

# 3.2 Surface Energy Balance

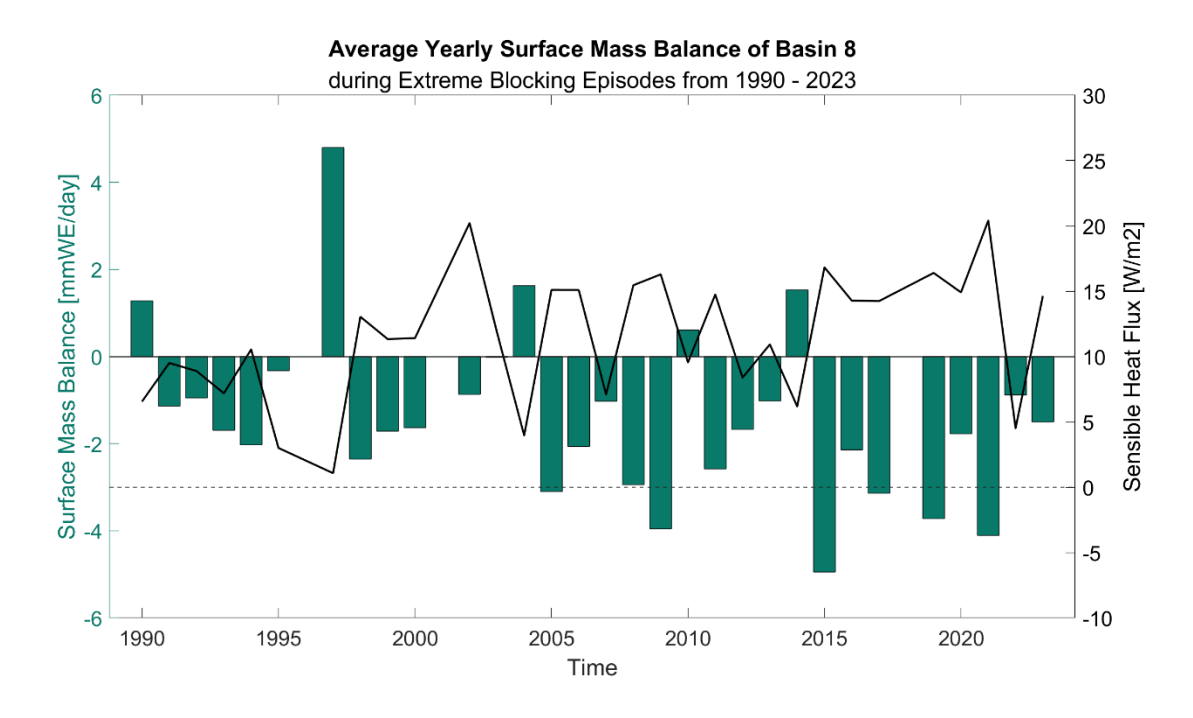
In section 3.1, it was found that surface mass loss in northwestern Greenland during extreme blocking events had increased over the study period. It was also found that not all extreme blocking events exclusively resulted in negative SMB, as several years had net surface mass gain on average. To further investigate possible reasons for why surface mass loss was increasing, as well as possibly explain what resulted in years with positive SMB, this thesis also examined surface energy balance variables during extreme blocking events.

Table 3.2: The average latent heat flux (W m<sup>-2</sup>) and sensible heat flux (W m<sup>-2</sup>) of Basin 8 during JJA extreme blocking events by decade, followed by the corresponding p-value of ANOVA testing meant to show the statistical difference in means between decades. Both turbulent heat fluxes had statistically significant changes in means over our study period where latent heat flux had significantly decreased, and sensible heat flux had significantly increased.

Basin 8	LHF [W/m <sup>2</sup> ]	SHF [W/m <sup>2</sup> ]
1990s	-5.699	8.379
2000s	-4.828	12.307
2010s	-5.005	12.858
2020s	-3.297	14.333
ANOVA p-value	0.034*	7.05E-05*



**Figure 3.3:** Average surface mass balance (mm w.e. day<sup>-1</sup>) (bars) and latent feat flux (W m<sup>-2</sup>) (line) of Basin 8 during JJA extreme blocking episodes from 1990–2023.



**Figure 3.4:** Average surface mass balance (mm w.e. day<sup>-1</sup>) (bars) and sensible heat flux (W m<sup>-2</sup>) (line) of Basin 8 during JJA extreme blocking episodes from 1990–2023.

In the long term, latent heat flux during extreme blocking events had a modest decrease of less than 0.5 W m<sup>-2</sup> decade over decade until the 2020s, where it dropped by over 1 W m<sup>-2</sup>, over twice as much as before (Figure 3.3, Table 3.2). Sensible heat flux on the other hand increased more irregularly, stagnating between the 2000s and 2010s before increasing again in the 2020s. When examining the year-by-year trend, latent heat and sensible heats fluxes had differences in their variability. Latent heat was more consistent and on average was confined to a much smaller range, despite its decreasing trend. Sensible heat flux however, had been more variable with a range of approximately 0 W m<sup>-2</sup> in 1997 to 20 W m<sup>-2</sup> in 2021 (Figure 3.4). While these are small differences in aggregate, they represented large differences in heat input when averaged over the entire ice drainage basin.

**Table 3.3:** This table shows the average snowfall (mm w.e. day<sup>-1</sup>) and rainfall (mm w.e. day<sup>-1</sup>) of Basin 8 during JJA extreme blocking events by decade, followed by the corresponding p-value of ANOVA testing meant to show the statistical difference in means between decades.

Basin 8	SF [mm w.e./day]	RF [mm w.e./day]
1990s	1.484	0.167
2000s	1.420	0.272
2010s	1.325	0.301
2020s	1.519	0.929
ANOVA p-value	0.911	6.83E-09*

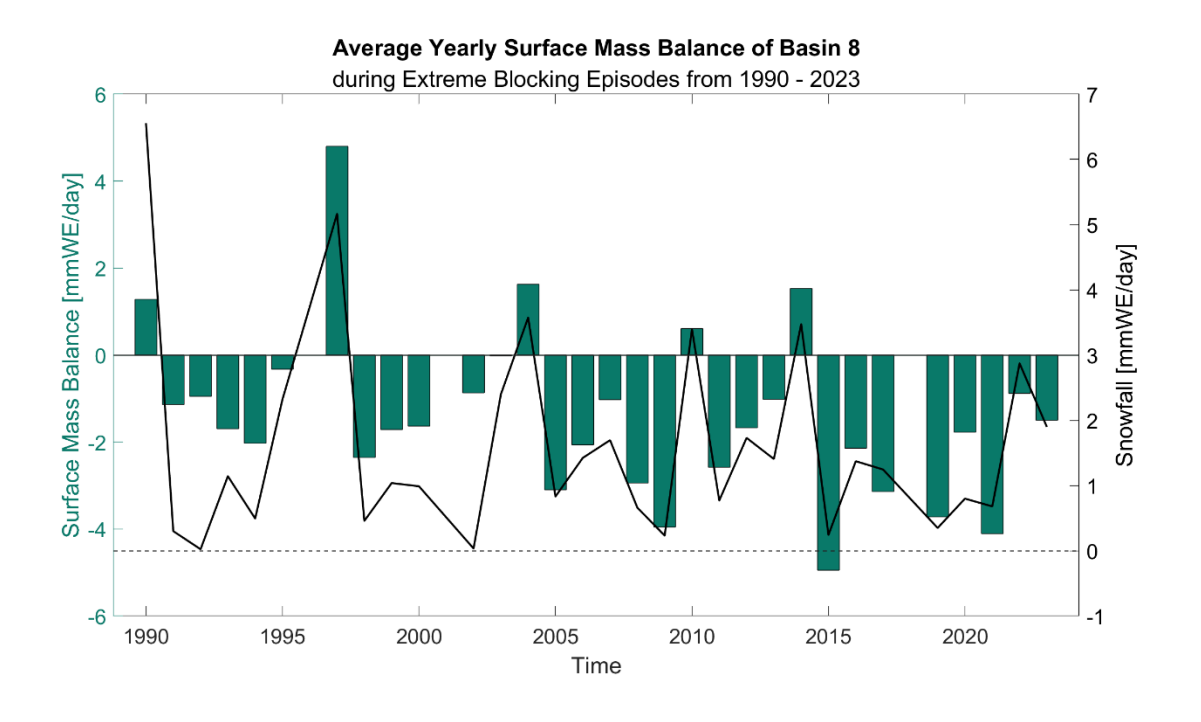


**Figure 3.5:** Average surface mass balance (mm w.e. day<sup>-1</sup>) (bars) and snowfall (mm w.e. day<sup>-1</sup>) (line) of Basin 8 during JJA extreme blocking episodes from 1990–2023.

Snowfall during JJA extreme blocking episodes overall tended to follow a negative relationship over time (Figure 3.5). Throughout the 1990s, there was a spike in snowfall production that would see years with high snowfall values. Through the 2000s and 2010s, this range of difference between yearly snowfall output, while still occurring, was not as drastic as it had been during the 1990s before ultimately shrinking yet again in the late 2010s and into the 2020s (Table 3.3). Snowfall during extreme blocking events in northwestern Greenland also seemed to follow a cyclical trend where every few years there would be a drastic increase in snowfall totals that would be reflected in positive SMB, or in the case of 2022, less surface mass loss than surrounding years.

Due to the cyclical variation in snowfall, I chose to further explore possible reasonings for this variation. As the relationship between the North Atlantic Oscillation (NAO) and blocking episodes over Greenland has already been established (Hanna et al., 2015), I began by comparing the years with high average snowfall to the average monthly NAO during the corresponding periods. While no significant relationship was found between NAO and high snowfall years, high snowfall totals did tend to occur when the NAO was in a weak negative to positive NAO phase (greater than -1). I followed this by also examining several years with much lower average snowfall and found that there were a few events that occurred during strong negative phases of the NAO (less than -2). While these results could be coincidental and not all-encompassing, it is worth pointing out due to the predetermined correlation between extreme blocking and the negative phase of the NAO.

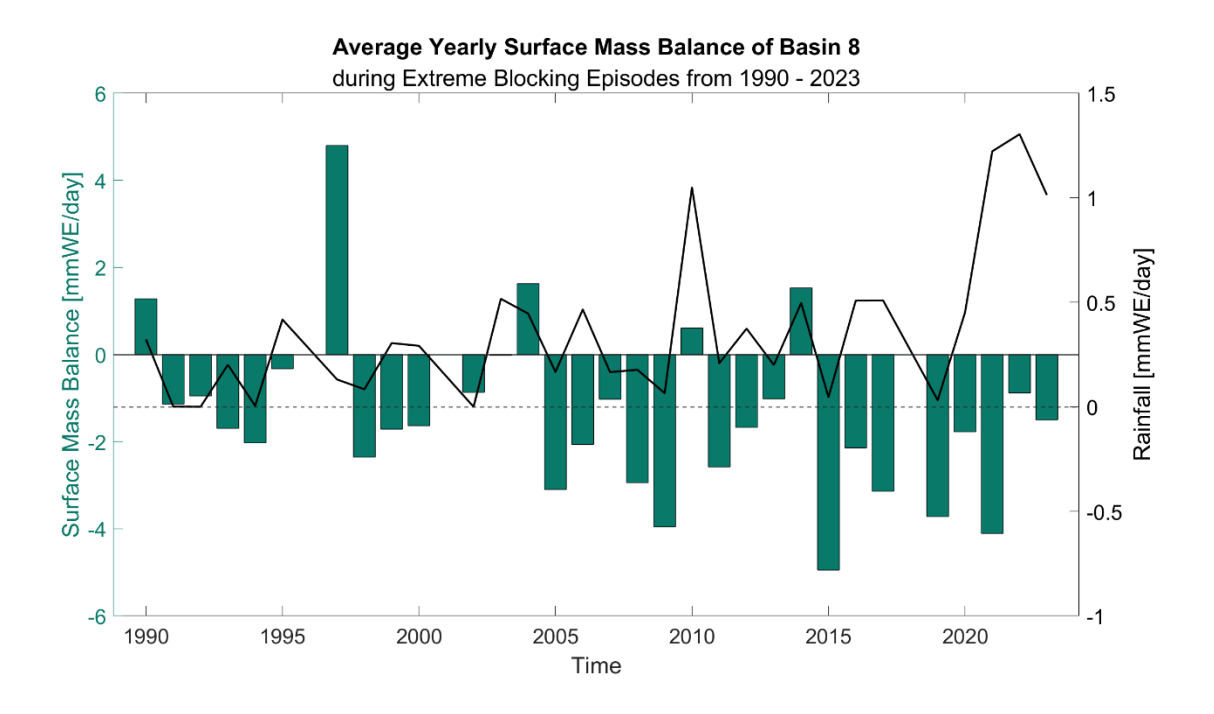


**Figure 3.6:** Average surface mass balance (mm w.e. day<sup>-1</sup>) (bars) and rainfall (mm w.e. day<sup>-1</sup>) (line) of Basin 8 during JJA extreme blocking episodes from 1990–2023.

As snowfall generally decreased over the 33-year period, rainfall had an opposite trend of gradually increasing totals for the better part of three decades before tripling on average in the 2020s. This represented an overall warming climate and an increased fraction of precipitation in summer falling as rain (Figure 3.6). Rainfall did also tend to be cyclical but with much smaller variation from year to year, with the exception of 2010 and 2019–2022. Unlike snowfall, however, rainfall did not seem to be obviously associated with surface mass losses (or gains), likely due to the overall small fraction of precipitation falling as rain in this region. Years with the most drastic ice mass losses, such as 2015, received similar rainfall during extreme blocking events as years that had large positive mass balance like 1997. It should also be noted that due to the spatial averaging of these results, it did not account for the spatial disparity in precipitation

type due to topography changes especially at higher elevations further inland where snowfall would be more prominent.

**Table 3.4:** This table shows the average runoff (mm w.e. day<sup>-1</sup>) and sublimation (mm w.e. day<sup>-1</sup>) of Basin 8 during JJA extreme blocking events by decade, followed by the corresponding p-value of ANOVA testing meant to show the statistical difference in means between decades.

Basin 8	RU [mm w.e./day]	SU [mm w.e./day]
1990s	2.258	0.166
2000s	3.137	0.150
2010s	3.764	0.141
2020s	4.206	0.101
ANOVA p-value	2.32E-23*	0.015*

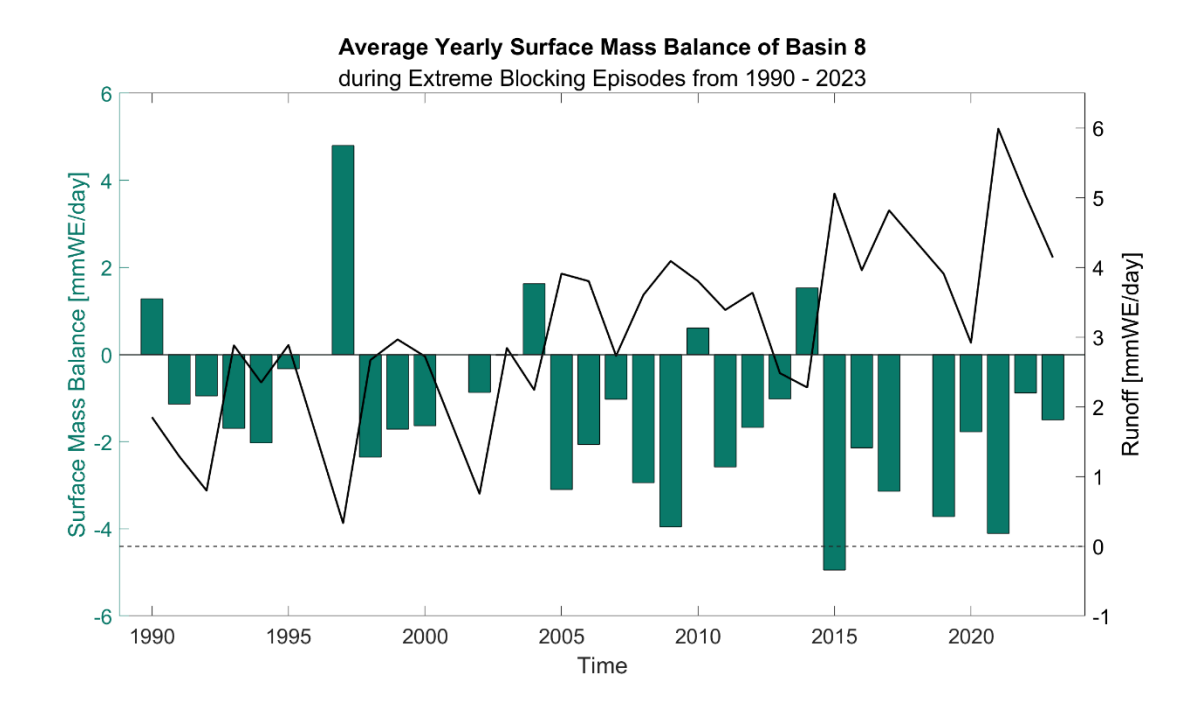


**Figure 3.7:** Average surface mass balance (mm w.e. day<sup>-1</sup>) (bars) and runoff (mm w.e. day<sup>-1</sup>) (line) of Basin 8 during JJA extreme blocking episodes from 1990–2023.

Unsurprisingly, runoff increased over the last several decades of extreme blocking episodes and followed a clear linear trend with cyclical variation (Table 3.4, Figure 3.7). As runoff is a crucial component of ablation in SMB, there was an obvious relationship between SMB magnitude and runoff in the time series. For example, in 1997 there was a sharp drop in runoff totals that coincided with large surface mass gain, and similarly in 2015 there was a large jump in runoff that coincided with large surface mass loss. However, this relationship did have exceptions. During 2017–2020, runoff decreased and yet SMB remained negative, with the magnitude of loss increasing during 2017–2019.

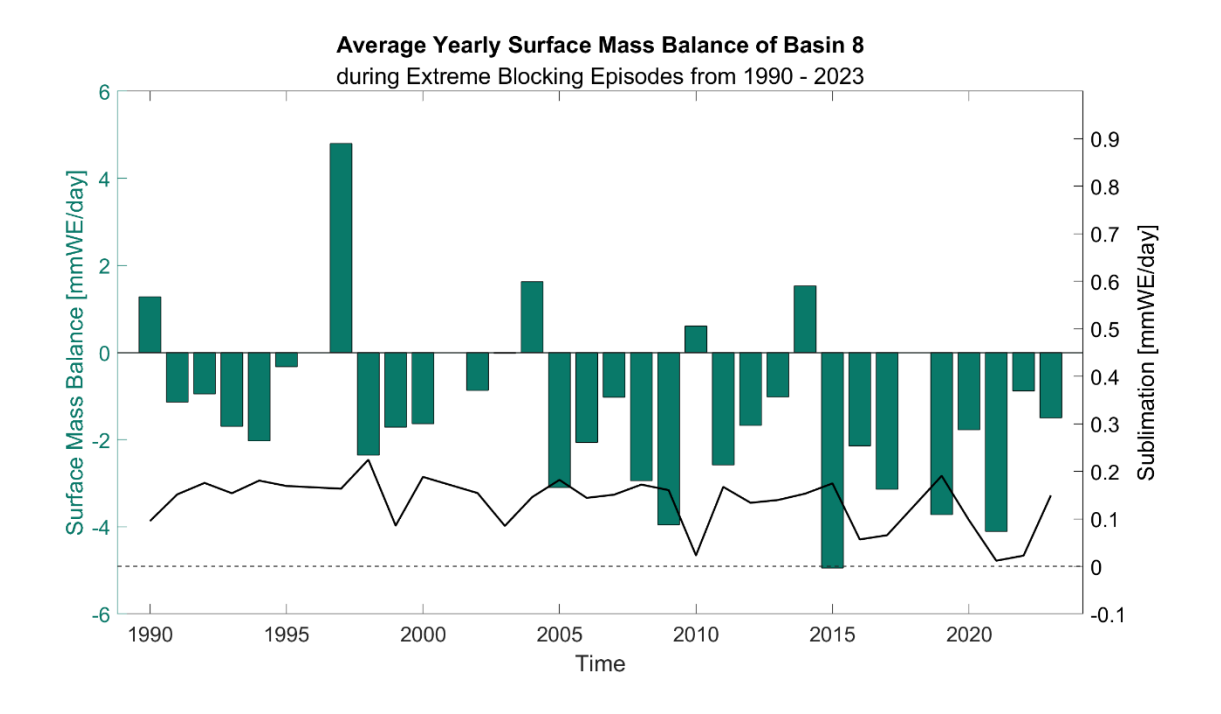


**Figure 3.8:** Average surface mass balance (mm w.e. day<sup>-1</sup>) (bars) and sublimation (mm w.e. day<sup>-1</sup>) (line) of Basin 8 during JJA extreme blocking episodes from 1990–2023.

Sublimation steadily decreased over time, perhaps in relation to the simultaneously decreasing snowfall totals (Figure 3.8). While this decrease was significant, sublimation was always at least an order of magnitude less than runoff and did not have as great of an impact on SMB.

**Table 3.5:** This table shows the average shortwave and longwave upwelling and downwelling radiation in (W m<sup>-2</sup>) of Basin 8 during JJA extreme blocking events by decade, followed by the corresponding p-value of ANOVA testing meant to show the statistical difference in means between decades.

Basin 8	SWD [W/m <sup>2</sup> ]	LWD [W/m <sup>2</sup> ]	SWU [W/m <sup>2</sup> ]	LWU [W/m <sup>2</sup> ]
1990s	314.850	227.277	247.969	284.907
2000s	289.180	232.464	226.529	287.010
2010s	285.422	233.291	220.969	288.435
2020s	263.703	240.660	206.230	290.920
ANOVA p-value	2.76E-05*	0.017*	1.87E-06*	0.004*

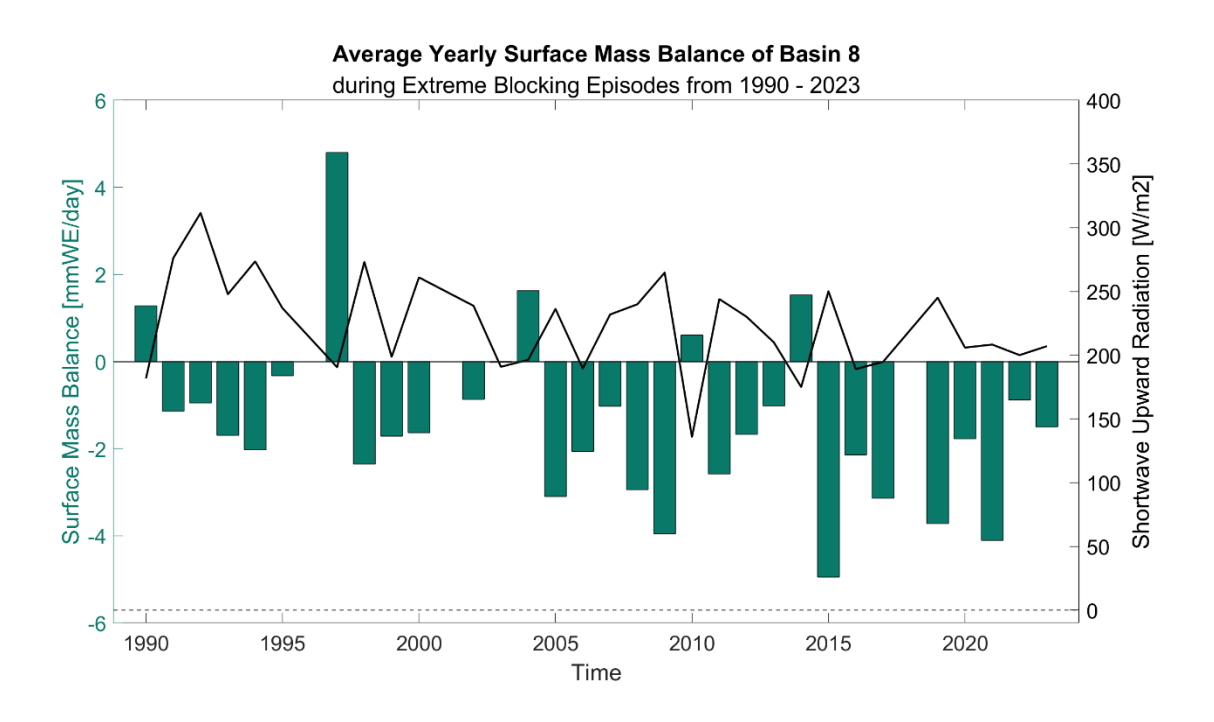


**Figure 3.9:** Average surface mass balance (mm w.e. day<sup>-1</sup>) (bars) and upwelling shortwave radiation (W m<sup>-2</sup>) (line) of Basin 8 during JJA extreme blocking episodes from 1990–2023.

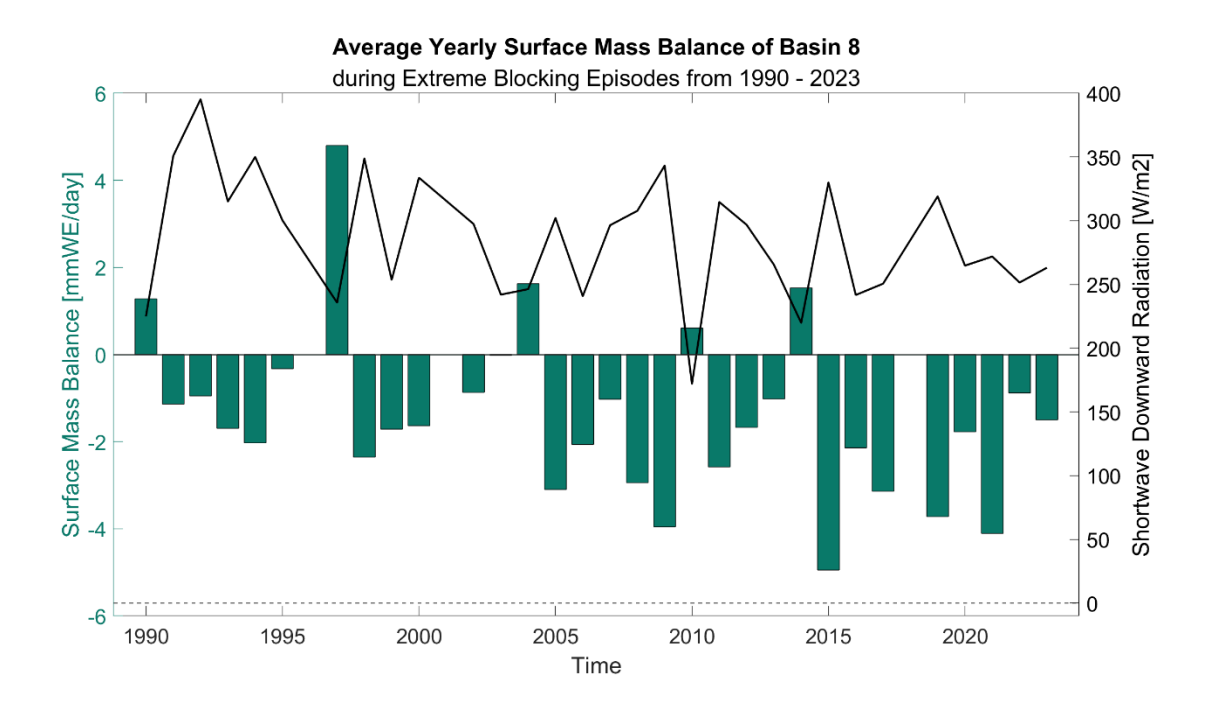


**Figure 3.10:** Average surface mass balance (mm w.e. day<sup>-1</sup>) (bars) and downwelling shortwave Radiation (W m<sup>-2</sup>) (line) of Basin 8 during JJA extreme blocking episodes from 1990–2023.

Shortwave downward and upward radiation both showed a significant consistent downward trend during extreme blocking events (Table 3.5, Figure 3.9, 3.10). Additionally, they both noticeably decreased during summers where SMB showed net positive gains. This pattern was not as consistent for summers of net negative SMB, as there were several years where shortwave radiation dropped and did not result in positive SMB.

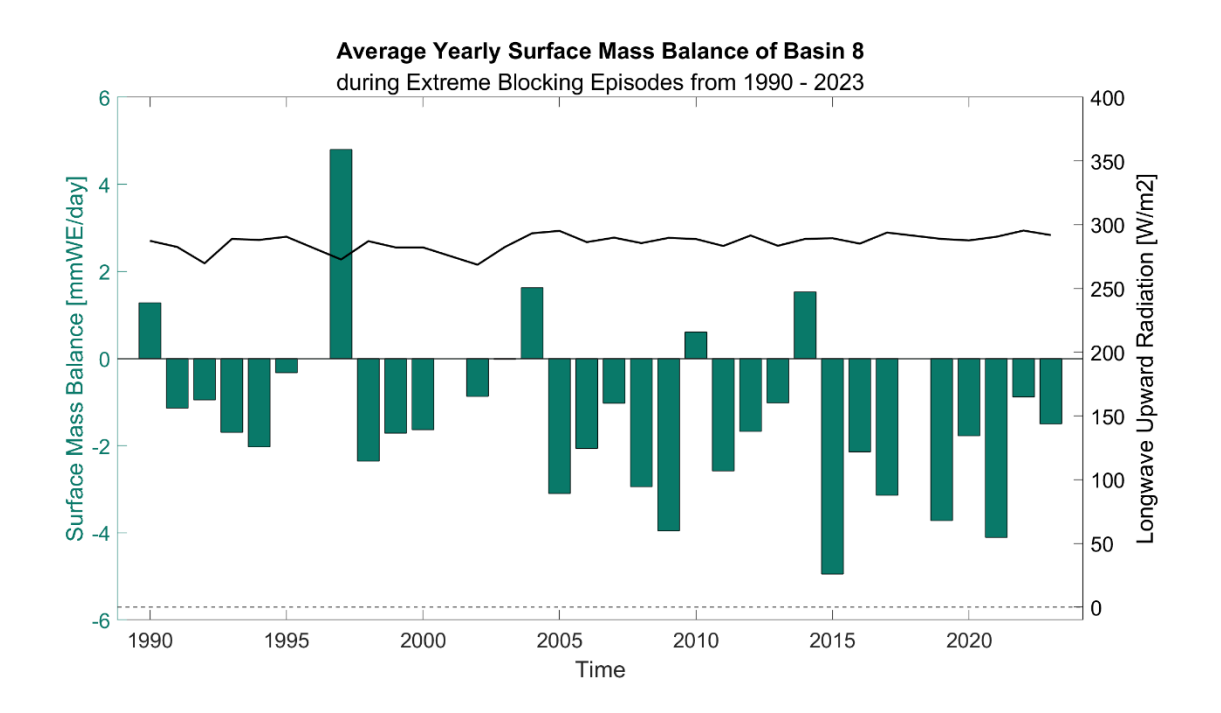


**Figure 3.11:** Average surface mass balance (mm w.e. day<sup>-1</sup>) (bars) and upwelling longwave radiation (W m<sup>-2</sup>) (line) of Basin 8 during JJA extreme blocking episodes from 1990–2023.

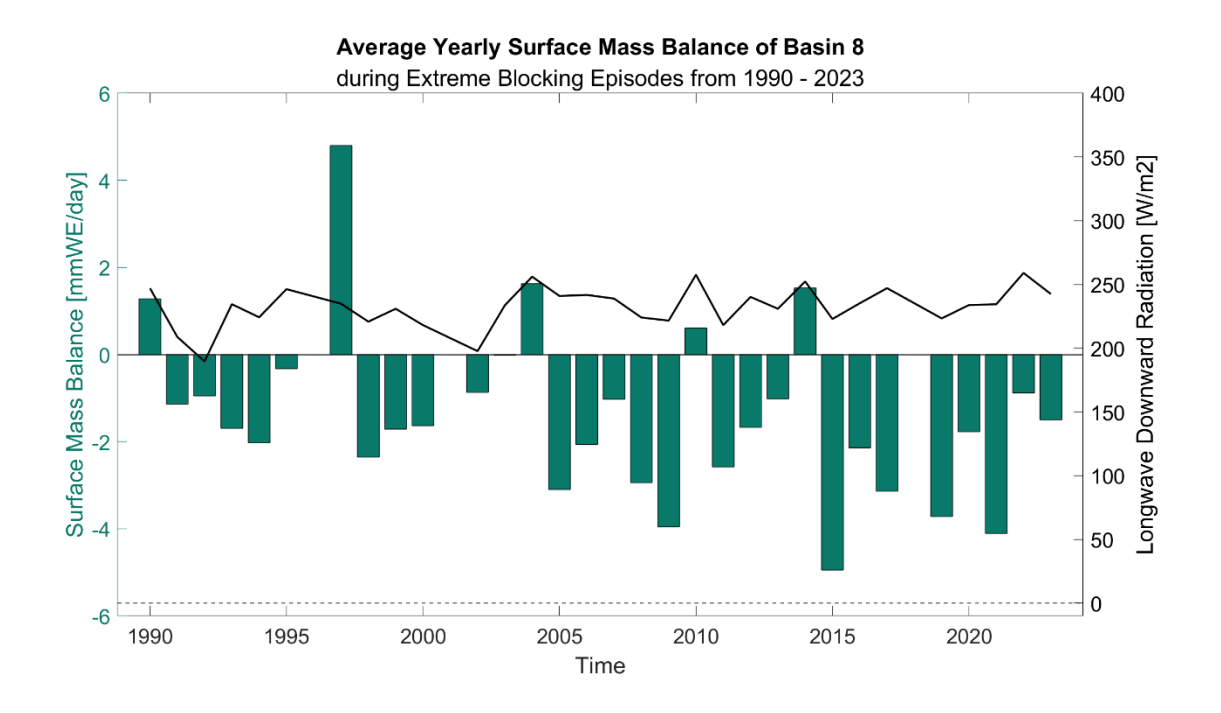


**Figure 3.12:** Average surface mass balance (mm w.e. day<sup>-1</sup>) (bars) and downwelling longwave radiation (W m<sup>-2</sup>) (line) of Basin 8 during JJA extreme blocking episodes from 1990–2023.

Compared to their shortwave counterparts, longwave upwards and downwards radiation tended to have much less variation. However, there was a noticeable pattern in the downward component where in years that resulted in positive SMB (or less negative SMB in 2022), longwave downward radiation would increase. In addition, longwave radiation significantly increased over time (Table 3.5, Figure 3.11, 3.12). Net radiation also tended to favor greater downwelling radiation than upwelling radiation, though over the decades the difference between the two seemed to be decreasing. The decreasing difference in downwelling and upwelling radiation could possibly indicate differences in cloud cover or cloud types, as thicker clouds would prevent more downwelling radiation from making it to the surface.

In summary, section 3.2 sought to visualize the long-term changes in various atmospheric and surface variables during summer extreme blocking events. While all examined variables with the exception of snowfall showed significant changes over the study period, a few key findings further stood out. Rainfall has become more prominent during extreme blocking events, especially since the beginning of the 2020s. While sensible heat flux has always been positive on average, the increased magnitude of positive sensible heat flux transferring greater melt energy to the surface is cause for concern. Lastly, years with positive SMB were often accompanied by less shortwave radiation and slightly higher longwave radiation, possibly supporting cloud cover as a factor in SMB.

While decadal trends were important for understanding the larger implications of extreme blocking, there were still yearly discrepancies in SMB that were not explained by long-term trends. To address this, two events from June 1997 and August 2014 were chosen as they resulted in positive SMB and two additional events from July 1994 and July/August 2019 were picked because they resulted in negative SMB. June 1997 and July/August 2019 were especially of

interest as they had the single highest daily gains/losses during the entire study period. By utilizing case studies, we were able to understand the situational variation that dictated whether extreme blocking resulted in surface mass gain or loss.

## 3.2.1 June 1997

From 1–6 June 1997, an extreme blocking event resulted in basin-wide surface mass gain in northwestern Greenland (Figure 3.13). During this blocking event, surface mass gain was very high, especially on 2 and 4 June, which had approximately 12.5 and 10 mm w.e. day<sup>-1</sup> of surface mass gain (Table 3.6), making them the second and fourth highest days of individual gain across the entire study period.

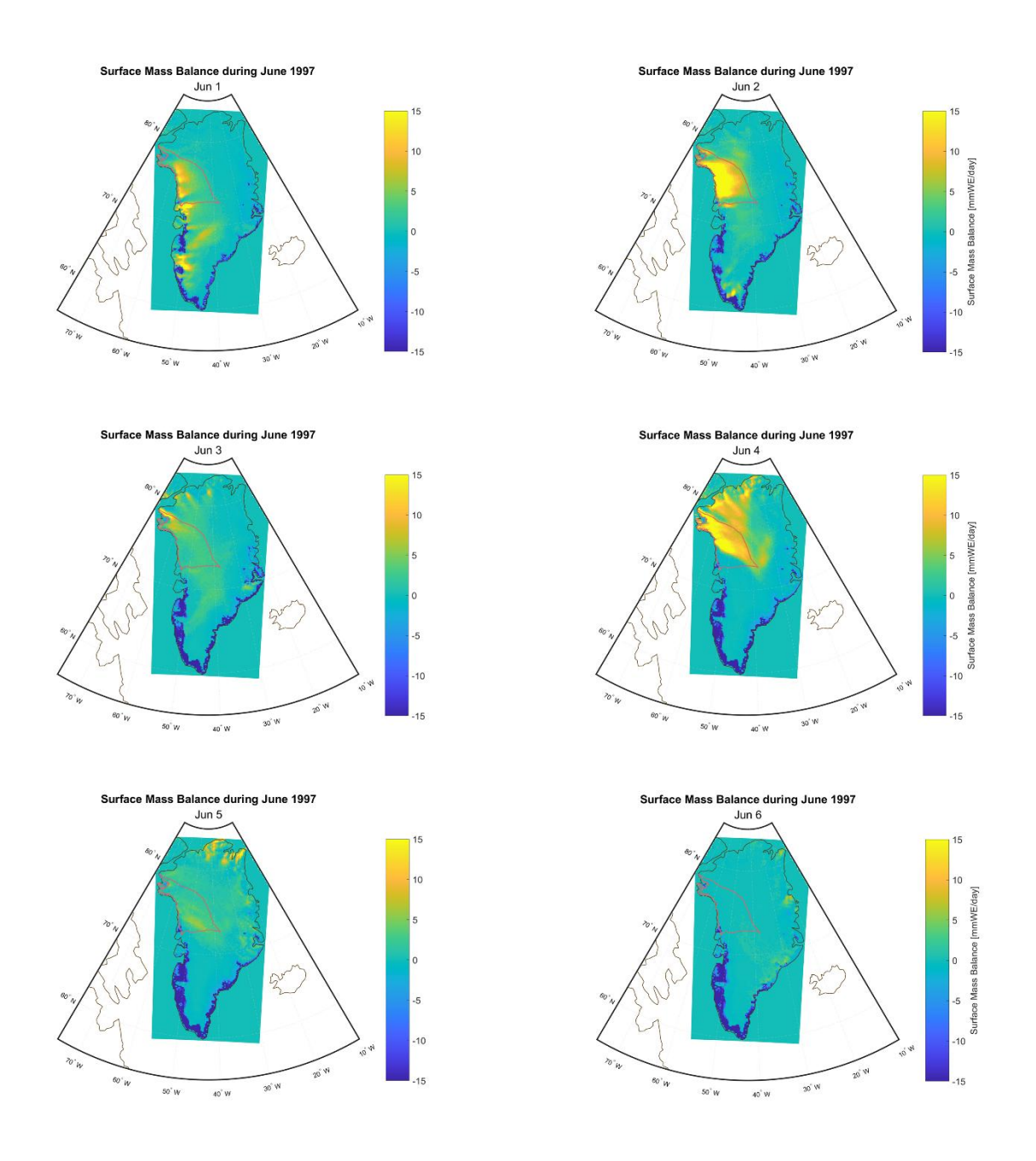


**Figure 3.13:** Average surface mass balance (mm w.e. day<sup>-1</sup>) for the extreme blocking event during 1–6 June 1997.

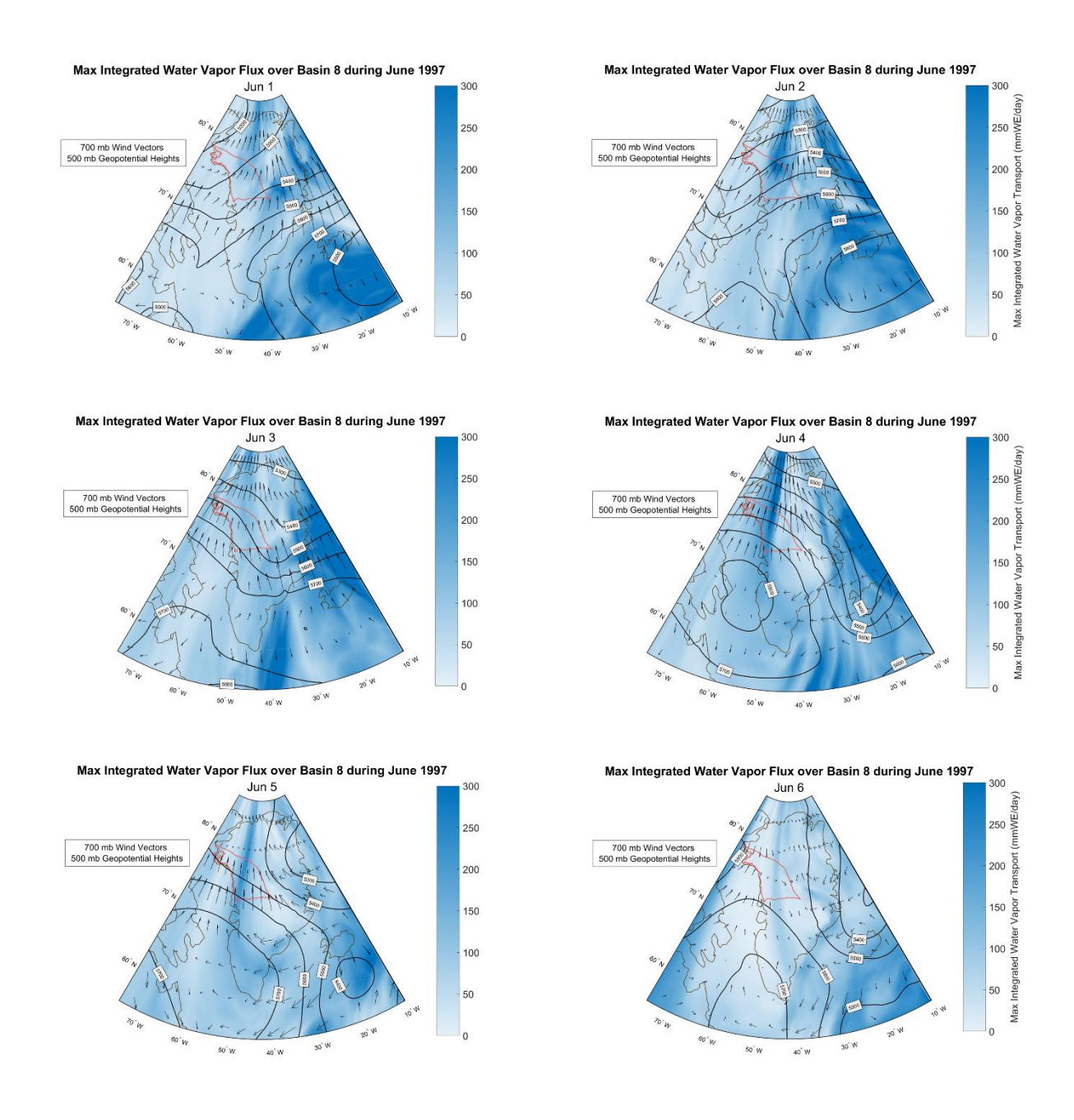


**Figure 3.14:** Average integrated water vapor transport (kg m<sup>-1</sup>s<sup>-1</sup>), 700 hPa wind vectors (m s<sup>-1</sup>), and 500 hPa geopotential heights for the extreme blocking event during 1–6 June 1997.

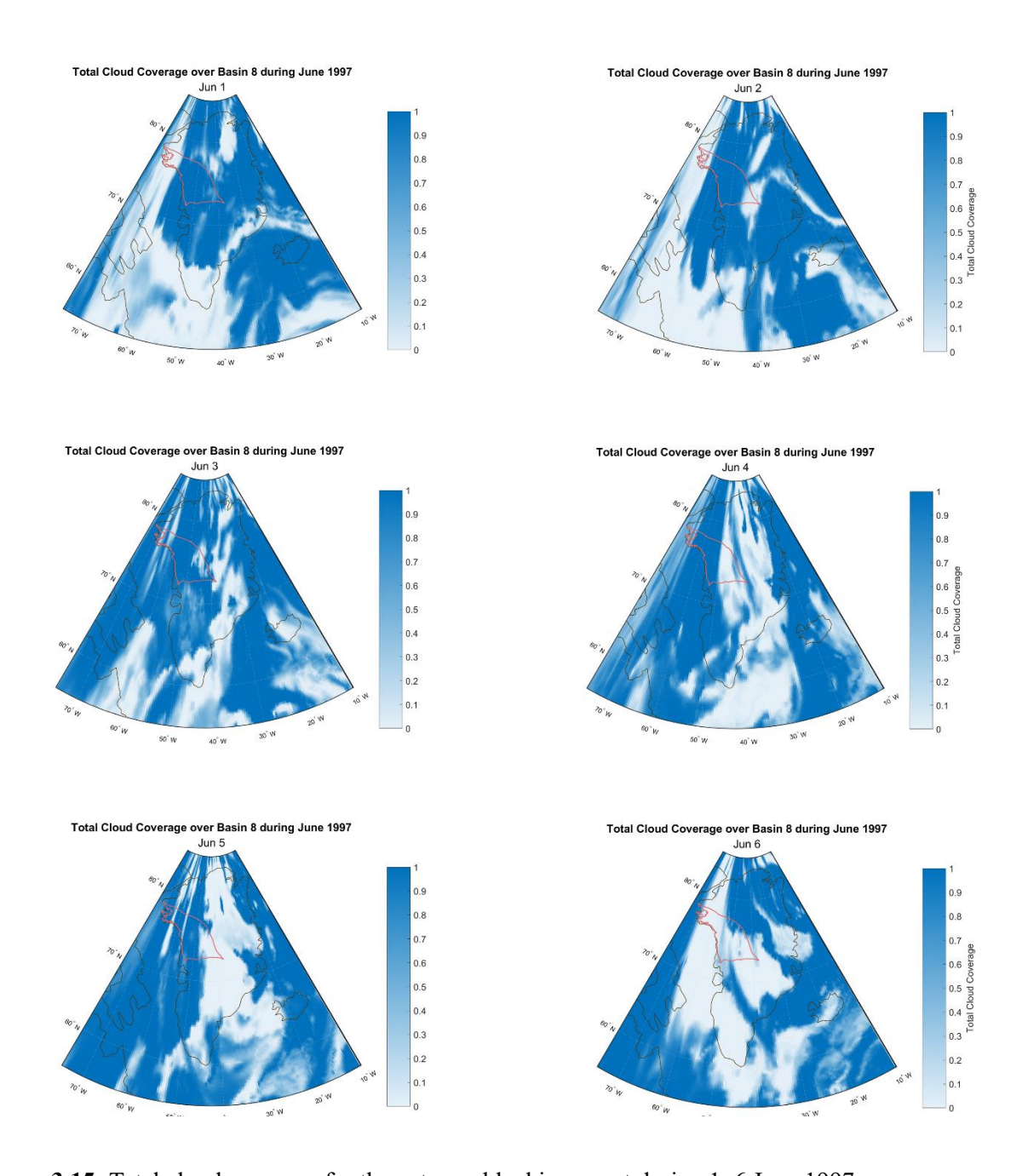


**Figure 3.15:** Total cloud coverage for the extreme blocking event during 1–6 June 1997.

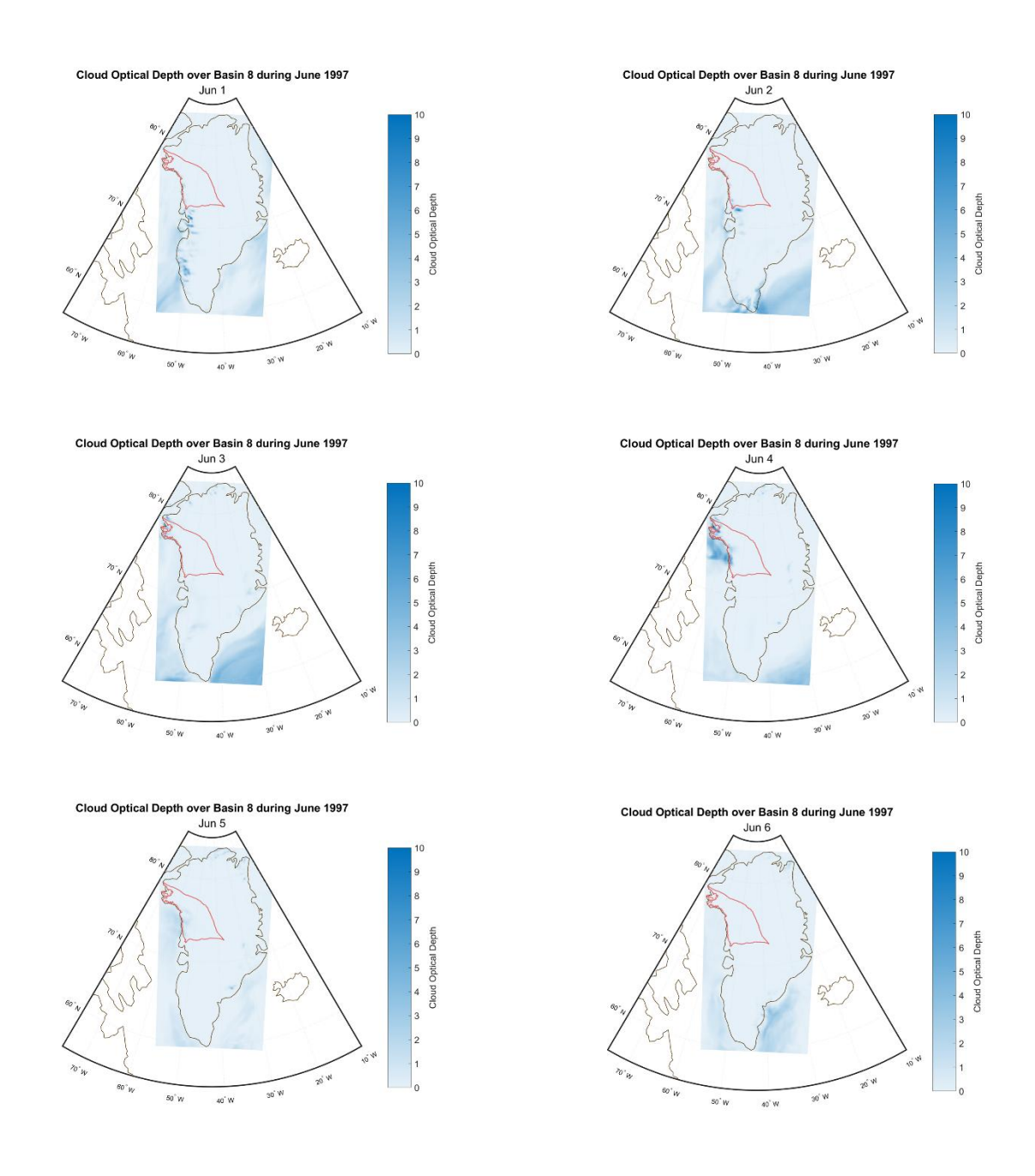


**Figure 3.16:** Cloud optical depth for the extreme blocking event during 1–6 June 1997.

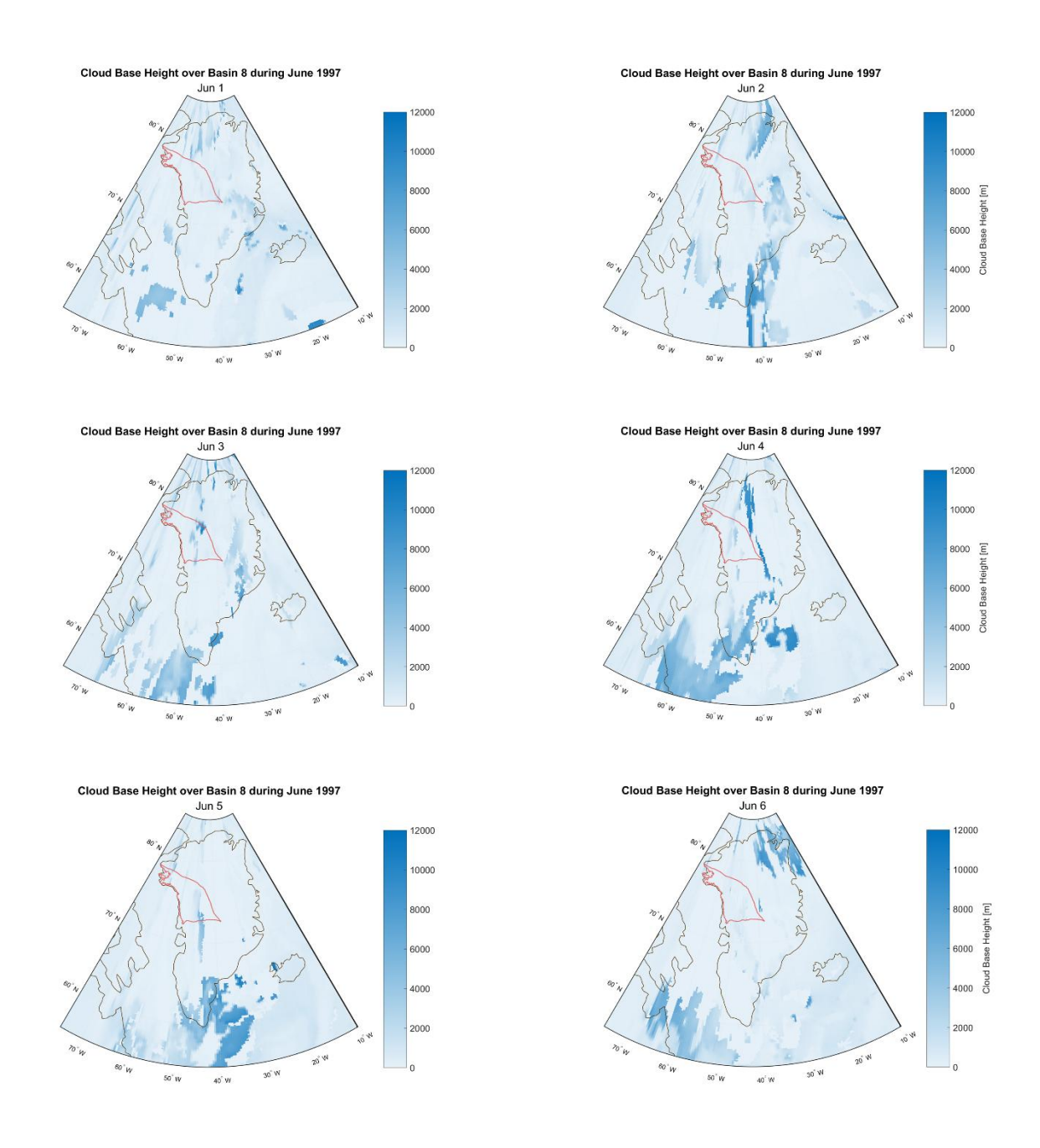


Figure 3.17: Cloud base height (m) for the extreme blocking event during 1–6 June 1997.

**Table 3.6:** Surface mass balance (SMB; mm w.e. day<sup>-1</sup>), average integrated water vapor transport (Avg IVT; kg m<sup>-1</sup>s<sup>-1</sup>), surface atmospheric temperature (Atm Temp; °C), surface skin temperature (Surface Temp; °C), latent heat flux (LHF; W m<sup>-2</sup>) and sensible heat flux (SHF; W m<sup>-2</sup>) averaged for spatially and temporally over Basin 8 for a blocking event during 1–6 June 1997.

Date	<b>SMB</b>	Avg IVT	<b>Atm Temp</b>	<b>Surface Temp</b>	LHF	SHF
6/1/1997	4.274	25.615	-12.037	-11.610	-9.041	-12.922
6/2/1997	12.497	155.486	-10.634	-10.100	-9.309	-12.293
6/3/1997	3.355	171.766	-13.263	-12.646	-5.855	-11.250
6/4/1997	9.920	155.679	-9.877	-9.677	-13.448	-6.631
6/5/1997	2.287	98.100	-9.113	-8.681	-7.191	-5.319
6/6/1997	-0.125	35.836	-11.075	-12.067	-3.659	8.099

**Table 3.7:** Cloud optical depth (COD), upper-middle- and lower-cloud coverage (CU; CM; CD) percentages averaged for spatially and temporally over Basin 8 for a blocking event during 1–6 June 1997.

Date	COD	CU	CM	CD
6/1/1997	0.034	0.793	0.941	0.940
6/2/1997	0.051	0.799	0.985	0.998
6/3/1997	0.075	0.496	0.772	0.911
6/4/1997	0.292	0.766	0.898	0.796
6/5/1997	0.128	0.543	0.604	0.772
6/6/1997	0.004	0.291	0.228	0.242

**Table 3.8:** Downwelling shortwave radiation (SWD), downwelling longwave radiation (LWD), upwelling shortwave radiation (SWU), upwelling longwave radiation (LWU, all W m<sup>-2</sup>) and albedo (ALB) averaged for spatially and temporally over Basin 8 for a blocking event during 1–6 June 1997.

Date	SWD	LWD	<b>SWU</b>	LWU	ALB
6/1/1997	263.874	241.174	213.574	265.444	0.811
6/2/1997	204.174	259.870	165.351	271.691	0.811
6/3/1997	280.975	225.420	227.814	261.193	0.812
6/4/1997	217.168	258.311	175.742	273.452	0.811
6/5/1997	322.939	232.222	259.978	277.443	0.806
6/6/1997	379.740	186.789	305.303	263.740	0.806

**Table 3.9:** Snowfall (SF), rainfall (RF), runoff (RU), sublimation (SU), melt (ME) and firn refreezing (RZ; all mm w.e. day<sup>-1</sup>) averaged for spatially and temporally over Basin 8 for a blocking event during 1–6 June 1997.

Date	SF	RF	RU	SU	ME	RZ
6/1/1997	4.538	0.000	0.003	0.278	0.008	0.003
6/2/1997	12.816	0.000	0.010	0.285	0.030	0.018
6/3/1997	3.523	0.000	0.001	0.177	0.010	0.012
6/4/1997	10.354	0.000	0.029	0.408	0.084	0.025
6/5/1997	2.565	0.000	0.056	0.217	0.415	0.153
6/6/1997	0.056	0.000	0.074	0.110	0.434	0.305

When examining the environmental context of this surface mass gain, several interesting patterns appeared. Non-radiative heat fluxes coincided well with SMB patterns. Latent heat flux values were consistently negative and had two peaks on 2 and 4 June at -9.3 W m<sup>-2</sup> and -13.4 W m<sup>-2</sup> (Table 3.6). Sensible heat flux was also negative except for the final day where it became positive, coinciding with the only day of net negative SMB. Surface and atmosphere temperature were both consistently well below freezing between -8 and -12° C and were within 1° C of each

other every day (Table 3.6). While for most days the temperature of the atmosphere was higher than that of the surface, this once again switched on the final day of extreme blocking.

Another trend to note was that precipitation through snowfall was generally high during this period and that rainfall was very low (Table 3.9). High snowfall accumulation was also not greatly offset by meltwater production and subsequent runoff or by sublimation, and some portion of meltwater would refreeze and contribute to positive SMB. Albedo was steady over this period, staying in the lower 80% range (Table 3.8). This higher albedo could possibly have been attributed to the large amount of fresh snowfall that was able to stay on the ground due to low surface temperatures.

In general, cloud coverage within the first few days was widespread throughout all layers of the lower atmosphere before dropping in the latter half of the blocking period (Table 3.7). It began consistently high with nearly the entire troposphere at 50 - 100% cloud coverage. On the final day, cloud coverage was still consistent across different elevations, but it was much more scattered with totals hovering around 20 - 30% across all parts of the troposphere. Clouds tended to be thin and low, though clouds that were optically thicker did appear offshore and over the coastal ablation zones (Figure 3.15, 3.16, 3.17).

With the added context regarding cloud coverage, radiation terms were also noticeably affected. Shortwave radiation dipped on 2 and 4 June compared to surrounding days, while the opposite was true for longwave radiation though not to the same magnitude (Table 3.8). The dampened shortwave and heightened longwave responses coincide well with days of greater cloud coverage extent across multiple layers of the troposphere, even if cloud optical depth itself was not particularly thick (Figure 3.15, 3.16). From June 2–4 through June, IVT was greater than 150 kg m<sup>-1</sup> s<sup>-1</sup>, signifying enhanced water vapor transport into Basin 8 (Table 3.6, Figure 3.14).

## 3.2.2 August 2014

August of 2014 was another example of an extreme blocking event that resulted in positive SMB, peaking at a daily surface mass gain of 12.66 mm w.e. day<sup>-1</sup> on 18 August, which was also the single highest day of surface mass gain across the entire study period (Table 3.10, Figure 3.18). Beginning with heat fluxes, latent and sensible heat flux were much different from the June 1997 event. Latent heat flux, while still negative, was much weaker in magnitude. Sensible heat flux was positive for most days, unlike sensible heat flux from 1997 that was strongly negative. Sensible heat flux also had two peaks, once on 16 August at 11.6 W m<sup>-2</sup>, which proceeded to drop to -0.35 W m<sup>-2</sup> before rebounding to 18 W m<sup>-2</sup> by 20 August. The days where sensible heat flux was nearest to 0, 17–18 August, were also the days with the greatest surface mass gain (Table 3.10).

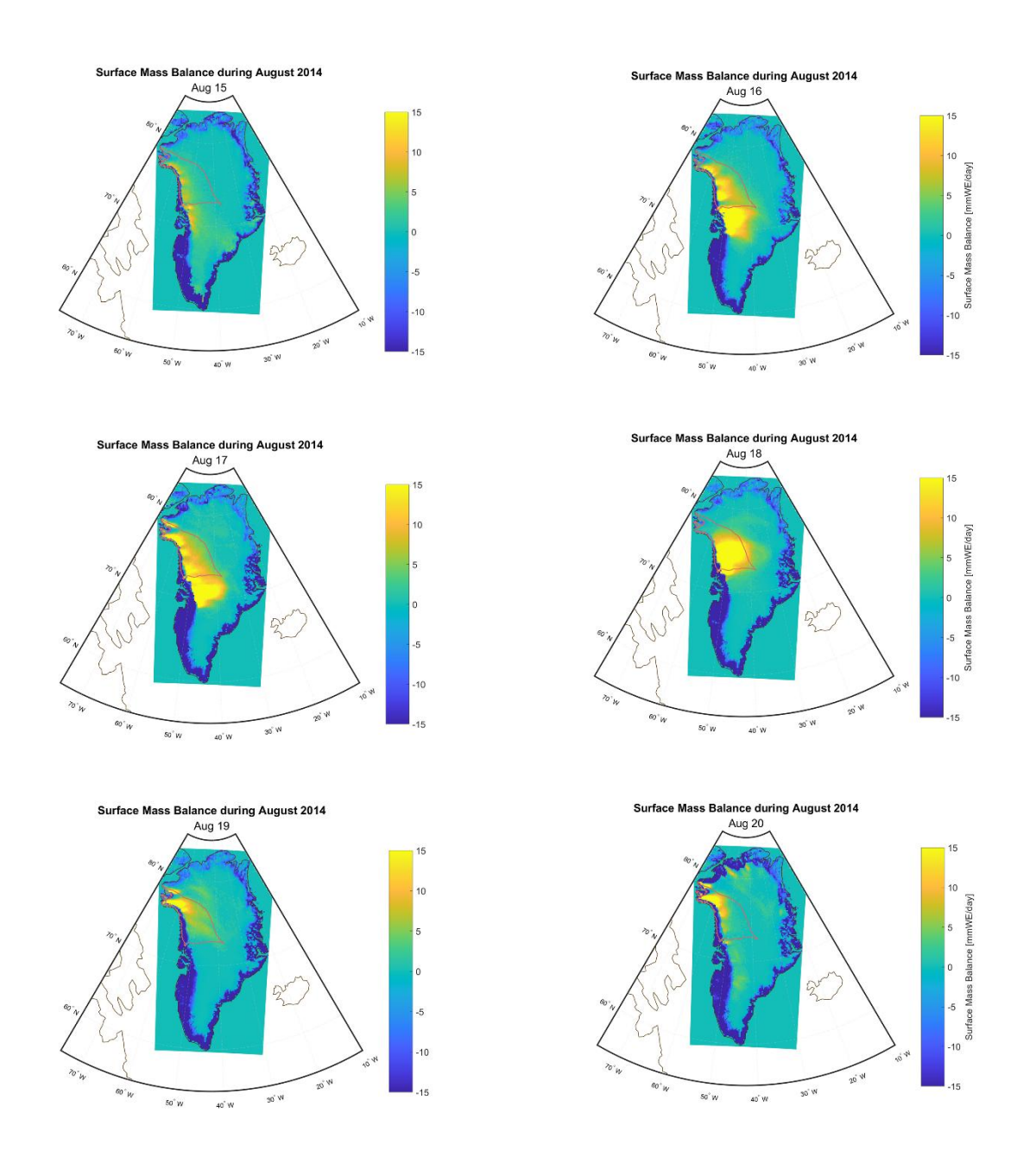


**Figure 3.18:** Average surface mass balance (mm w.e. day<sup>-1</sup>) for the extreme blocking event during 15–20 August 2014.

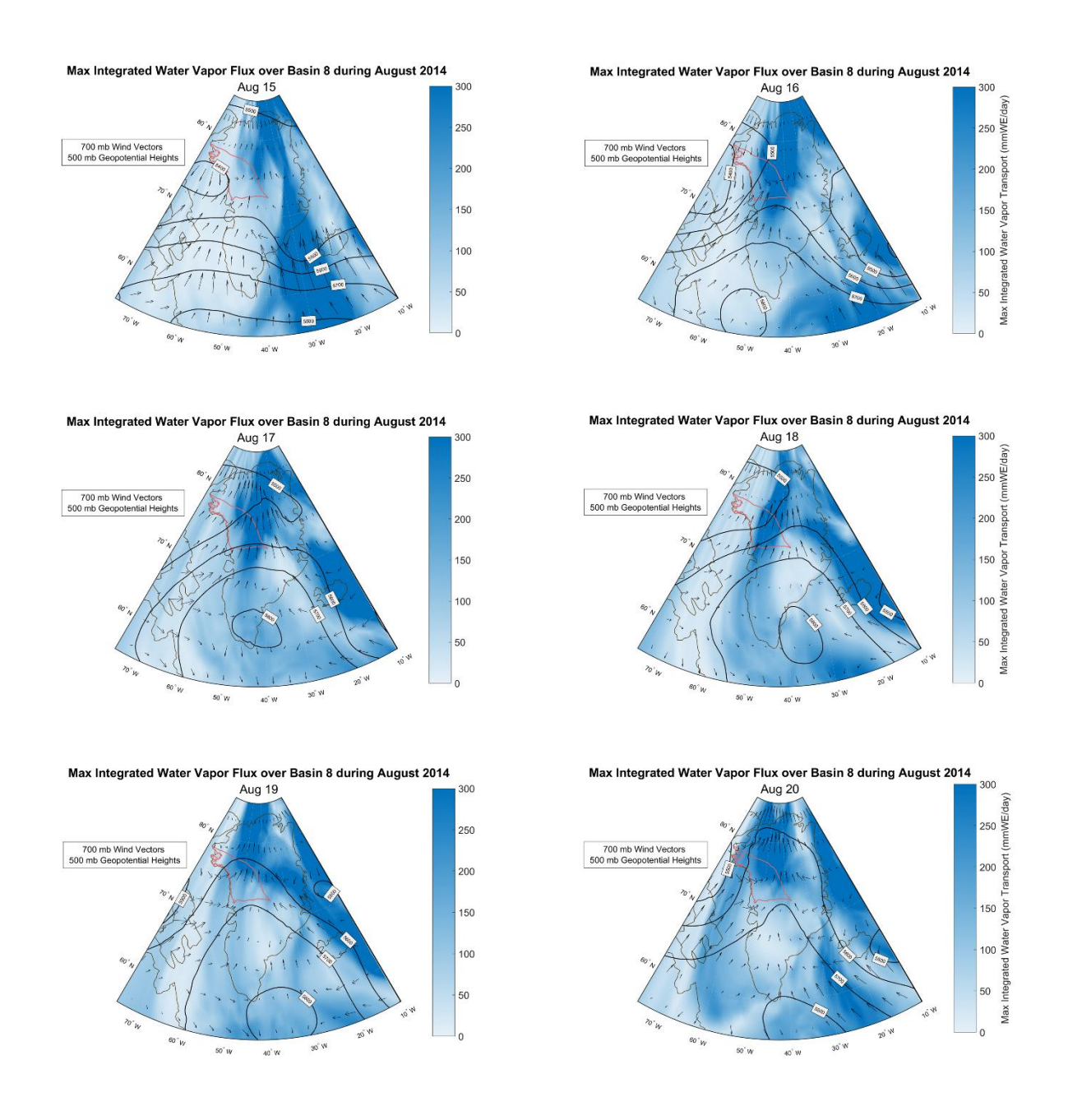


**Figure 3.19:** Average integrated water vapor transport (kg m<sup>-1</sup>s<sup>-1</sup>), 700 hPa wind vectors (m s<sup>-1</sup>), and 500 hPa geopotential heights for the extreme blocking event during 15–20 August 2014.

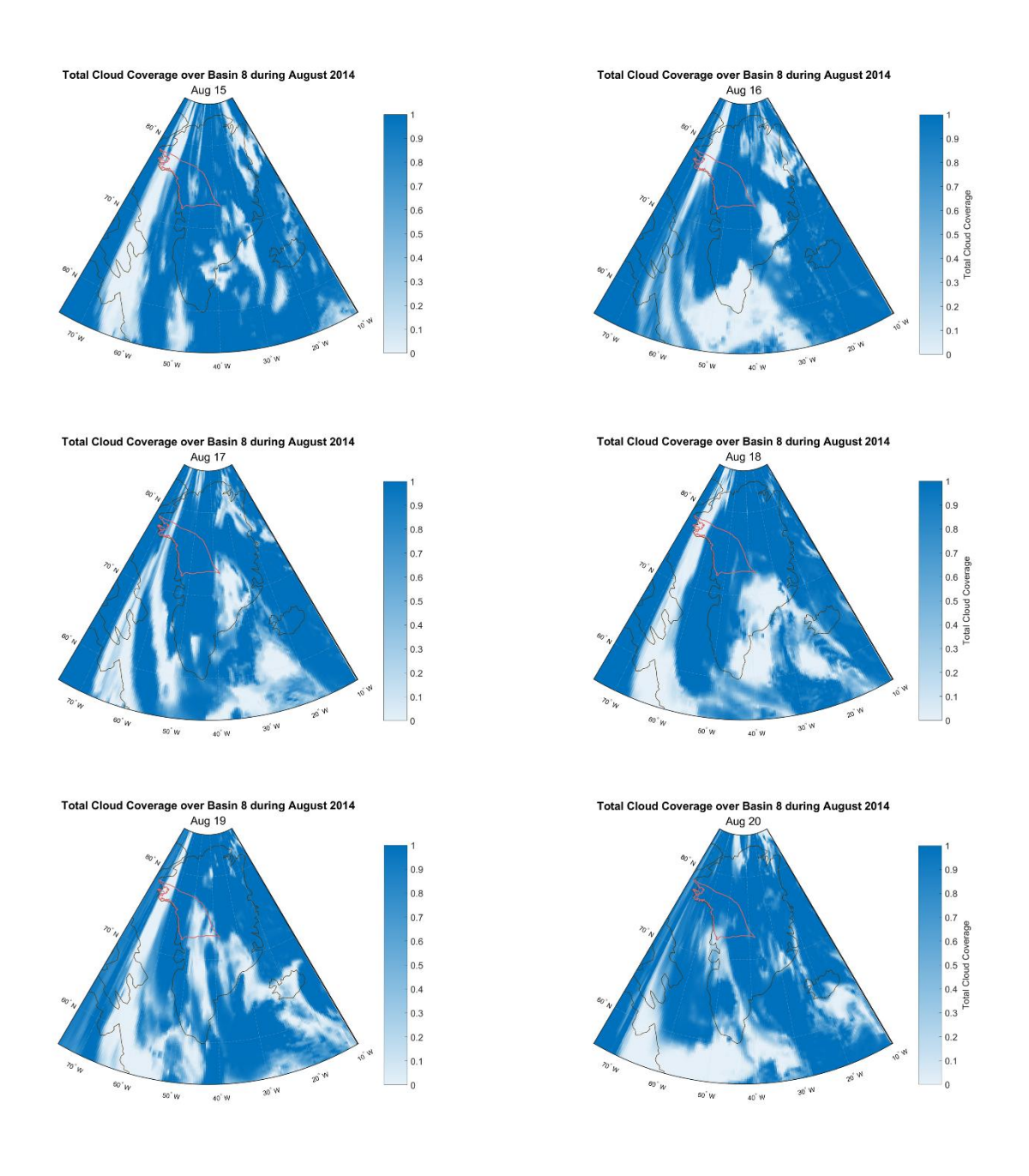


Figure 3.20: Total cloud coverage percentage for the extreme blocking event during 15–20 August 2014.

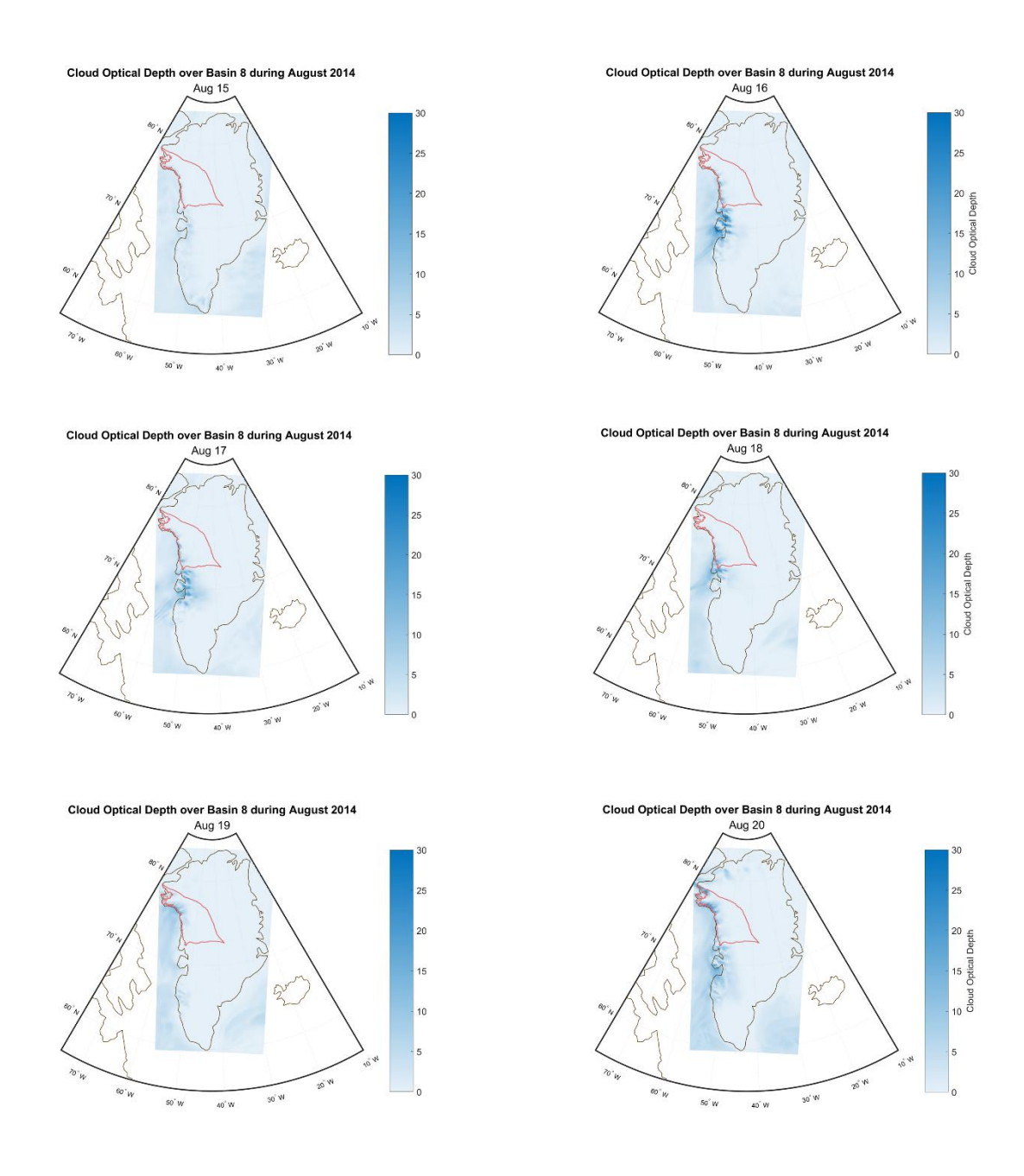


Figure 3.21: Cloud optical depth for the extreme blocking event during 15–20 August 2014.

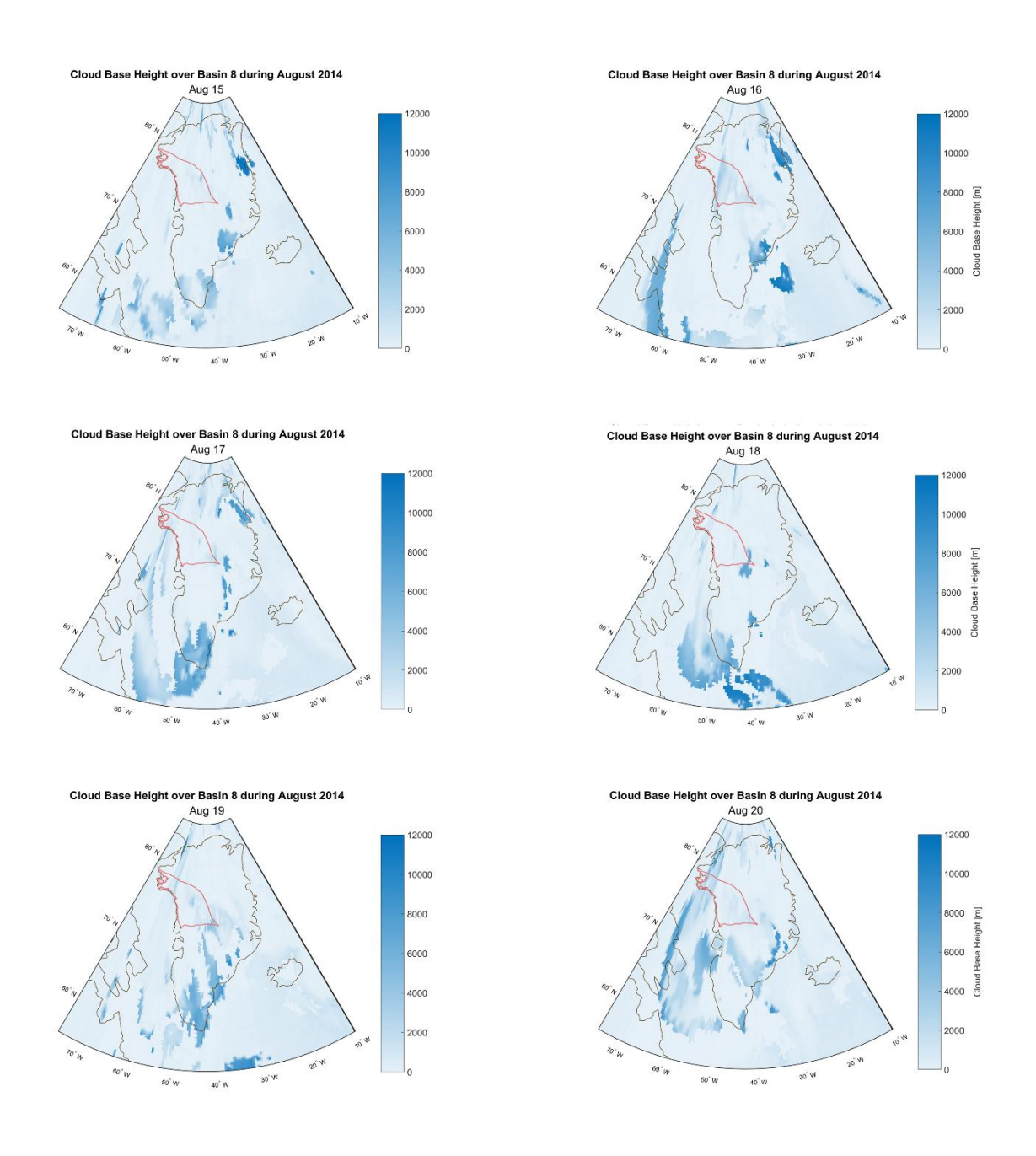


Figure 3.22: Cloud base height (m) for the extreme blocking event during 15–20 August 2014.

**Table 3.10:** Surface mass balance (SMB; mm w.e. day<sup>-1</sup>), average integrated water vapor transport (Avg IVT; kg m<sup>-1</sup>s<sup>-1</sup>), surface atmospheric temperature (Atm Temp; °C), surface skin temperature (Surface Temp; °C), latent heat flux (LHF; W m-2) and sensible heat flux (SHF; W m<sup>-2</sup>) averaged for spatially and temporally over Basin 8 for a blocking event during 15–20 August 2014.

Date	<b>SMB</b>	Avg IVT	Atm Temp	<b>Surface Temp</b>	LHF	SHF
8/15/2014	1.757	43.436	-8.244	-8.576	-2.861	2.115
8/16/2014	5.475	88.075	-7.290	-8.123	-2.761	11.595
8/17/2014	7.635	113.687	-5.160	-5.172	-3.411	-0.348
8/18/2014	12.660	67.108	-4.681	-4.962	-2.790	1.477
8/19/2014	2.769	38.418	-3.603	-4.480	-3.360	15.011
8/20/2014	2.142	42.943	-5.296	-6.404	-1.237	18.005

**Table 3.11:** Cloud optical depth (COD), upper-middle- and lower-cloud coverage (CU; CM; CD) percentages averaged for spatially and temporally over Basin 8 for a blocking event during 15–20 August 2014.

Date	COD	CU	CM	CD
8/15/2014	0.161	0.797	0.856	0.844
8/16/2014	0.600	0.629	0.810	0.825
8/17/2014	0.589	0.648	0.862	0.975
8/18/2014	0.581	0.775	0.748	0.905
8/19/2014	0.859	0.890	0.776	0.676
8/20/2014	1.800	0.675	0.493	0.588

**Table 3.12:** Downwelling shortwave radiation (SWD), downwelling longwave radiation (LWD), upwelling shortwave radiation (SWU), upwelling longwave radiation (LWU, all W m<sup>-2</sup>) and albedo (ALB) averaged for spatially and temporally over Basin 8 for a blocking event during 15–20 August 2014.

Date	SWD	LWD	SWU	LWU	ALB
8/15/2014	183.006	244.754	147.699	278.427	0.808
8/16/2014	120.929	257.556	97.223	280.862	0.800
8/17/2014	142.472	274.497	114.667	292.660	0.806
8/18/2014	137.658	273.793	111.413	293.717	0.813
8/19/2014	140.975	270.154	112.084	295.999	0.797
8/20/2014	140.015	255.564	113.432	288.041	0.794

**Table 3.13:** Snowfall (SF), rainfall (RF), runoff (RU), sublimation (SU), melt (ME) and firn refreezing (RZ; all mm w.e. day<sup>-1</sup>) averaged for spatially and temporally over Basin 8 for a blocking event during 15–20 August 2014.

Date	SF	RF	RU	SU	ME	RZ
8/15/2014	2.656	0.236	1.073	0.067	0.845	0.272
8/16/2014	6.646	1.013	2.115	0.060	1.973	0.275
8/17/2014	8.592	0.870	1.740	0.089	1.094	0.358
8/18/2014	13.538	2.218	3.000	0.068	1.251	0.408
8/19/2014	5.025	1.378	3.556	0.072	3.805	0.444
8/20/2014	4.556	3.071	5.476	0.011	3.631	0.724

There was a consistent influx of enhanced water vapor traveling through the middle of the basin, especially after 15 August (Figure 3.19). Surface and atmospheric temperatures were well below zero and of similar values (Table 3.10). The consistently freezing atmosphere allowed precipitation to again be dominated by snowfall totals, though there was also steadily increasing rainfall. Meltwater production was greater during this event and subsequently so was runoff and meltwater refreezing, though the former was at least four times greater than the latter (Table 3.13). Unsurprisingly, albedo was high during this period, between 79 – 81% (Table 3.12).

Cloud coverage was once again widespread throughout the upper, middle, and lower troposphere, similar to as it was in June 1997 (Figure 3.20), and cloud base heights were mostly low (Figure 3.22). However, optical depth was greater, especially over the coastal ablation zone where it steadily increased in scope with each passing day (Table 3.11, Figure 3.21). Interestingly, the greatest areas of surface mass gain on 19–20 August coincide very well with areas of highest cloud optical thickness, which was not the case for the first several days. Shortwave radiation was much lower than it had been in June 1997, and longwave radiation was slightly higher (Table 3.12).

July 1994 was an extreme blocking event that began on 5 July with approximately 0.5 mm w.e. day<sup>-1</sup> of surface mass gain before quickly resulting in daily consecutive surface mass loss (Figure 3.23, Table 3.14). Unlike previous case studies, there was not a clear stream of enhanced moisture that passed through basin boundaries, though there were a few spots that had slightly higher IVT values (Figure 3.24). Latent heat flux was consistently negative but slightly decreasing. Sensible heat flux was positive and continued to increase day-over-day (Table 3.14). Again, surface and atmospheric temperatures were well below freezing, though surface temperatures tended to be up to 1.5 °C lower than the atmosphere (Table 3.14).

Precipitation was lower during this event compared to previously discussed events but had much higher meltwater production (Table 3.17). Though freezing surface temperatures did help some meltwater refreeze, the losses from runoff were still 1.5 - 2.5 times as high as refreezing gains. Albedo was also slightly lower during this time, gradually decreasing with each subsequent day as more meltwater was introduced into the snowpack (Table 3.16).

Cloud coverage also varied from previous case studies in that there was a lack of consistency in cloud coverage through the layers (Table 3.15). The upper troposphere tended to have the greatest cloud coverage, peaking on 7 July at over 80% before dropping the following days but still being much higher than the lower cloud layers. The middle and lower layers had cloud coverage peak on 6 July with around 50% coverage before dropping and staying very low for the rest of the period (Figure 3.25, 3.27, Table 3.15). Across all days, cloud optical depth was very low (Figure 3.26), and cloud base heights were mostly low with the exception of line of clouds in the eastern portion of the basin where heights tended to be higher (Figure 3.27).

The first few days of more widespread, multi-layer cloud coverage were also reflected by lower shortwave radiation and slightly higher longwave radiation. Beginning on 8 July however, as cloud coverage became scarcer there was a noticeable increase in shortwave radiation and decrease in longwave radiation.

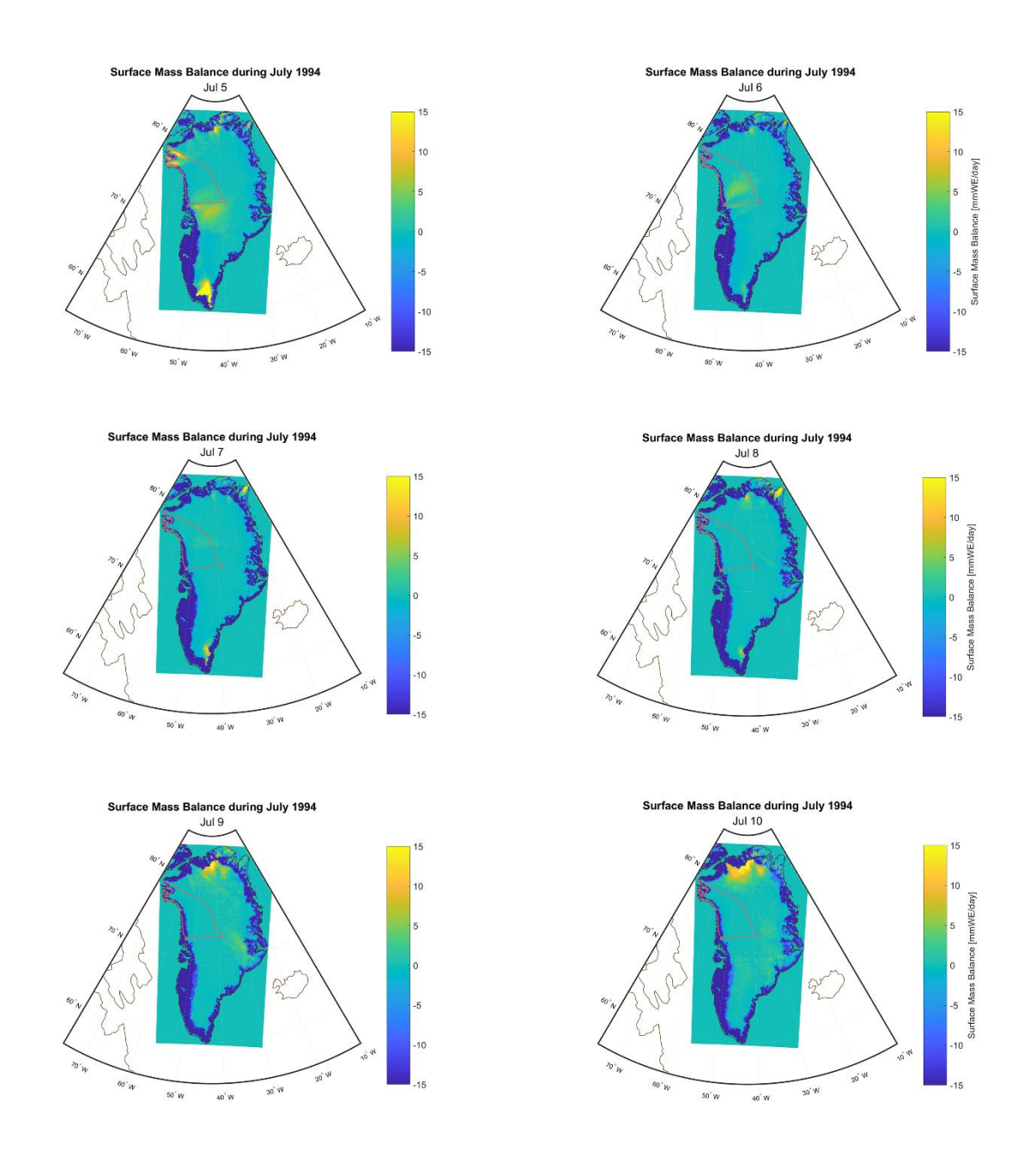


**Figure 3.23:** Average surface mass balance (mm w.e. day<sup>-1</sup>) for the extreme blocking event during 5–10 July 1994.

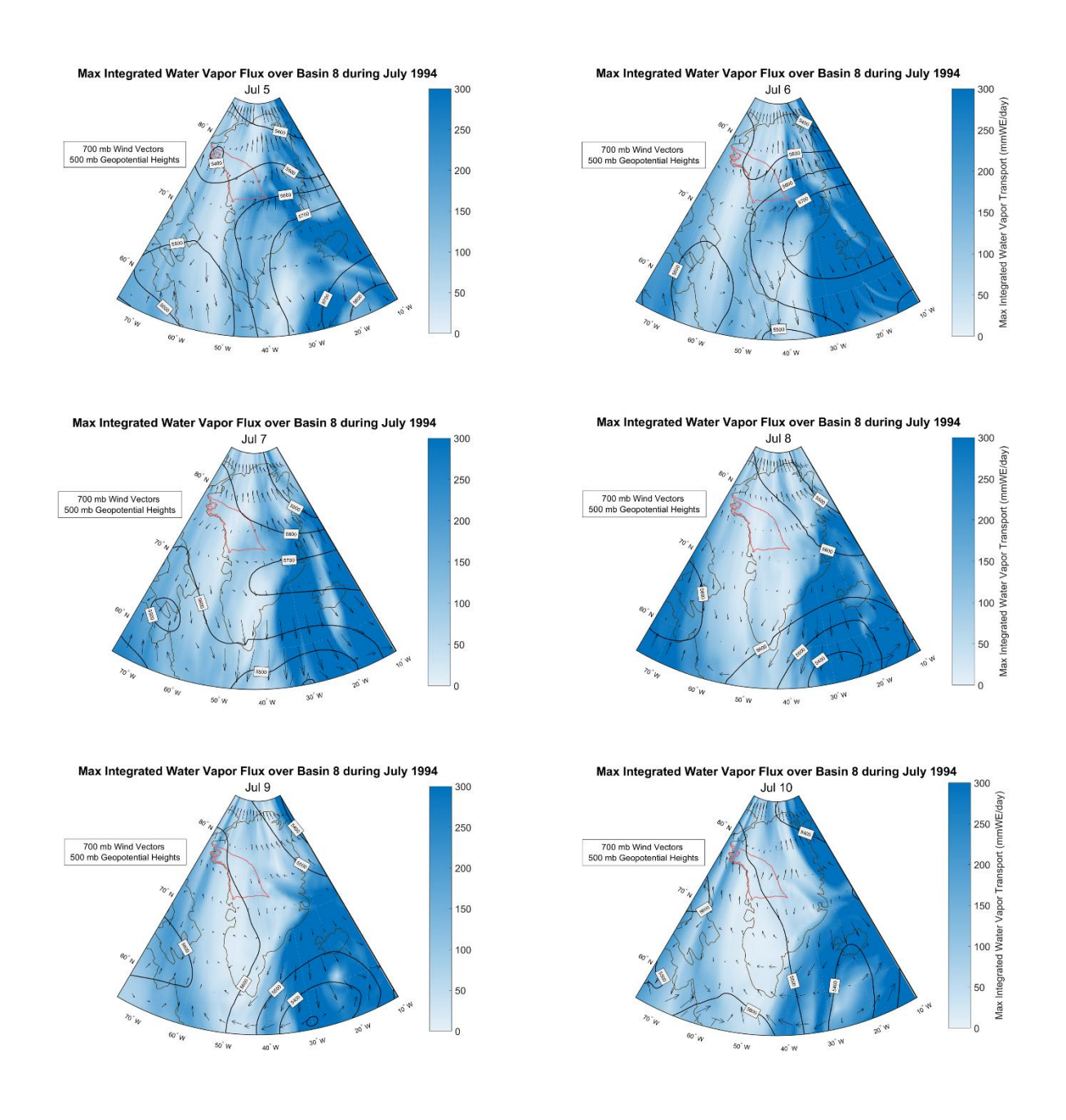


**Figure 3.24:** Average integrated water vapor transport (kg m<sup>-1</sup>s<sup>-1</sup>), 700 hPa wind vectors (m s<sup>-1</sup>), and 500 hPa geopotential heights for the extreme blocking event during 5–10 July1994.

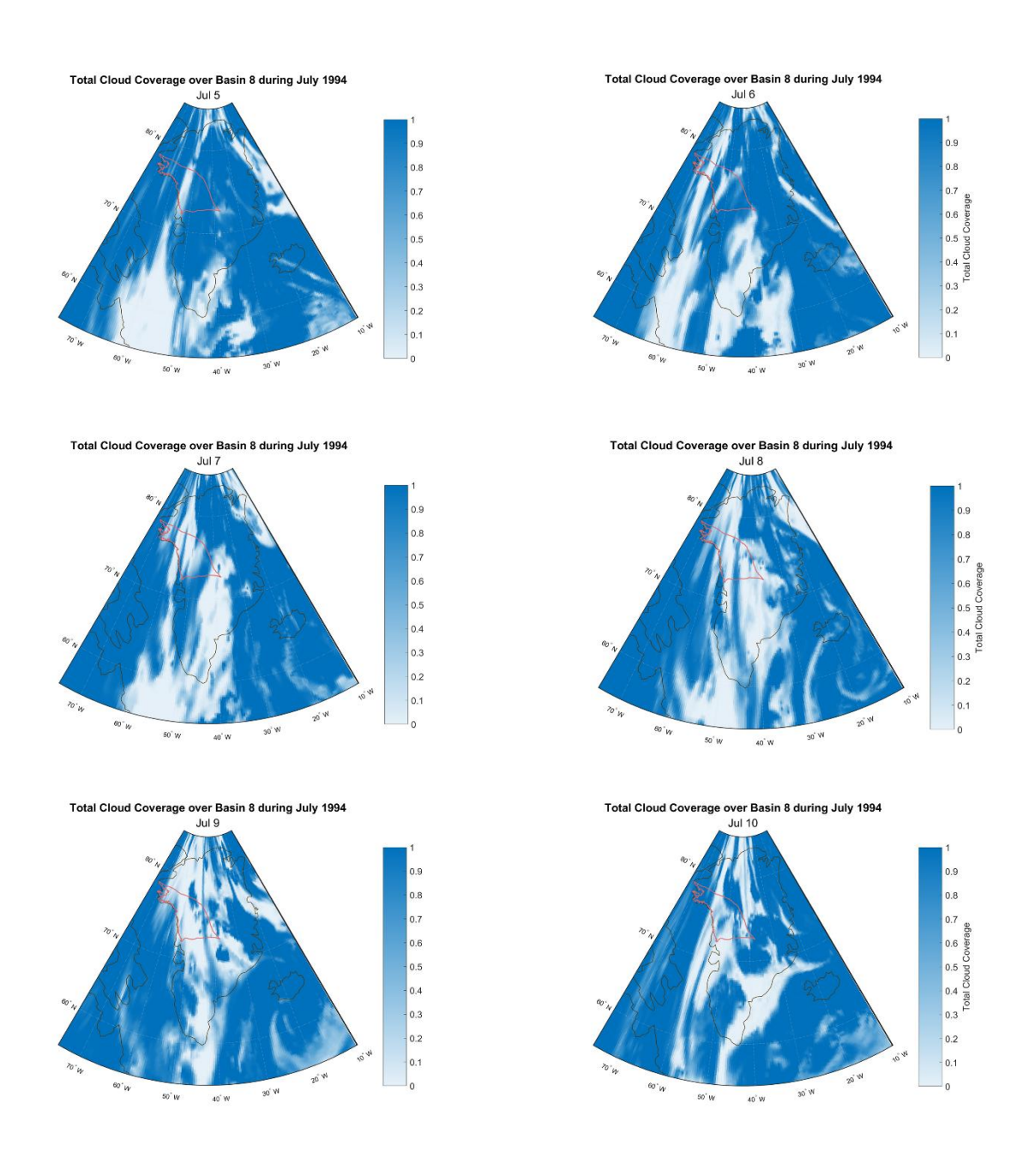


Figure 3.25: Total cloud coverage percentage for the extreme blocking event during 5–10 July1994.

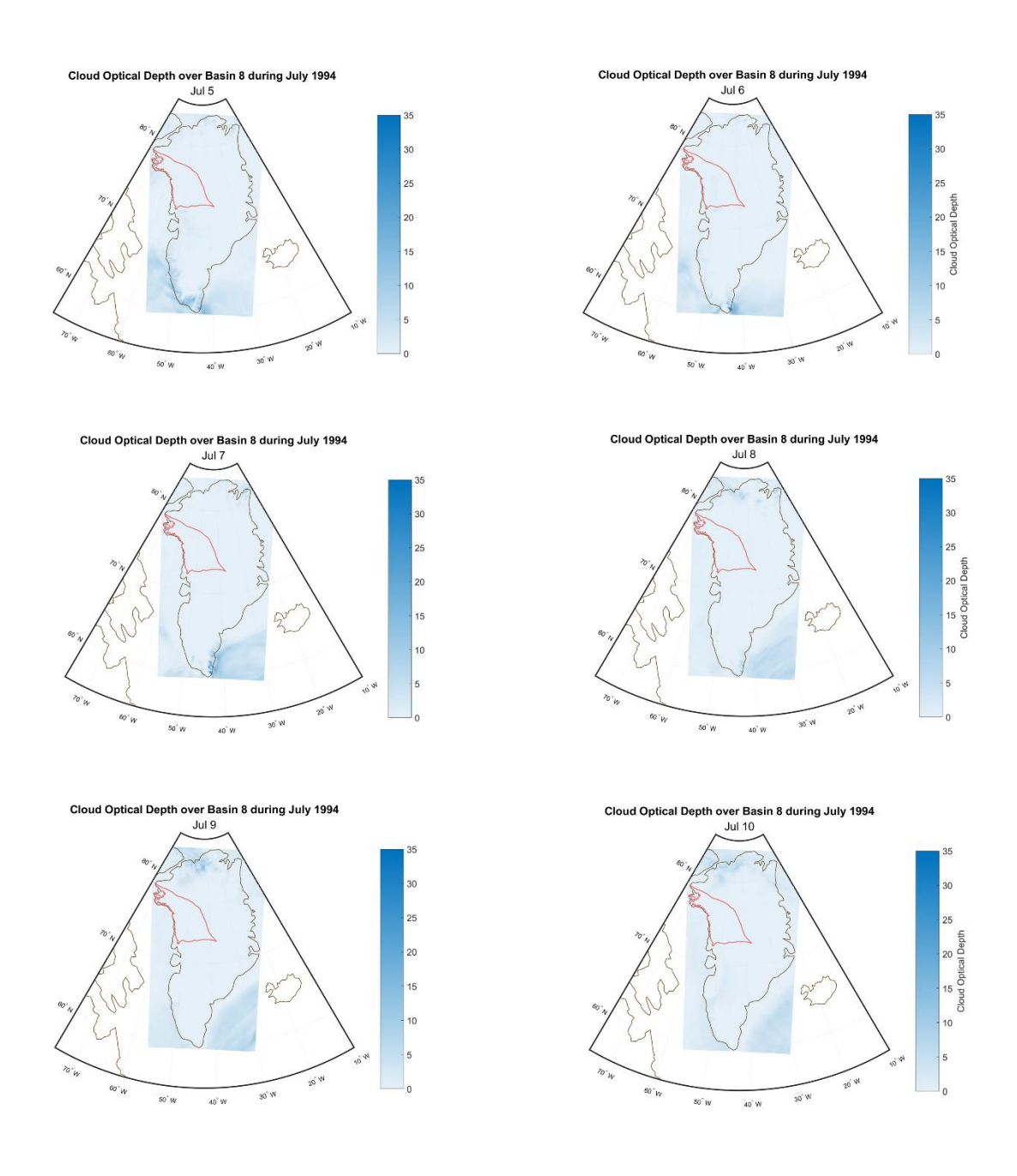


Figure 3.26: Cloud optical depth for the extreme blocking event during 5–10 July 1994.

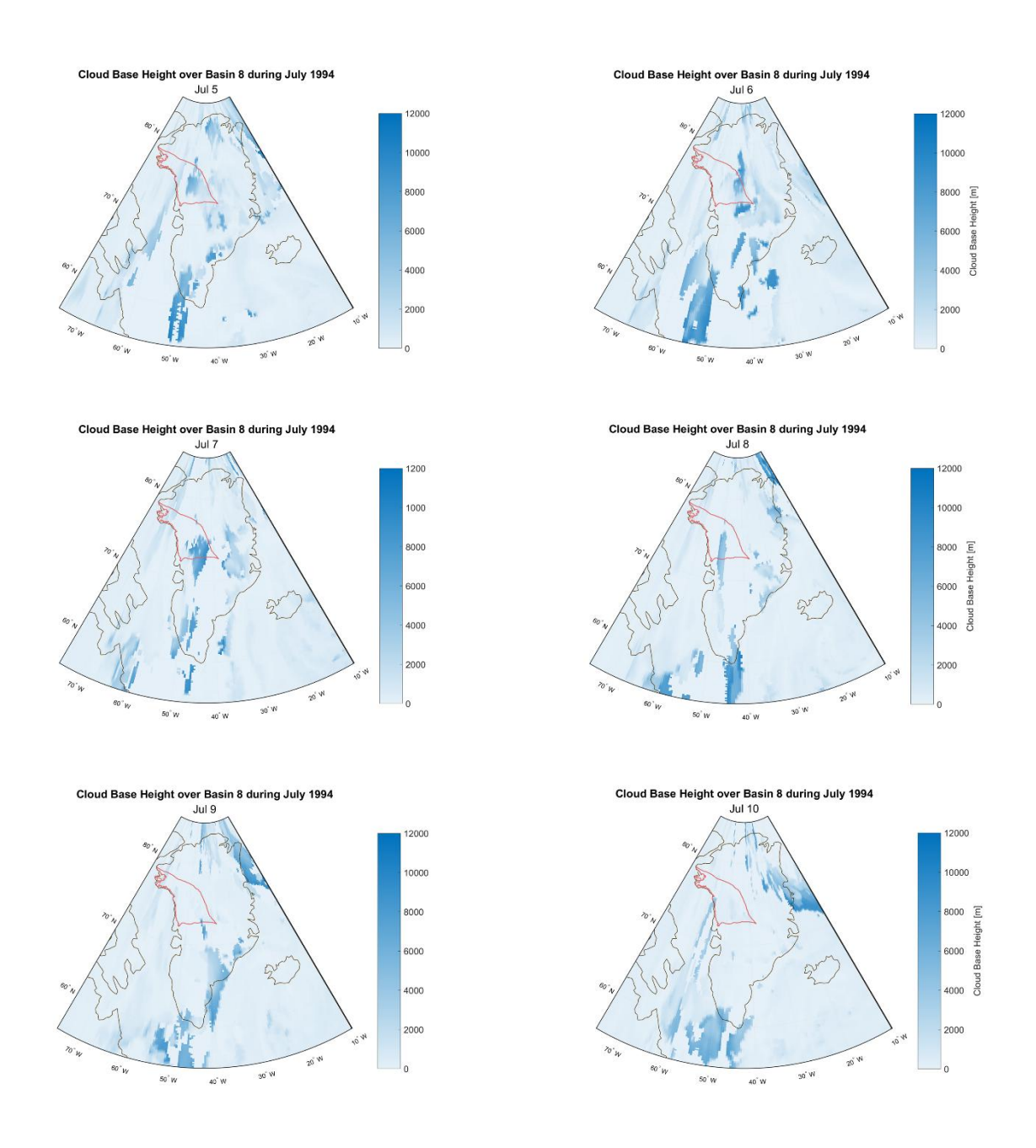


Figure 3.27: Cloud base height (m) for the extreme blocking event during 5–10 July1994.

**Table 3.14:** Surface mass balance (SMB; mm w.e. day<sup>-1</sup>), average integrated water vapor transport (Avg IVT; kg m<sup>-1</sup>s<sup>-1</sup>), surface atmospheric temperature (Atm Temp; °C), surface skin temperature (Surface Temp; °C), latent heat flux (LHF; W m<sup>-2</sup>) and sensible heat flux (SHF; W m<sup>-2</sup>) averaged for spatially and temporally over Basin 8 for a blocking event during 5–10 July 1994.

Date	SMB	Avg IVT	Atm Temp	Surface Temp	LHF	SHF
7/5/1994	0.543	64.374	-8.385	-9.164	-7.245	4.205
7/6/1994	-0.497	72.818	-4.046	-4.889	-6.049	5.795
7/7/1994	-2.951	43.022	-3.264	-4.594	-6.733	12.713
7/8/1994	-2.883	21.978	-4.168	-5.668	-4.453	10.492
7/9/1994	-3.133	25.506	-5.409	-7.000	-5.902	14.846
7/10/1994	-3.254	23.072	-5.369	-6.952	-5.258	15.209

**Table 3.15:** Cloud optical depth (COD), upper-middle- and lower-cloud coverage (CU; CM; CD) percentages averaged for spatially and temporally over Basin 8 for a blocking event during 5–10 July 1994.

Date	COD	CU	CM	CD
7/5/1994	0.039	0.478	0.499	0.498
7/6/1994	0.096	0.642	0.533	0.493
7/7/1994	0.023	0.823	0.344	0.185
7/8/1994	0.015	0.311	0.127	0.063
7/9/1994	0.006	0.131	0.032	0.116
7/10/1994	0.004	0.360	0.050	0.048

**Table 3.16:** Downwelling shortwave radiation (SWD), downwelling longwave radiation (LWD), upwelling shortwave radiation (SWU), upwelling longwave radiation (LWU, all W m<sup>-2</sup>) and albedo (ALB) averaged for spatially and temporally over Basin 8 for a blocking event during 5–10 July 1994.

Date	SWD	LWD	SWU	LWU	ALB
7/5/1994	328.200	222.887	262.473	276.433	0.803
7/6/1994	320.793	245.129	254.263	294.318	0.795
7/7/1994	332.029	241.064	258.975	295.782	0.783
7/8/1994	369.971	219.205	285.945	290.963	0.775
7/9/1994	377.598	209.122	292.090	285.472	0.775
7/10/1994	371.514	208.021	287.796	285.519	0.776

**Table 3.17:** Snowfall (SF), rainfall (RF), runoff (RU), sublimation (SU), melt (ME) and firn refreezing (RZ; all mm w.e. day<sup>-1</sup>) averaged for spatially and temporally over Basin 8 for a blocking event during 5–10 July 1994.

Date	SF	RF	RU	SU	ME	RZ
7/5/1994	1.547	0.003	0.796	0.221	1.327	0.322
7/6/1994	1.197	0.025	1.531	0.183	3.289	0.694
7/7/1994	0.191	0.000	2.934	0.205	5.837	1.362
7/8/1994	0.010	0.000	2.762	0.135	5.295	1.936
7/9/1994	0.016	0.000	2.971	0.179	5.379	1.959
7/10/1994	0.003	0.000	3.100	0.159	4.884	1.660

# 3.2.4 July/August 2019

Another extreme blocking event occurred at the end of July through the middle of August over approximately 20 days. For the purposes of this case study, we examined six core days that had the greatest surface mass loss, peaking on 31 July with nearly 10 mm w.e. day<sup>-1</sup> (Figure 3.28, Table 3.18). This portion of the event did have consistent, widespread enhanced water vapor, especially in the first half of the event, which differs greatly from previous case studies (Figure 3.29).

Sensible heat flux was high especially in the first three days before dropping by 1 August and continuing to drop throughout the last three days. It did remain high compared to the sensible heat flux values from previous case studies. Latent heat flux did not follow as straightforward of a trend, instead fluctuating between negative and positive values for the first few days before dropping to just under -5 W m<sup>-2</sup> on 2 August (Table 3.18).

Rainfall and snowfall totals were small, especially when compared to the meltwater production and runoff that occurred during the same time period (Table 3.21). Meltwater

production, particularly on 30 July – 1 August was very high, averaging between 14 – 15.5 mm w.e. day<sup>-1</sup> (Table 3.21). Most of this meltwater production transferred into high runoff values that were consistently over twice as large in magnitude as gains made from refreezing. Albedo was at its lowest during this event, remaining between low to mid 70% (Table 3.20). This possibly was due to the lack of fresh snowfall from this event compared to the previous case studies (Table 3.21). Surface temperatures were lower than atmospheric temperatures, which for a three-day period climbed to above freezing. Overall, temperatures remained near or just below freezing, which was quite abnormal compared to previous case studies (Table 3.18).

Cloud optical depth was once again thin across all six days (Figure 3.31), and cloud coverage itself varied throughout the layers of the troposphere (Figure 3.30, Table 3.19). Cloud coverage at the top layer was fairly consistent around 50% while the middle and bottom layers had much lower cloud coverage except on 1 August. Given the optical thickness of the clouds, especially the first few days, it was not surprising that short wave radiation values were also high initially (Table 3.20). However, on 1 August when cloud optical depth increased and all layers of the troposphere had 40 – 50% cloud coverage, shortwave radiation dropped for that single day. Following 1 August, cloud optical depth and cloud coverage decreased again, and shortwave radiation rose as a result. The reverse pattern was also found for longwave radiation, which tended to increase with increasing cloud optical depth and coverage (Table 3.19, 3.20). Finally, the base heights of clouds were higher overall than during previous case studies, with several days having large areas of medium to high cloud bases over large portions of the basin (Figure 3.32).

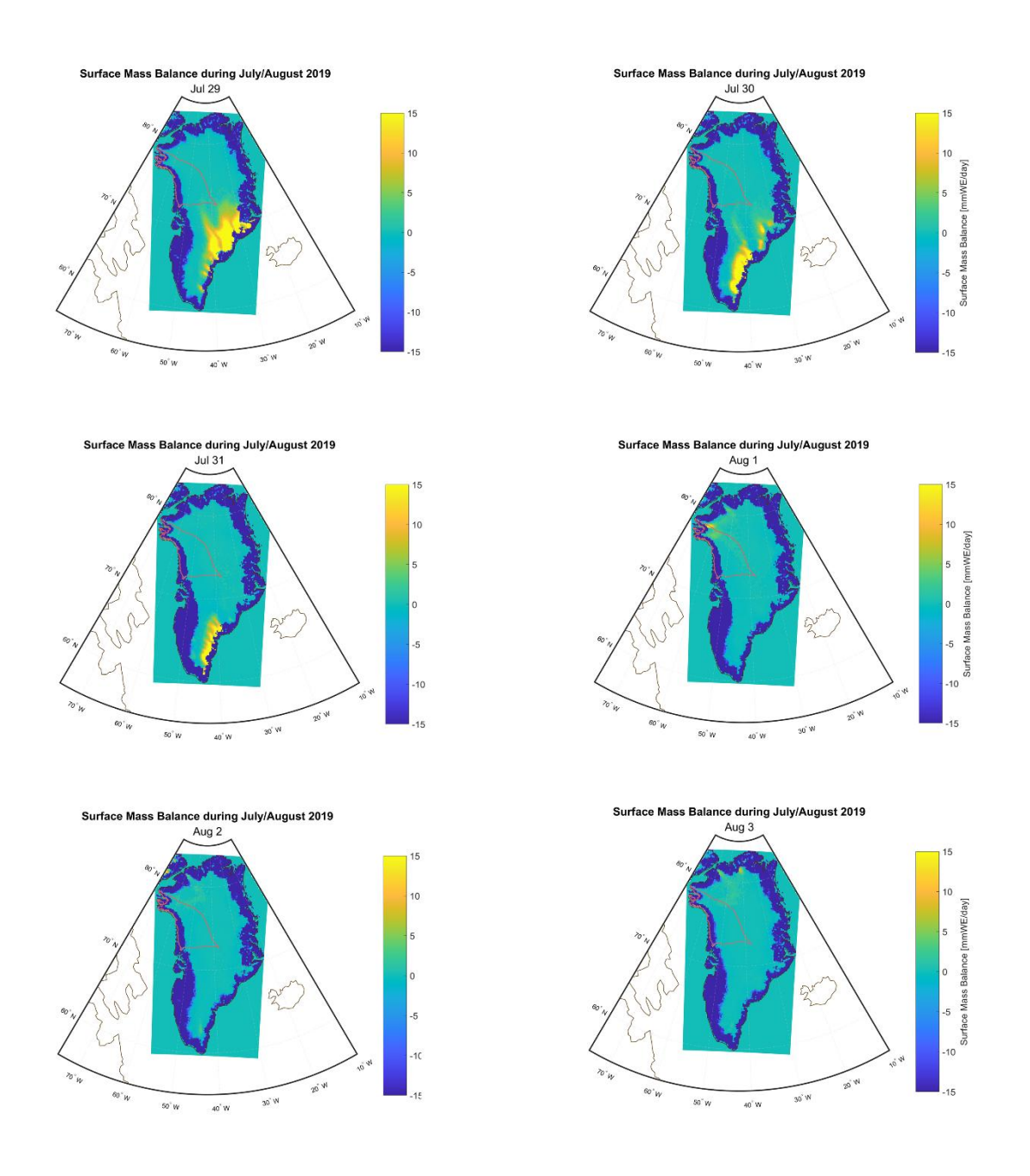


**Figure 3.28:** Average surface mass balance (mm w.e. day<sup>-1</sup>) for the extreme blocking event during 29 July – 3 August 2019.

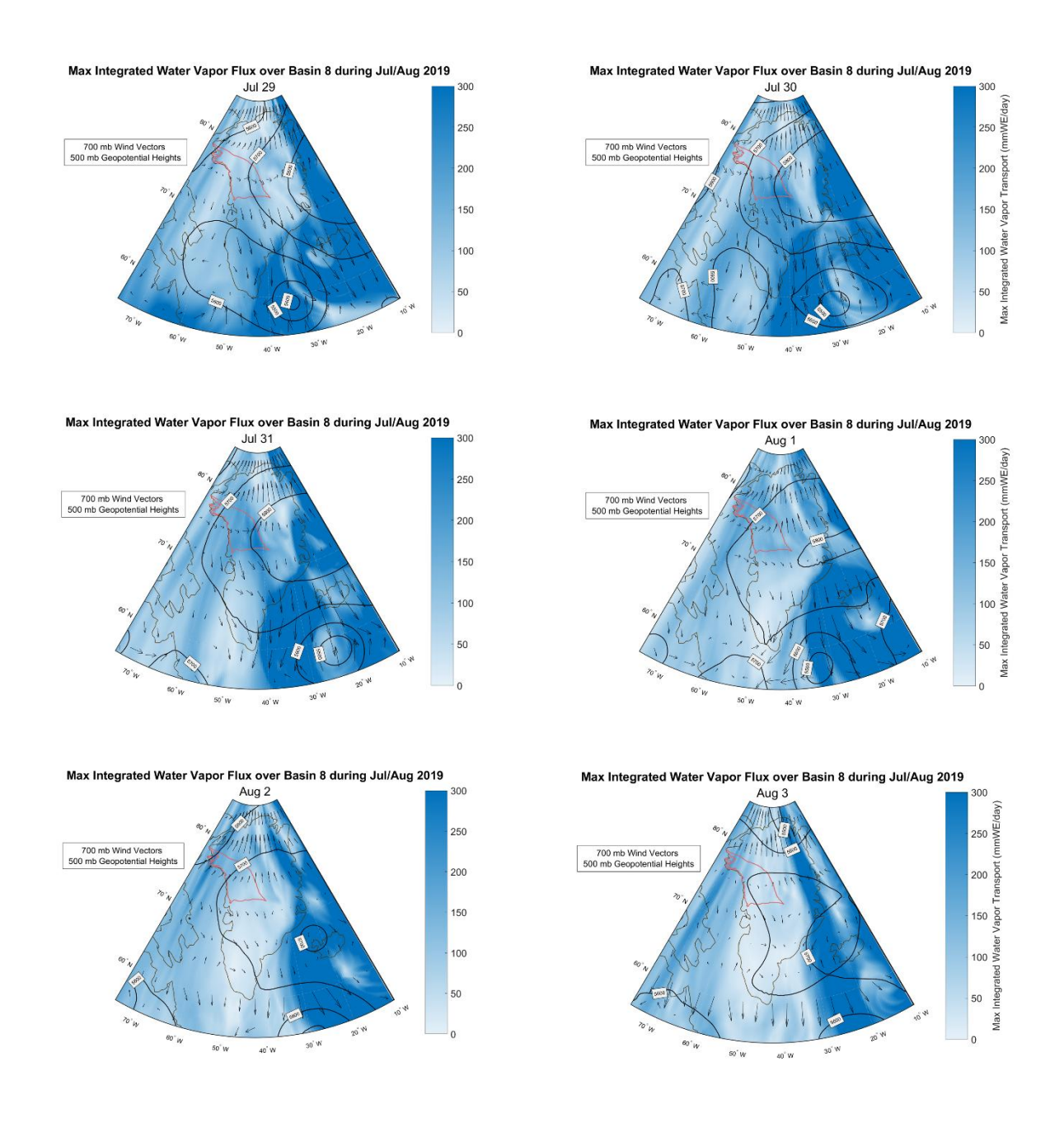


**Figure 3.29.** Average integrated water vapor transport (kg m<sup>-1</sup>s<sup>-1</sup>), 700 hPa wind vectors (m s<sup>-1</sup>), and 500 hPa geopotential heights for the extreme blocking event during 29 July – 3 August 2019.

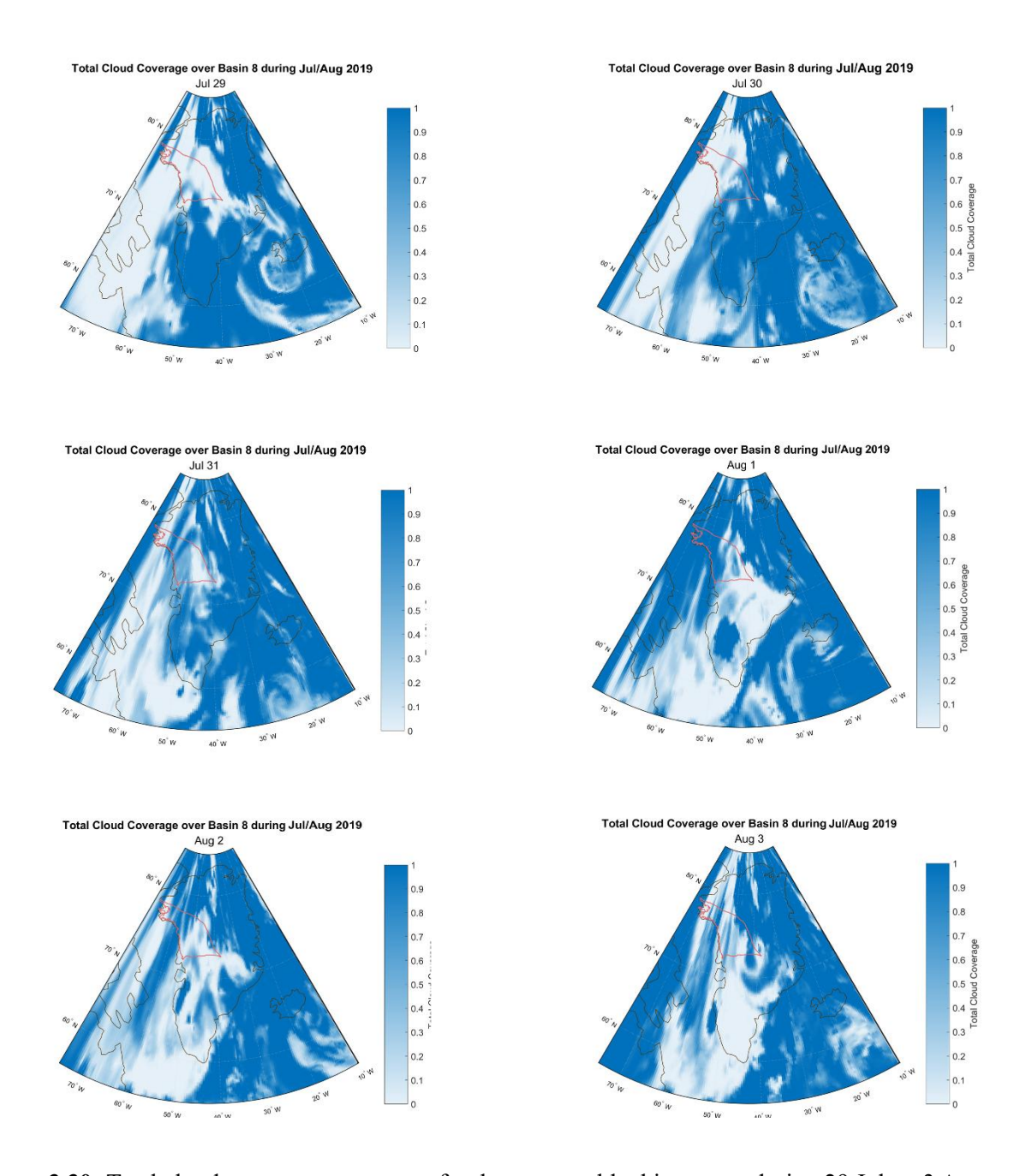


**Figure 3.30:** Total cloud coverage percentage for the extreme blocking event during 29 July – 3 August 2019.

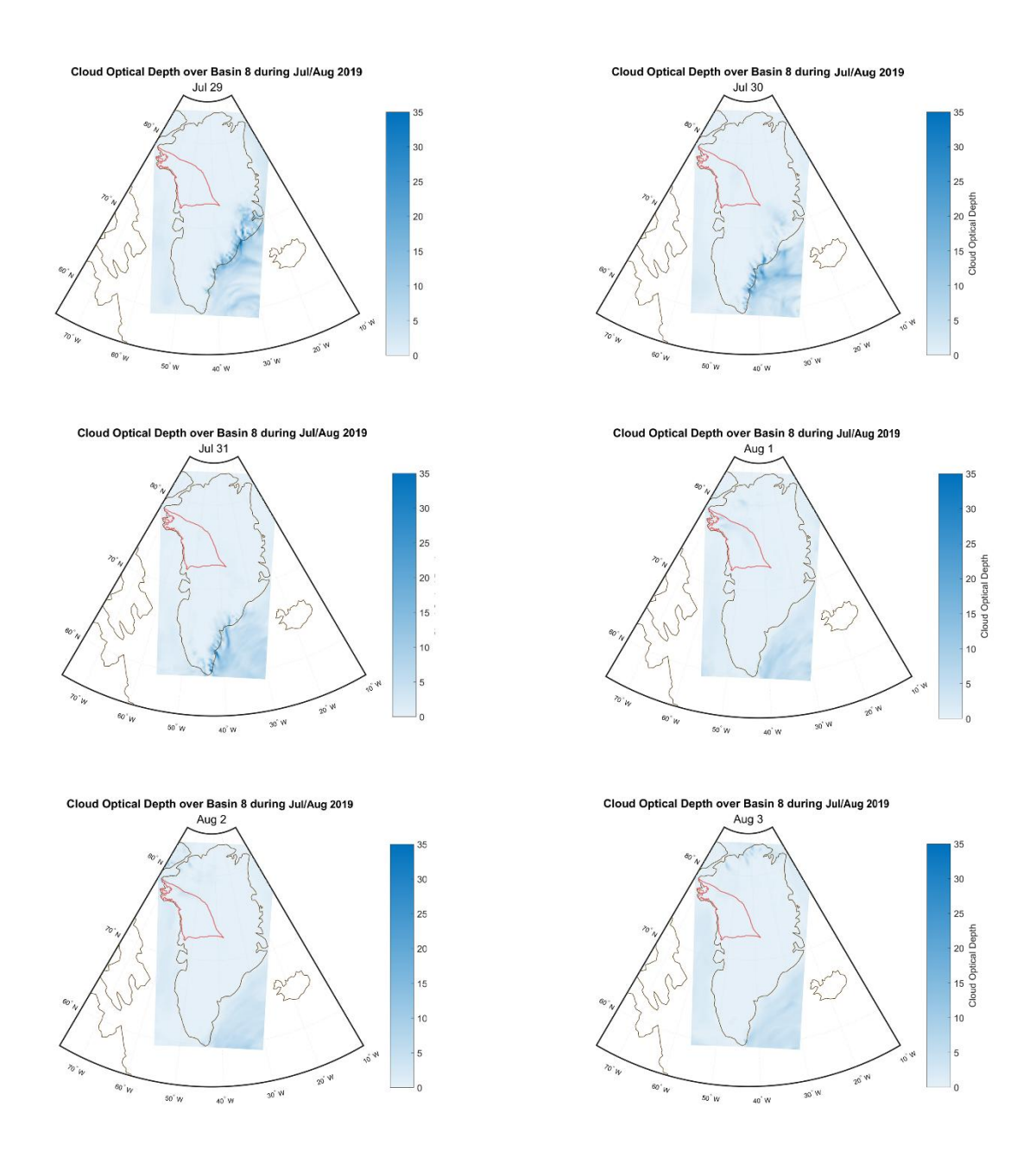


Figure 3.31: Cloud optical depth for the extreme blocking event during 29 July – 3 August 2019.

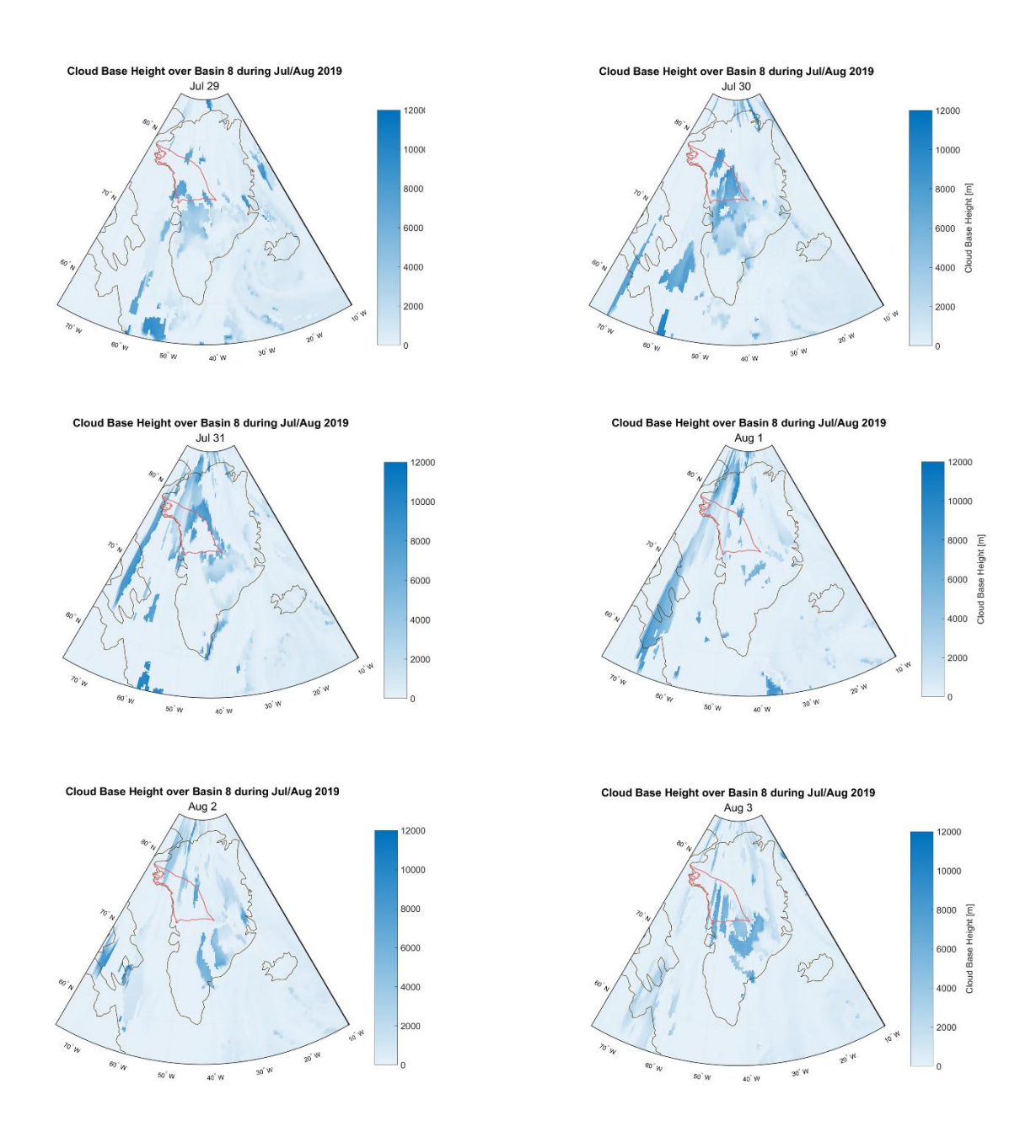


Figure 3.32: Cloud base height (m) for the extreme blocking event during 29 July – 3 August 2019.

**Table 3.18:** Surface mass balance (SMB; mm w.e. day<sup>-1</sup>), average integrated water vapor transport (Avg IVT; kg m<sup>-1</sup>s<sup>-1</sup>), surface atmospheric temperature (Atm Temp; °C), surface skin temperature (Surface Temp; °C), latent heat flux (LHF; W m<sup>-2</sup>) and sensible heat flux (SHF; W m<sup>-2</sup>) averaged for spatially and temporally over Basin 8 for a blocking event during 29 July – 3 August 2019.

Date	SMB	Avg IVT	Atm Temp	Surface Temp	LHF	SHF
7/29/2019	-5.56277	43.502	-1.899	-3.994	-2.065	34.075
7/30/2019	-8.397814	46.986	1.362	-1.045	1.393	44.179
7/31/2019	-9.71502	35.843	0.736	-1.562	-0.570	41.687
8/1/2019	-8.272496	31.912	0.040	-1.512	0.561	25.072
8/2/2019	-6.752306	68.123	-1.807	-3.438	-4.804	20.979
8/3/2019	-4.675633	64.939	-3.516	-5.092	-2.929	15.536

**Table 3.19:** Cloud optical depth (COD), upper-middle- and lower-cloud coverage (CU; CM; CD) percentages averaged for spatially and temporally over Basin 8 for a blocking event during 29 July – 3

August 2019.

Date	COD	$\mathbf{C}\mathbf{U}$	$\mathbf{CM}$	CD
7/29/2019	0.003	0.491	0.142	0.055
7/30/2019	0.169	0.548	0.148	0.120
7/31/2019	0.057	0.466	0.172	0.059
8/1/2019	0.571	0.474	0.454	0.406
8/2/2019	0.231	0.525	0.196	0.139
8/3/2019	0.071	0.496	0.036	0.089

**Table 3.20:** Downwelling shortwave radiation (SWD), downwelling longwave radiation (LWD), upwelling shortwave radiation (SWU), upwelling longwave radiation (LWU, all W m<sup>-2</sup>) and albedo (ALB) averaged for spatially and temporally over Basin 8 for a blocking event during 29 July – 3 August 2019.

Date	SWD	LWD	SWU	LWU	Albedo
7/29/2019	294.390	229.345	225.241	298.128	0.768
7/30/2019	281.381	247.409	203.180	311.750	0.725
7/31/2019	276.801	244.983	201.606	309.383	0.727
8/1/2019	236.478	266.662	170.393	309.795	0.720
8/2/2019	266.877	240.215	196.033	300.850	0.733
8/3/2019	284.518	223.533	210.355	293.562	0.740

**Table 3.21:** Snowfall (SF), rainfall (RF), runoff (RU), sublimation (SU), melt (ME) and firn refreezing (RZ; all mm w.e. day<sup>-1</sup>) averaged for spatially and temporally over Basin 8 for a blocking event during 29 July – 3 August 2019.

Date	SF	$\mathbf{RF}$	RU	SU	ME	RZ
7/29/2019	0.060	0.000	5.564	0.061	7.729	0.852
7/30/2019	0.038	0.008	8.487	-0.049	15.476	3.074
7/31/2019	0.009	0.001	9.720	0.009	15.322	4.422
8/1/2019	0.452	0.172	8.901	-0.029	14.077	4.082
8/2/2019	0.055	0.025	6.684	0.141	9.064	3.299
8/3/2019	0.056	0.004	4.644	0.087	6.409	2.717

#### **CHAPTER 4**

#### **DISCUSSION**

Atmospheric blocking events – defined as a quasi-stationary area of anticyclonic circulation which inhibits longwave atmospheric patterns and smaller weather systems – have noticeable effects on SMB of the Greenland ice sheet. Greenland atmospheric blocking can be measured using the Greenland Blocking Index (Hanna et al., 2016). To select days of anomalous blocking conditions, GBI was calculated for each day during meteorological summer (JJA) during 1990–2023. The top 10% of GBI days were selected to represent anomalous blocking conditions, further known as "extreme blocking" conditions.

Past research has concluded that extreme atmospheric blocking affects SMB of the Greenland ice sheet (Barrett et al., 2020; Henderson et al., 2021; McLeod & Mote, 2015, 2016; Preece et al., 2022), but effects are not spatially homogeneous (Preece et al., 2022). In particular, northwestern Greenland is one of the largest contributors to total GrIS mass loss, as well as the second largest acceleration in mass loss in the last few decades (Mouginot et al., 2019; Velicogna et al., 2014). This study aimed to further examine how northwestern GrIS reacts to extreme blocking conditions, as well as give greater insight as to how the relationship between atmospheric blocking and SMB has changed over a 33-year period.

Results showed that over a 33-year period from 1990-2023, most major ice drainage basins had a weak negative trend in SMB during summer extreme blocking episodes, meaning that there tended to be greater surface mass loss on average in the most recent decade of the

record. For the ice sheet as a whole, one concern is that the Arctic is expected to more regularly see these intense blocking episodes, and if this trend continues – or potentially accelerates –the risk of greater surface mass losses would also increase, contributing to global sea level rise.

While most extreme blocking events were associated with negative SMB, this was not exclusively the case. In the past, most basins had at least a single extreme blocking event that resulted in surface mass gain, meaning that there was greater accumulation of mass than ablation. Since 2015 however, positive SMB during extreme blocking has become a rarity.

Of particular interest to this study, northwestern Greenland had consistently exhibited negative SMB during the last several summers. This could suggest a stronger relationship between extreme blocking and negative SMB in northwestern Greenland (Basin 8), although it does not necessarily support the hypothesis that the magnitude of negative SMB had accelerated disproportionately to other basins

### 4.1 Surface Energy Balance

As SMB of northwestern Greenland has varied over the past several decades in response to extreme blocking events, it is important to understand the responses of the energy budget components to blocking, including sensible and latent heat fluxes, radiation budget components, and precipitation amount and types. Using output from a regional climate model for Greenland that includes a sophisticated treatment of SMB (MAR), I extracted surface energy budget variables for northwestern Greenland (Basin 8) on extreme blocking days during JJA from 1990 – 2023. This was done to understand differences in the surface energy budget of extreme blocking events during the 33-year period, and, in turn, to better understand possible causes for the acceleration of GrIS surface mass loss in this region.

#### 4.1.1 Latent and Sensible Heat Flux

Latent heat is the energy exchanged between water and the atmosphere as water cycles between its different phases. Notably, as water vapor condenses into liquid such as in the formation of clouds, it releases latent heat into its surrounding environment and warms it. When latent energy moves between the atmosphere and the surface, this is known as latent heat flux (LHF). Sensible heat flux (SHF) is the exchange of heat between the surface and the atmosphere that is not associated with the phase change of water and can be "sensed" as a change in temperature.

The magnitude of LHF has steadily decreased with each subsequent decade during extreme blocking events, but the direction of latent heat flux continued to be mostly negative, indicating a movement of energy from the surface to the atmosphere through sublimation and evaporation during extreme blocking. While it is not possible to pinpoint the sources of the LHF term from the available MAR data, the increase in LHF during extreme blocking events may be related to greater evaporation of meltwater or sublimation from snow. During years where the magnitude of negative LHF was weaker, sublimation was also much lower. The inverse was also true, where stronger negative LHF would coincide with years of higher sublimation values. SHF, on the other hand, remained positive and increased over the 33-year period. A positive SHF means a transfer of energy from the atmosphere to the surface that warms the surface and enhances the potential for melt and runoff. While this thesis only examined periods associated with extreme blocking, these periods often constituted major melt events that accounted for a significant portion of the annual melt and runoff. Additionally, the mean SHF component was roughly four times as large as the LHF component during extreme blocking events. Therefore,

increased SHF during extreme blocking was expected to be associated with increased extreme ablation and runoff events.

Previous studies have established a positive relationship between turbulent heat fluxes and melt energy (Fausto et al., 2016; Mattingly et al., 2020; Neff et al., 2014). In this thesis, the findings regarding SHF supported prior findings as SMB increased during years with low average sensible heat flux. If SHF continues to increase in the future, the enhanced melt energy will increase runoff and further increase surface mass loss, if not offset by simultaneous increases in snowfall or meltwater refreezing.

# 4.1.2 Surface Accumulation and Ablation

SMB is the net of mass gains through accumulation and deposition and mass losses through runoff and sublimation. Snowfall is the primary accumulation that increases SMB, while some modest increase may be due to deposition; sublimation and runoff decrease SMB and are therefore known as net ablation terms.

To examine the impact of changes in mass inputs during extreme blocking events, accumulation and ablation variables were extracted for JJA extreme blocking days and then spatially averaged over Basin 8. Time was split over 4 decades: 1990s, 2000s, 2010s, and the beginning of the 2020s, graphed using timeseries superimposed with yearly SMB values, and then analyzed. Snowfall during extreme blocking events decreased since the 1990s. The apparent cyclical nature of snowfall contributions led to an examination of possible low-frequency atmospheric circulation features that could be coincident or driving blocking, such as changes in the North Atlantic Oscillation (NAO). The negative phase of the NAO is correlated with blocking episodes over Greenland (Hanna et al., 2015). While there was not a relationship

between NAO and snowfall during extreme blocking that captured all events, some years did share similarities. For example, high snowfall totals tended to occur during weaker negative NAO phases (-1 – 0) as well as positive NAO phases. This is a significant finding as blocking events are strongly related to negative NAO (e.g., Woollings et al. 2018). Negative NAO, with extreme blocking episodes, should produce strong sensible heat advection and limit snowfall production, which is counterintuitive to large surface mass gains. (Some blocking events with the greatest surface mass loss and lowest snowfall totals occurred in months with a strongly negative NAO (< -2)). In sum, extreme blocking with a weakly negative NAO was conducive to snowfall, but when it occurred with strongly negative NAO, the result was a reduction in snowfall and more mass loss.

During events with greater snowfall, the periods of extreme blocking appeared shorter than the low/no snowfall events. Greater snowfall tended to occur during blocking periods of between 5-10 days, while periods of long extreme blocking – often exceeding greater than 2 weeks of concurrent extreme blocking conditions – occurred in years that resulted in average snowfall totals of < 1 mm.

This region showed similar or increasing rainfall later in the record. This supported results that identified increasing positive trends across the entire ice sheet, but particularly in northwestern Greenland (Box et al., 2023; Collins et al., 2013; Huai et al., 2022; Niwano et al., 2021). An increase in liquid precipitation in a warm environment plays a role in ablation due to raising the liquid water content of the snow and lowering the surface albedo, as well as cloud condensation releasing latent heat. Lower surface albedo and latent heat release further result in above-average temperatures from heat release and increased radiation absorption because of lower albedo. Above-average temperatures make it harder for liquid precipitation to refreeze as

well as facilitating the melting of ground snow, both of which lead to increased runoff amounts, as is reflected in the increased runoff.

The significance of the changing trends in precipitation brought on by extreme blocking events lies in its implications for future surface melt. Prior to the mid-2010s, extreme blocking events had the capabilities to bring large amounts of snowfall that would positively impact SMB. Instead of bringing large amounts of snowfall, some of this precipitation is falling as rain instead, and less of this rain is refreezing and contributing mass to the firn.

Sublimation resulting from extreme blocking decreased and played a smaller part in surface ablation as it was an order of magnitude smaller than runoff. Less sublimation implicitly means that less surface energy is being used to transition snow to vapor, which even if not as significant to SMB, still increases the temperature of the firn (Zolles & Born, 2024). The changes in sublimation did not appear to contribute meaningfully to the changes observed in SMB.

Runoff increased during extreme blocking events during the study period. While a portion of this increase is probably attributed to greater rainfall, throughout this thesis we have discussed the possibility of meltwater refreezing as a means of offsetting surface mass losses from runoff. During normal circumstances, meltwater refreezing currently prevents approximately 50% of meltwater being produced from turning into runoff (Amory et al., 2024); however, in the context of a warming snowpack due to extreme blocking, this process is not as straightforward as it seems. Studies have already documented decreasing firn thickness in Greenland (Brils et al., 2022; Kuipers Munneke et al., 2015; Medley et al., 2022). When surface ice initially begins to melt, the small pockets of space between the molecules of snow (firn) will become even smaller as higher liquid water content will lead to a denser snowpack. As meltwater refreezing depends on the retention of water in the firn, the denser the snowpack becomes the

less capable it is retaining and refreezing meltwater and potentially also forming an impermeable layer near the surface of the firn, therefore allowing for greater runoff potential (Amory et al., 2024; Braithwaite et al., 1994; Harper et al., 2012; Pfeffer et al., 1991). In sum, it is possible that a portion of the increase in runoff over the course of our study period is attributed to the densification of firn limiting the capacity of meltwater refreezing and allowing for greater runoff.

## 4.1.3 Radiation Balance

The surface energy budget, which is the balance between incoming and outgoing shortwave and longwave radiation, is affected by abnormally clear or cloudy conditions associated with blocking. Incoming shortwave radiation from the sun passes through the atmosphere on its way to the surface, but a component is backscattered away from the surface by hydrometeors in clouds and the clear atmosphere. Differences in cloud properties, including water droplet size, shape, and overall liquid water content all play a role in the absorption, reflection, and transmission potential of radiation in clouds (W. Wang et al., 2018).

Shortwave radiation is also reflected at the surface as a function of the surface albedo. Although no surface absorbs or reflects 100% of radiation, lighter objects have higher rates of radiation reflection than darker objects. Snow is highly reflective, and fresh snow can reflect more than 80% of incident shortwave radiation. Older snow is darker due to an accumulation of impurities and growth in the size of snow grains and therefor absorbs more heat than freshly fallen snow. Snow that has gone throw melt-freeze metamorphosis also is less reflective, but the addition of fresh snowfall will increase the albedo. Reduced cloudiness during blocking may be associated with anomalously low snowfall amounts, additionally lowering the overall albedo of the ice sheet (Rajewicz & Marshall, 2014; Tedesco & Fettweis, 2020; W. Wang et al., 2021).

Extreme blocking events drive changes in cloud cover distribution, which directly affects the radiation balance through cloud radiative forcing (i.e., clouds reduce downwelling shortwave radiation and increasing downwelling longwave radiation,) and indirectly affects the radiation balance by altering the surface albedo through melt and new snow accumulation. As previously discussed, blocking events have been connected to reductions in cloud cover that can enhance surface melt and heatwaves. The results in Chapter 3 demonstrated several key variables associated with reduced cloud cover, including greater downwelling shortwave radiation.

The time series of extreme blocking events demonstrated several changes in the surface energy budget components during the period of record. The changes in the radiation budget suggested increased cloud cover in northwestern Greenland (Basin 8), allowing enhanced surface melt. Previous research by Bennartz et al. (2013) has suggested that low-level liquid clouds have played a large role during ice-sheet wide summer melt events in the past (Bennartz et al., 2013; Noël et al., 2019; Shupe & Intrieri, 2004; Van Tricht et al., 2016). These clouds are unique in that they have a low optical thickness, thin enough that it allowed shortwave radiation to pass through yet thick enough to prevent a greater fraction of longwave radiation from radiating into space. Bennartz et al. (2013) found that this cloud type did also tend to occur most often during the summer.

More recent patterns of extreme blocking may have enhanced negative SMB through increased clouds and resulting changes in cloud radiative forcing. While the evidence presented through the regional averages is not conclusive, downwelling shortwave radiation decreased and longwave radiation increased on average during extreme blocking events, which suggested increased cloud cover. SHF increased and was critical in bringing greater melt energy into the firn, which had a reduced albedo in later extreme blocking events due to less fresh snowfall and

greater rainfall amounts. This wetter, warmer snowpack was also shown to have a lower surface albedo than it did in the past; despite less shortwave radiation reaching the surface, a higher fraction of this radiation could be absorbed and further warm the firn.

This current trend is important to highlight due to a likely positive feedback loop. As the snowpack continues to warm and become wetter through longwave and shortwave radiation absorption, as well as less snowfall and more rainfall, it will continue to lower the surface albedo. Consequently, lower surface albedo will also allow even greater radiation absorption, more surface melt from warmer conditions, and therefore an even lower surface albedo, continuing the loop. Further, as the firn densifies, the water holding capacity decreases, allowing runoff to begin earlier in the season and less meltwater refrozen in the pack. As blocking events are expected to become more frequent and perhaps longer or more amplified, there may be more opportunities to trigger the feedback loop and continue the acceleration of mass loss. This feedback loop is not exclusive to extreme blocking events, as a warmer surface and lower albedo would continue to act after an extreme blocking phase has concluded.

#### 4.2 Case Studies

Several case studies, chosen during different periods within the record, were examined to provide a different perspective on research questions that cannot be conclusively addressed in the previous analysis. While the case studies themselves are also not conclusive, together with the previous analysis they provide greater insight. Four extreme blocking events were chosen for further study based on loss/gain of SMB and whether they occurred earlier and later in the study period.

While these case studies came from separate blocking events, they had similar patterns. First, the blocking events that resulted in positive SMB required considerable snowfall. The accumulation of snowfall is instrumental in offsetting possible losses through meltwater production and runoff. However, snowfall itself was not the only important factor, the snow also needed to stay on the ground and not melt. This is where surface and atmospheric temperatures as well as sensible heat flux became critical. Temperatures that were well below freezing, especially on the ground would be important to keep fresh snowfall intact and help meltwater refreeze, thereby positively impacting SMB. It would also help prevent substantial meltwater production.

A negative SHF, which means heat transfer from the surface to the atmosphere thereby cooling the surface, also reduced mass losses. The inverse of this is also true, as reflected by the July/August 2019 event, which had several days with an anomalously high SHF. Not only did the additional melt energy prime ice for meltwater production, but it therefore also reduced the surface albedo by raising the liquid water content of the ice pack.

The case studies, while informative, are insufficient to conclusively establish a pattern between cloud radiative forcing effects on mass balance and extreme blocking events. However, variability in cloud cover appeared to play a role in SMB. First, optically thin clouds, such as most of the clouds that occurred during our case studies, tended to let more shortwave radiation reach the surface. However, when we had multiple layers of clouds across the upper, middle, and lower troposphere, it tended to function similarly to optically thick clouds. For example, June 1997 had large mass gains while having thin clouds that were widespread amongst all layers of the troposphere. Shortwave and longwave radiation were affected by this cloud coverage, i.e., days of greater cloud extent had reduced downwelling shortwave radiation and reduced

upwelling longwave radiation. The finding of multiple thin cloud layers acting like an optically thick cloud layer and thereby affecting GrIS mass balance has not been discussed in previous research and is a unique contribution of this thesis.

Another interesting distinction between the negative and positive SMB case studies was in the magnitude of landfalling water vapor transport. June 1997 and August 2014 had higher average IVT than the negative SMB events, especially June 1997 where IVT averaged over the period was over 2.5 times as large as during the negative SMB events. The higher average IVT could possibly be connected to several key factors in positive SMB, including cloud coverage and enhanced snowfall which both rely on water vapor to form. Previously we discussed that cloud coverage and snowfall also seemed to be two of the most influential contributors to positive SMB, so it stands to reason that greater water vapor transport could have been a supporting factor for this gain.

Cloud coverage was not the only factor in mitigating or enhancing the effects of surface radiation budget; albedo also played a critical role. Events that had positive SMB produced snowfall that raised the albedo of the surface. Higher albedos reflected more shortwave radiation and thereby prevented absorption of shortwave radiation. As a result, events with high shortwave radiation would not necessarily have proportionately greater surface absorption.

In summary, positive SMB from extreme blocking events often depended on large snowfall amounts and surface temperatures that were well below 0°C to ensure snowfall remains without melt-freeze metamorphism and meltwater production minimized. Negative SMB events were characterized by high surface melt energy through positive SHF and surface temperatures near freezing. Additionally, a lack of fresh snowfall not only fails to offset surface mass losses but also contributed to lower surface albedo and increased the absorption of downwelling

radiation. This contributed to a positive feedback loop which coupled with a continually warming atmosphere that also further enhances surface melt conditions, and these events were more common at the end of the study period. The trends in extreme blocking-related events suggest they will more likely contribute to large mass loss events, which is discussed in the final chapter.

#### CHAPTER 5

#### CONCLUSION

Recent research has indicated that the northwestern Greenland ice sheet is experiencing surface mass loss at increasingly accelerated rates. This is due in part to synoptic-scale, quasistationary high-pressure systems known as atmospheric blocks, where some of the most intense "extreme" blocks are increasingly resulting in significant ice-sheet wide surface melt and runoff, and recent events appear less likely to produce heavy snowfall that can mitigate mass losses. As some research has suggested that blocking events will become more frequent and higher amplitude – albeit contrary to current climate model projections – the current definition of "extreme" blocking will also change, shifting the normal distribution curve further and redefining the spectrum of blocking. Additionally, the nature of surface and atmospheric conditions resulting from atmospheric blocking, such changes in sensible and latent heat and cloud radiative forcing, is likely to change with this redefinition of blocking. For these reasons, extreme blocking and its effect on the SMB of the Greenland ice sheet needs greater attention and research.

# 5.1 Summary of Key Findings

While previous research has found discrepancies in blocking effects over various parts of the ice sheet (Preece et al., 2022; H. Wang et al., 2024), a more detailed explanation for how blocking conditions affect northwestern Greenland has not been conducted prior to this thesis. Further exploring the relationship between extreme blocking episodes and surface melt in northwestern Greenland is critical due to the rapid warming occurring at high latitudes. While a

warming atmosphere, by itself, will contribute to enhanced ice sheet melt, changes in atmospheric circulation that include more high amplitude blocking may further increase the magnitude of surface melt and mass loss. Extreme blocking episodes may also contribute to a feedback, or a "memory" effect, that lasts beyond the blocking event. For instance, a blocking event that contributes to a warming of the firn (i.e., a reduction of the "cold content" of the ice) or alters the surface albedo through melt-freeze metamorphism, may lead to increased melt and runoff later through positive feedbacks. Conversely, a blocking event that produces high snowfall rates and increases surface albedo may produce a negative feedback.

To explore the relationship between extreme blocking and SMB in northwestern Greenland, this study used downscaled regional climate data from Modèle Atmosphérique Régionale (MAR) and ERA5-Reanalysis to look at long-term trends and individual extreme blocking events through time series of the surface energy budget components associated with these events and through case studies of positive and negative SMB events that occurred earlier and later in the study period.

Our first research question sought to answer how SMB during summertime extreme blocking has changed over a 33-year period from 1990-2023 in northwestern Greenland, and how SMB compares to other portions of the ice sheet. Our findings revealed that recent extreme blocking more often resulted in negative SMB than earlier in the study period, particularly since the mid-2010s as Basin 8 had not shown a positive SMB summer since 2014. In relation to the other 7 major ice drainage basins, Basin 8 surface mass loss was the fourth highest in the 2020s, showing an acceleration that surpassed that of one other basin since the 1990s. Overall, our results do support the notion of surface mass loss acceleration as a result of extreme blocking conditions in northwestern Greenland.

Our second research question sought to address how surface energy balance components during extreme blocking events have changed since the beginning of the study period, and perhaps even more importantly, how the components interact with SMB and what dictates mass loss versus mass gain. Recent extreme blocking was commonly associated with lower albedo, greater rainfall, less snowfall, and more positive SHF, leading to increased surface melt energy and greater meltwater production, similar to results from previous work (Blau et al., 2024; W. Wang et al., 2021). Meltwater increasingly resulted in runoff, instead of refreezing in the firn. Lower surface albedo spawned by a larger proportion of liquid water content, contributed to the lower albedo and greater absorption of downwelling shortwave radiation, even as shortwave radiation itself was decreasing due to changes in cloud cover.

Extreme blocking episodes that resulted in positive SMB were mostly dominated by high snowfall and low temperatures but still resulted in meltwater production and runoff. The magnitude of snowfall at higher elevations of the region could overwhelm the losses through runoff at lower elevations. Our case studies suggested that greater snowfall totals and cloud extent could have been spawned by greater water vapor flux into the region. Additionally, several years with high snowfall that resulted in positive SMB occurred in tandem with a weak negative or positive NAO. Our results also suggested that multiple layers of widespread thin clouds could function similarly to more optically thick clouds.

While the surface-albedo feedback loop is a well-documented phenomenon (Guo et al., 2025; Janoski et al., 2023; Ryan, 2024), the positive feedback loop as it relates to and is enhanced by Greenland blocking is less studied. Recent research has correlated Greenland blocking to lower surface albedo (Lewis et al., 2021). More recent extreme blocking events brought greater SHF from the atmosphere to the surface, increasing melt energy. As ice melts and

the liquid water content of the snowpack increases, reduced albedo allows for greater absorption of downwelling radiation and further warming of the snowpack, contributing to the positive feedback. Furthermore, recent extreme blocking was less likely to produce heavy snowfall that would counter surface mass losses. Rainfall has increased in more recent extreme blocking events, at the expense of snowfall; rain introduces additional heat into the ice and contributes to lower surface albedo. Finally, despite extreme blocking episodes showing a trend of decreasing shortwave radiation and increasing longwave radiation, the simultaneous lowering of surface albedo during more recent extreme blocking allowed more shortwave absorption.

### 5.2 Future Research

In the future, research could further focus on utilizing this methodology in a variety of ways. First, this body of work only encompassed summer extreme blocking events and could be expanded to include spring, fall, and wintertime extreme blocks to parse out trends. Prior studies have included blocking seasonality components (Barrett et al., 2020; Barriopedro et al., 2006; Lupo, 2021), but to our knowledge none have looked at seasonality of extreme blocking specifically to Greenland on a basin scale. Continuing to study extreme blocking conditions by categorizing by blocking type similar to work done by Preece et al (2022) could also yield further reasons behind blocking and surface melt in individual basins. Alternatively, continuing to focus on other components of extreme blocking such as duration or the link between extreme blocking episodes and other natural phenomena such as teleconnections or enhanced moisture transport could also produce interesting results.

Additionally, while these results document a negative trend in SMB under extreme blocking conditions, this work was entirely focused on the recent historical record. Using similar methods with the Climate Model Intercomparison Project 6 (CMIP6) output could allow greater

insight into melt events based off of different climate scenarios as laid out in the Representative Concentration Pathways (RCP), particularly as some research suggests that there have been improvements in CMIP6 resolving blocking episodes compared to prior iterations (D'Andrea & Davini, 2020). This could also prove extremely useful for physical and social scientists, as well as local communities as they navigate serious consequences such as environmental loss and flooding due to Greenland's diminishing ice sheet.

### **REFERENCES**

- Amory, C., Buizert, C., Buzzard, S., Case, E., Clerx, N., Culberg, R., Datta, R. T., Dey, R., Drews, R., Dunmire, D., Eayrs, C., Hansen, N., Humbert, A., Kaitheri, A., Keegan, K., Kuipers Munneke, P., Lenaerts, J. T. M., Lhermitte, S., Mair, D., The Firn Symposium team. (2024). Firn on ice sheets. Nature Reviews Earth & Environment, 5(2), 79–99. <a href="https://doi.org/10.1038/s43017-023-00507-9">https://doi.org/10.1038/s43017-023-00507-9</a>
- Barrett, B. S., Henderson, G. R., McDonnell, E., Henry, M., & Mote, T. (2020). Extreme

  Greenland blocking and high-latitude moisture transport. *Atmospheric Science Letters*,

  21(11), e1002. <a href="https://doi.org/10.1002/asl.1002">https://doi.org/10.1002/asl.1002</a>
- Barriopedro, D., García-Herrera, R., Lupo, A. R., & Hernández, E. (2006). A Climatology of Northern Hemisphere Blocking. *Journal of Climate*, *19*(6), 1042–1063. https://doi.org/10.1175/JCLI3678.1
- Black, E., Blackburn, M., Harrison, G., Hoskins, B., & Methven, J. (2004). Factors contributing to the summer 2003 European heatwave. *Weather*, *59*(8), 217–223. https://doi.org/10.1256/wea.74.04
- Blau, M. T., Ha, K.-J., & Chung, E.-S. (2024). Extreme summer temperature anomalies over Greenland largely result from clear-sky radiation and circulation anomalies.

  Communications Earth & Environment, 5(1), 1–13. <a href="https://doi.org/10.1038/s43247-024-01549-7">https://doi.org/10.1038/s43247-024-01549-7</a>

- Box, J. E., Nielsen, K. P., Yang, X., Niwano, M., Wehrlé, A., van As, D., Fettweis, X., Køltzow, M. A. Ø., Palmason, B., Fausto, R. S., van den Broeke, M. R., Huai, B., Ahlstrøm, A. P., Langley, K., Dachauer, A., & Noël, B. (2023). Greenland ice sheet rainfall climatology, extremes and atmospheric river rapids. *Meteorological Applications*, 30(4), e2134. https://doi.org/10.1002/met.2134
- Braithwaite, R. J., Laternser, M., & Pfeffer, W. T. (1994). Variations of near-surface firn density in the lower accumulation area of the Greenland ice sheet, Pâkitsoq, West Greenland.

  Journal of Glaciology, 40(136), 477–485. https://doi.org/10.3189/S002214300001234X
- Brils, M., Kuipers Munneke, P., van de Berg, W. J., & van den Broeke, M. (2022). Improved representation of the contemporary Greenland ice sheet firn layer by IMAU-FDM v1.2G. Geoscientific Model Development, 15(18), 7121–7138. <a href="https://doi.org/10.5194/gmd-15-7121-2022">https://doi.org/10.5194/gmd-15-7121-2022</a>
- Brun, E., Martin, E., Simon, V., Gendre, C., & Coleou, C. (1989). An Energy and Mass Model of Snow Cover Suitable for Operational Avalanche Forecasting. *Journal of Glaciology*, 35(121), 333–342. <a href="https://doi.org/10.3189/S0022143000009254">https://doi.org/10.3189/S0022143000009254</a>
- C3S. (2018). ERA5 hourly data on single levels from 1940 to present [Dataset]. [object Object]. https://doi.org/10.24381/CDS.ADBB2D47
- Cazenave, A., & Remy, F. (2011). Sea level and climate: Measurements and causes of changes.

  WIREs Climate Change, 2(5), 647–662. https://doi.org/10.1002/wcc.139
- Chen, J. L., Wilson, C. R., & Tapley, B. D. (2006). Satellite Gravity Measurements Confirm Accelerated Melting of Greenland Ice Sheet. *Science*, *313*(5795), 1958–1960. https://doi.org/10.1126/science.1129007

- Collins, M., R. Knutti, J. Arblaster, J.-L. Dufresne, T. Fichefet, P. Friedlingstein, X. Gao, W.J. Gutowski, et al. (2013). Long-term climate change: Projections, commitments and irreversibility. In Climate change 2013: The physical science basis. Contribution of working group I to the fifth assessment report on the intergovernmental panel on climate change, ed. Stocker et al., 1029–1136. Cambridge University Press.
- Copernicus Climate Change Service. (2018). *ERA5 hourly data on pressure levels from 1940 to present* [Dataset]. [object Object]. <a href="https://doi.org/10.24381/CDS.BD0915C6">https://doi.org/10.24381/CDS.BD0915C6</a>
- Dacre, H. F., Clark, P. A., Martinez-Alvarado, O., Stringer, M. A., & Lavers, D. A. (2015). How Do Atmospheric Rivers Form? *Bulletin of the American Meteorological Society*, *96*(8), 1243–1255. https://doi.org/10.1175/BAMS-D-14-00031.1
- D'Andrea, F., & Davini, P. (2020). Northern Hemisphere atmospheric blocking simulation in present and future climate. 18294. https://doi.org/10.5194/egusphere-egu2020-18294
- Davini, P., Cagnazzo, C., Gualdi, S., & Navarra, A. (2012). Bidimensional Diagnostics,

  Variability, and Trends of Northern Hemisphere Blocking. *Journal of Climate*, 25(19),
  6496–6509. <a href="https://doi.org/10.1175/JCLI-D-12-00032.1">https://doi.org/10.1175/JCLI-D-12-00032.1</a>
- Ettema, J., Van Den Broeke, M. R., Van Meijgaard, E., & Van De Berg, W. J. (2010). Climate of the Greenland ice sheet using a high-resolution climate model Part 2: Near-surface climate and energy balance. *The Cryosphere*, 4(4), 529–544. <a href="https://doi.org/10.5194/tc-4-529-2010">https://doi.org/10.5194/tc-4-529-2010</a>
- Fang, B., & Lu, M. (2020). Heatwave and Blocking in the Northeastern Asia: Occurrence,

  Variability, and Association. *Journal of Geophysical Research: Atmospheres*, 125(6),
  e2019JD031627. https://doi.org/10.1029/2019JD031627

- Fausto, R. S., van As, D., Box, J. E., Colgan, W., Langen, P. L., & Mottram, R. H. (2016). The implication of nonradiative energy fluxes dominating Greenland ice sheet exceptional ablation area surface melt in 2012. *Geophysical Research Letters*, 43(6), 2649–2658. https://doi.org/10.1002/2016GL067720
- Fettweis, X. (2022). Modèle Atmosphérique Régional (MAR) version 3.11 regional climate model output, 1979-2019, Greenland domain, 10 kilometer (km) horizontal resolution. https://doi.org/10.18739/A28G8FJ7F
- Fettweis, X., Box, J. E., Agosta, C., Amory, C., Kittel, C., Lang, C., van As, D., Machguth, H., & Gallée, H. (2017). Reconstructions of the 1900–2015 Greenland ice sheet surface mass balance using the regional climate MAR model. *The Cryosphere*, *11*(2), 1015–1033. https://doi.org/10.5194/tc-11-1015-2017
- Fettweis, X., Franco, B., Tedesco, M., Van Angelen, J. H., Lenaerts, J. T. M., Van Den Broeke,
  M. R., & Gallée, H. (2013). Estimating the Greenland ice sheet surface mass balance
  contribution to future sea level rise using the regional atmospheric climate model MAR.
  The Cryosphere, 7(2), 469–489. https://doi.org/10.5194/tc-7-469-2013
- Fettweis, X., Gallée, H., Lefebre, F., & van Ypersele, J.-P. (2005). Greenland surface mass balance simulated by a regional climate model and comparison with satellite-derived data in 1990–1991. *Climate Dynamics*, 24(6), 623–640. <a href="https://doi.org/10.1007/s00382-005-0010-y">https://doi.org/10.1007/s00382-005-0010-y</a>
- Franco, B., Fettweis, X., Lang, C., & Erpicum, M. (2012). Impact of spatial resolution on the modelling of the Greenland ice sheet surface mass balance between 1990–2010, using the regional climate model MAR. *The Cryosphere*, *6*(3), 695–711. <a href="https://doi.org/10.5194/tc-6-695-2012">https://doi.org/10.5194/tc-6-695-2012</a>

- Gallée, H., & Schayes, G. (1994). Development of a three-dimensional meso-γ primitive equation model: Katabatic winds simulation in the area of Terra Nova Bay, Antarctica.

  Monthly Weather Review, 122(4), 671–685. https://doi.org/10.1175/1520-0493(1994)122<0671:doatdm&gt;2.0.co;2
- Gimeno, L., Dominguez, F., Nieto, R., Trigo, R., Drumond, A., Reason, C. J. C., Taschetto, A. S., Ramos, A. M., Kumar, R., & Marengo, J. (2016). Major mechanisms of atmospheric moisture transport and their role in extreme precipitation events. *Annual Review of Environment and Resources*, 41(1), 117–141. doi: 10.1146/annurev-environ-110615-085558
- Guo, S., Dai, Y., Yuan, H., & Liang, H. (2025). Enhanced MOIDS-derived ice physical properties within CoLM revealing bare ice-snow-albedo feedback over Greenland. EGUsphere, 1–34. https://doi.org/10.5194/egusphere-2025-230
- Hanna, E., Cropper, T. E., Hall, R. J., Cornes, R. C., & Barriendos, M. (2022). Extended North
   Atlantic Oscillation and Greenland Blocking Indices 1800–2020 from New
   Meteorological Reanalysis. *Atmosphere*, 13(3), Article 3.
   <a href="https://doi.org/10.3390/atmos13030436">https://doi.org/10.3390/atmos13030436</a>
- Hanna, E., Cropper, T. E., Hall, R. J., & Cappelen, J. (2016). Greenland blocking index 1851–2015: A regional climate change signal. *International Journal of Climatology*, 36(15), 4847–4861. doi: 10.1002/joc.4673

- Hanna, E., Cropper, T. E., Jones, P. D., Scaife, A. A., & Allan, R. (2015). Recent seasonal asymmetric changes in the NAO (a marked summer decline and increased winter variability) and associated changes in the AO and Greenland Blocking Index: RECENT SEASONAL ASYMMETRIC CHANGES IN THE NAO. *International Journal of Climatology*, 35(9), 2540–2554. https://doi.org/10.1002/joc.4157
- Hanna, E., Fettweis, X., Mernild, S. H., Cappelen, J., Ribergaard, M. H., Shuman, C. A., Steffen, K., Wood, L., & Mote, T. L. (2014). Atmospheric and oceanic climate forcing of the exceptional Greenland ice sheet surface melt in summer 2012. *International Journal of Climatology*, 34(4), 1022–1037. <a href="https://doi.org/10.1002/joc.3743">https://doi.org/10.1002/joc.3743</a>
- Hanna, E., Jones, J. M., Cappelen, J., Mernild, S. H., Wood, L., Steffen, K., & Huybrechts, P.
  (2013). The influence of North Atlantic atmospheric and oceanic forcing effects on 1900–2010 Greenland summer climate and ice melt/runoff. *International Journal of Climatology*, 33(4), 862–880. <a href="https://doi.org/10.1002/joc.3475">https://doi.org/10.1002/joc.3475</a>
- Harper, J., Humphrey, N., Pfeffer, W. T., Brown, J., & Fettweis, X. (2012). Greenland ice-sheet contribution to sea-level rise buffered by meltwater storage in firn. Nature, 491(7423), 240–243. <a href="https://doi.org/10.1038/nature11566">https://doi.org/10.1038/nature11566</a>
- Helsen, M. M., van de Wal, R. S. W., van den Broeke, M. R., van de Berg, W. J., & Oerlemans, J. (2012). Coupling of climate models and ice sheet models by surface mass balance gradients: Application to the Greenland Ice Sheet. *The Cryosphere*, 6(2), 255–272. https://doi.org/10.5194/tc-6-255-2012
- Henderson, G. R., Barrett, B. S., Wachowicz, L. J., Mattingly, K. S., Preece, J. R., & Mote, T. L. (2021). Local and remote atmospheric circulation drivers of arctic change: A Review.

  Frontiers in Earth Science, 9. doi: 10.3389/feart.2021.709896

- Hersbach, H., Bell, B., Berrisford, P., Hirahara, S., Horányi, A., Muñoz-Sabater, J., Nicolas, J.,
  Peubey, C., Radu, R., Schepers, D., Simmons, A., Soci, C., Abdalla, S., Abellan, X.,
  Balsamo, G., Bechtold, P., Biavati, G., Bidlot, J., Bonavita, M., ... Thépaut, J. (2020).
  The ERA5 global reanalysis. *Quarterly Journal of the Royal Meteorological Society*,
  146(730), 1999–2049. https://doi.org/10.1002/qj.3803
- Hofer, S., Tedstone, A. J., Fettweis, X., & Bamber, J. L. (2017). Decreasing cloud cover drives the recent mass loss on the Greenland ice sheet. *Science Advances*, **3**(6). doi: 10.1126/sciadv.1700584
- Hoskins, B. J., & Sardeshmukh, P. D. (1987). A Diagnostic Study of the Dynamics of the Northern Hemisphere Winter of 1985-86. *Quarterly Journal of the Royal Meteorological Society*, 113(477), 759–778. <a href="https://doi.org/10.1002/qj.49711347705">https://doi.org/10.1002/qj.49711347705</a>
- Hoskins, B. J., McIntyre, M. E., & Robertson, A. W. (1985). On the use and significance of isentropic potential vorticity maps. *Quarterly Journal of the Royal Meteorological Society*, 111(470), 877–946. <a href="https://doi.org/10.1002/qj.49711147002">https://doi.org/10.1002/qj.49711147002</a>
- Huai, B., van den Broeke, M. R., Reijmer, C. H., & Noël, B. (2022). A Daily 1-km Resolution Greenland Rainfall Climatology (1958–2020) From Statistical Downscaling of a Regional Atmospheric Climate Model. *Journal of Geophysical Research: Atmospheres*, 127(17), e2022JD036688. https://doi.org/10.1029/2022JD036688
- Janoski, T. P., Previdi, M., Chiodo, G., Smith, K. L., & Polvani, L. M. (2023). Ultrafast Arctic amplification and its governing mechanisms. Environmental Research: Climate, 2(3), 035009. <a href="https://doi.org/10.1088/2752-5295/ace211">https://doi.org/10.1088/2752-5295/ace211</a>

- Kautz, L.-A., Martius, O., Pfahl, S., Pinto, J. G., Ramos, A. M., Sousa, P. M., & Woollings, T. (2022). Atmospheric blocking and weather extremes over the Euro-Atlantic Sector A Review. *Weather and Climate Dynamics*, *3*(1), 305–336. <a href="https://doi.org/110.5194/wcd-3-305-2022">https://doi.org/110.5194/wcd-3-305-2022</a>
- Khan, S. A., Aschwanden, A., Bjørk, A. A., Wahr, J., Kjeldsen, K. K., & Kjær, K. H. (2015).

  Greenland ice sheet mass balance: A review. *Reports on Progress in Physics*, 78(4), 046801. https://doi.org/10.1088/0034-4885/78/4/046801
- Kuipers Munneke, P., Ligtenberg, S. R. M., Noël, B. P. Y., Howat, I. M., Box, J. E., Mosley-Thompson, E., McConnell, J. R., Steffen, K., Harper, J. T., Das, S. B., & van den Broeke, M. R. (2015). Elevation change of the Greenland Ice Sheet due to surface mass balance and firn processes, 1960–2014. The Cryosphere, 9(6), 2009–2025.
  <a href="https://doi.org/10.5194/tc-9-2009-2015">https://doi.org/10.5194/tc-9-2009-2015</a>
- Lambin, C., Fettweis, X., Kittel, C., Fonder, M., & Ernst, D. (2023). Assessment of future wind speed and wind power changes over South Greenland using the Modèle Atmosphérique Régional regional climate model. *International Journal of Climatology*, 43(1), 558–574. <a href="https://doi.org/10.1002/joc.7795">https://doi.org/10.1002/joc.7795</a>
- Leeson, A. A., Eastoe, E., & Fettweis, X. (2018). Extreme temperature events on Greenland in observations and the MAR regional climate model. *The Cryosphere*, *12*(3), 1091–1102. <a href="https://doi.org/10.5194/tc-12-1091-2018">https://doi.org/10.5194/tc-12-1091-2018</a>

- Lewis, G., Osterberg, E., Hawley, R., Marshall, H. P., Meehan, T., Graeter, K., McCarthy, F., Overly, T., Thundercloud, Z., Ferris, D., Koffman, B. G., & Dibb, J. (2021). Atmospheric Blocking Drives Recent Albedo Change Across the Western Greenland Ice Sheet Percolation Zone. Geophysical Research Letters, 48(10), e2021GL092814.
  https://doi.org/10.1029/2021GL092814
- Lupo, A. R. (2021). Atmospheric blocking events: A Review. *Annals of the New York Academy of Sciences*, 1504(1), 5–24. doi: 10.1111/nyas.14557
- Lupo, A., Jensen, A., Mokhov, I., Timazhev, A., Eichler, T., & Efe, B. (2019). Changes in global blocking character in recent decades. *Atmosphere*, *10*(2), 92. doi; 10.3390/atmos10020092
- Maddison, J. W., Catto, J. L., Hanna, E., Luu, L. N., & Screen, J. A. (2024). Missing Increase in Summer Greenland Blocking in Climate Models. Geophysical Research Letters, 51(11), e2024GL108505. https://doi.org/10.1029/2024GL108505
- Matsueda, M. (2009). Blocking Predictability in Operational Medium-Range Ensemble Forecasts. *Sola*, *5*, 113–116. https://doi.org/10.2151/sola.2009-029
- Mattingly, K. S., Mote, T. L., Fettweis, X., van As, D., Van Tricht, K., Lhermitte, S., Pettersen,
  C., & Fausto, R. S. (2020). Strong summer atmospheric rivers trigger Greenland ice sheet
  melt through spatially varying surface energy balance and cloud regimes. *Journal of Climate*, 33(16), 6809–6832. doi: 10.1175/jcli-d-19-0835.1
- Mattingly, K. S., Mote, T. L., & Fettweis, X. (2018). Atmospheric River impacts on Greenland Ice Sheet Surface Mass Balance. *Journal of Geophysical Research: Atmospheres*, 123(16), 8538–8560. https://doi.org/10.1029/2018jd028714

- Mattingly, K. S., Ramseyer, C. A., Rosen, J. J., Mote, T. L., & Muthyala, R. (2016). Increasing water vapor transport to the Greenland Ice Sheet revealed using self-organizing maps.

  \*Geophysical Research Letters\*, 43(17), 9250–9258.

  https://doi.org/10.1002/2016GL070424
- McLeod, J. T., & Mote, T. L. (2016). Linking interannual variability in extreme Greenland blocking episodes to the recent increase in summer melting across the Greenland ice sheet. *International Journal of Climatology*, *36*(3), 1484–1499.

  <a href="https://doi.org/10.1002/joc.4440">https://doi.org/10.1002/joc.4440</a>
- McLeod, J. T., & Mote, T. L. (2015). Assessing the role of precursor cyclones on the formation of extreme Greenland blocking episodes and their impact on summer melting across the Greenland ice sheet. *Journal of Geophysical Research: Atmospheres*, *120*(24), 12357–12377. https://doi.org/10.1002/2015JD023945
- Medley, B., Neumann, T. A., Zwally, H. J., Smith, B. E., & Stevens, C. M. (2022). Simulations of firn processes over the Greenland and Antarctic ice sheets: 1980–2021. The Cryosphere, 16(10), 3971–4011. https://doi.org/10.5194/tc-16-3971-2022
- Michel, C., Madonna, E., Spensberger, C., Li, C., & Outten, S. (2021). Dynamical drivers of Greenland blocking in climate models. *Weather and Climate Dynamics*, *2*(4), 1131–1148. https://doi.org/10.5194/wcd-2-1131-2021
- Mouginot, J., Rignot, E., Bjørk, A. A., van den Broeke, M., Millan, R., Morlighem, M., Noël, B., Scheuchl, B., & Wood, M. (2019). Forty-six years of Greenland Ice Sheet mass balance from 1972 to 2018. Proceedings of the National Academy of Sciences, 116(19), 9239–9244. https://doi.org/10.1073/pnas.1904242116

- Nakamura, N., & Huang, C. S. Y. (2018). Atmospheric blocking as a traffic jam in the jet stream. Science (New York, N.Y.), 361(6397), 42–47. https://doi.org/10.1126/science.aat0721
- Neff, W. (2018). Atmospheric rivers melt Greenland. *Nature Climate Change*, 8(10), 857–858. https://doi.org/10.1038/s41558-018-0297-4
- Neff, W., Compo, G. P., Martin Ralph, F., & Shupe, M. D. (2014). Continental heat anomalies and the extreme melting of the Greenland ice surface in 2012 and 1889. *Journal of Geophysical Research: Atmospheres*, 119(11), 6520–6536.

  <a href="https://doi.org/10.1002/2014JD021470">https://doi.org/10.1002/2014JD021470</a>
- Newell, R. E., Newell, N. E., Zhu, Y., & Scott, C. (1992). Tropospheric rivers? A pilot study. Geophysical Research Letters, 19(24), 2401–2404. https://doi.org/10.1029/92GL02916
- Nghiem, S. V., Hall, D. K., Mote, T. L., Tedesco, M., Albert, M. R., Keegan, K., Shuman, C. A., DiGirolamo, N. E., & Neumann, G. (2012). The extreme melt across the Greenland ice sheet in 2012. *Geophysical Research Letters*, 39(20). https://doi.org/10.1029/2012GL053611
- Niwano, M., Box, J. E., Wehrlé, A., Vandecrux, B., Colgan, W. T., & Cappelen, J. (2021).
  Rainfall on the Greenland Ice Sheet: Present-Day Climatology From a High-Resolution
  Non-Hydrostatic Polar Regional Climate Model. *Geophysical Research Letters*, 48(15),
  e2021GL092942. https://doi.org/10.1029/2021GL092942
- Noël, B., van de Berg, W. J., Lhermitte, S., & van den Broeke, M. R. (2019). Rapid ablation zone expansion amplifies north Greenland mass loss. *Science Advances*, *5*(9), eaaw0123. <a href="https://doi.org/10.1126/sciadv.aaw0123">https://doi.org/10.1126/sciadv.aaw0123</a>

- Noël, B., Fettweis, X., Van De Berg, W. J., Van Den Broeke, M. R., & Erpicum, M. (2014).

  Sensitivity of Greenland Ice Sheet surface mass balance to perturbations in sea surface temperature and sea ice cover: A study with the regional climate model MAR. *The Cryosphere*, 8(5), 1871–1883. https://doi.org/10.5194/tc-8-1871-2014
- North Atlantic Oscillation (NAO) | National Centers for Environmental Information (NCEI).

  (n.d.). Retrieved May 5, 2025, from <a href="https://www.ncei.noaa.gov/access/monitoring/nao/">https://www.ncei.noaa.gov/access/monitoring/nao/</a>
- Pelly, J. L., & Hoskins, B. J. (2003). A New Perspective on Blocking. *Journal of the Atmospheric Sciences*, 60(5), 743–755. <a href="https://doi.org/10.1175/1520-0469(2003)060<0743:ANPOB>2.0.CO;2">https://doi.org/10.1175/1520-0469(2003)060<0743:ANPOB>2.0.CO;2</a>
- Pfeffer, W. T., Meier, M. F., & Illangasekare, T. H. (1991). Retention of Greenland runoff by refreezing: Implications for projected future sea level change. Journal of Geophysical Research: Oceans, 96(C12), 22117–22124. https://doi.org/10.1029/91JC02502
- Preece, J. R., Wachowicz, L. J., Mote, T. L., Tedesco, M., & Fettweis, X. (2022). Summer Greenland Blocking Diversity and Its Impact on the Surface Mass Balance of the Greenland Ice Sheet. *Journal of Geophysical Research: Atmospheres*, 127(4), e2021JD035489. <a href="https://doi.org/10.1029/2021JD035489">https://doi.org/10.1029/2021JD035489</a>
- Previdi, M., Smith, K. L., & Polvani, L. M. (2021). Arctic amplification of climate change: A review of underlying mechanisms. *Environmental Research Letters*, *16*(9), 093003. https://doi.org/10.1088/1748-9326/ac1c29
- Rajewicz, J., & Marshall, S. J. (2014). Variability and trends in anticyclonic circulation over the Greenland ice sheet, 1948–2013. *Geophysical Research Letters*, 41(8), 2842–2850. https://doi.org/10.1002/2014GL059255

- Ralph, F. M., Dettinger, M., Lavers, D., Gorodetskaya, I. V., Martin, A., Viale, M., White, A. B.,
  Oakley, N., Rutz, J., Spackman, J. R., Wernli, H., & Cordeira, J. (2017). Atmospheric
  Rivers Emerge as a Global Science and Applications Focus. *Bulletin of the American Meteorological Society*, 98(9), 1969–1973. <a href="https://doi.org/10.1175/BAMS-D-16-0262.1">https://doi.org/10.1175/BAMS-D-16-0262.1</a>
- Rantanen, M., Karpechko, A. Y., Lipponen, A., Nordling, K., Hyvärinen, O., Ruosteenoja, K., Vihma, T., & Laaksonen, A. (2022). The Arctic has warmed nearly four times faster than the globe since 1979. *Communications Earth & Environment*, 3(1), 1–10. <a href="https://doi.org/10.1038/s43247-022-00498-3">https://doi.org/10.1038/s43247-022-00498-3</a>
- Rex, D. F. (1950). Blocking Action in the Middle Troposphere and its Effect upon Regional Climate. *Tellus*, 2(4), 275–301. https://doi.org/10.3402/tellusa.v2i4.8603
- Rignot, E., Velicogna, I., van den Broeke, M. R., Monaghan, A., & Lenaerts, J. T. M. (2011).

  Acceleration of the contribution of the Greenland and Antarctic ice sheets to sea level rise. *Geophysical Research Letters*, 38(5). <a href="https://doi.org/10.1029/2011GL046583">https://doi.org/10.1029/2011GL046583</a>
- Ryan, J. C. (2024). Contribution of surface and cloud radiative feedbacks to Greenland Ice Sheet meltwater production during 2002–2023. *Communications Earth & Environment*, 5(1), 1–9. <a href="https://doi.org/10.1038/s43247-024-01714-y">https://doi.org/10.1038/s43247-024-01714-y</a>
- Ryan, J. C., Smith, L. C., Cooley, S. W., Pearson, B., Wever, N., Keenan, E., & Lenaerts, J. T. M. (2022). Decreasing surface albedo signifies a growing importance of clouds for Greenland Ice Sheet meltwater production. Nature Communications, 13(1), 4205. https://doi.org/10.1038/s41467-022-31434-w
- Schwierz, C., Croci-Maspoli, M., & Davies, H. C. (2004). Perspicacious indicators of atmospheric blocking. *Geophysical Research Letters*, *31*(6). https://doi.org/10.1029/2003GL019341

- Serreze, M. C., Barrett, A. P., Stroeve, J. C., Kindig, D. N., & Holland, M. M. (2009). The emergence of surface-based Arctic amplification. *The Cryosphere*, *3*(1), 11–19. https://doi.org/10.5194/tc-3-11-2009
- Setchell, H. (2020, February 19). *ECMWF Reanalysis v5* [Text]. ECMWF. https://www.ecmwf.int/en/forecasts/dataset/ecmwf-reanalysis-v5
- Shepherd, A., Ivins, E. R., A, G., Barletta, V. R., Bentley, M. J., Bettadpur, S., Briggs, K. H., Bromwich, D. H., Forsberg, R., Galin, N., Horwath, M., Jacobs, S., Joughin, I., King, M. A., Lenaerts, J. T. M., Li, J., Ligtenberg, S. R. M., Luckman, A., Luthcke, S. B., ... Zwally, H. J. (2012). A Reconciled Estimate of Ice-Sheet Mass Balance. *Science*, 338(6111), 1183–1189. https://doi.org/10.1126/science.1228102
- Shupe, M. D., & Intrieri, J. M. (2004). Cloud Radiative Forcing of the Arctic Surface: The Influence of Cloud Properties, Surface Albedo, and Solar Zenith Angle. *Journal of Climate*, 17(3), 616–628. <a href="https://doi.org/10.1175/1520-0442(2004)017<0616:CRFOTA>2.0.CO;2">https://doi.org/10.1175/1520-0442(2004)017<0616:CRFOTA>2.0.CO;2</a>
- Sousa, P. M., Trigo, R. M., Barriopedro, D., Soares, P. M. M., & Santos, J. A. (2018). European temperature responses to blocking and ridge regional patterns. *Climate Dynamics*, *50*(1), 457–477. https://doi.org/10.1007/s00382-017-3620-2
- Steinfeld, D., & Pfahl, S. (2019). The role of latent heating in atmospheric blocking dynamics: A global climatology. *Climate Dynamics*, *53*(9), 6159–6180. https://doi.org/10.1007/s00382-019-04919-6
- Tedesco, M., & Fettweis, X. (2020). Unprecedented atmospheric conditions (1948–2019) drive the 2019 exceptional melting season over the Greenland ice sheet. *The Cryosphere*, *14*(4), 1209–1223. https://doi.org/10.5194/tc-14-1209-2020

- Tedesco, M., Mote, T., Fettweis, X., Hanna, E., Jeyaratnam, J., Booth, J. F., Datta, R., & Briggs, K. (2016). Arctic cut-off high drives the poleward shift of a new Greenland melting record. *Nature Communications*, 7(1), 11723. https://doi.org/10.1038/ncomms11723
- Tedesco, M., Fettweis, X., Mote, T., Wahr, J., Alexander, P., Box, J. E., & Wouters, B. (2013). Evidence and analysis of 2012 Greenland records from spaceborne observations, a regional climate model and reanalysis data. *The Cryosphere*, 7(2), 615–630. <a href="https://doi.org/10.5194/tc-7-615-2013">https://doi.org/10.5194/tc-7-615-2013</a>
- Tedesco, M., & Fettweis, X. (2012). 21st century projections of surface mass balance changes for major drainage systems of the Greenland ice sheet. *Environmental Research Letters*, 7(4), 045405. https://doi.org/10.1088/1748-9326/7/4/045405
- Tyrlis, E., & Hoskins, B. J. (2008). Aspects of a Northern Hemisphere Atmospheric Blocking Climatology. *Journal of the Atmospheric Sciences*, 65(5), 1638–1652. https://doi.org/10.1175/2007JAS2337.1
- Van Den Broeke, M. R., Smeets, C. J. P. P., & Van De Wal, R. S. W. (2011). The seasonal cycle and interannual variability of surface energy balance and melt in the ablation zone of the west Greenland ice sheet. *The Cryosphere*, *5*(2), 377–390. <a href="https://doi.org/10.5194/tc-5-377-2011">https://doi.org/10.5194/tc-5-377-2011</a>
- Van Tricht, K., Lhermitte, S., Lenaerts, J. T. M., Gorodetskaya, I. V., L'Ecuyer, T. S., Noël, B., van den Broeke, M. R., Turner, D. D., & van Lipzig, N. P. M. (2016). Clouds enhance Greenland ice sheet meltwater runoff. *Nature Communications*, 7(1), 10266. <a href="https://doi.org/10.1038/ncomms10266">https://doi.org/10.1038/ncomms10266</a>

- Velicogna, I., Sutterley, T. C., & van den Broeke, M. R. (2014). Regional acceleration in ice mass loss from Greenland and Antarctica using GRACE time-variable gravity data.

  \*\*Geophysical Research Letters\*, 41(22), 8130–8137.\*\*

  https://doi.org/10.1002/2014GL061052
- Wachowicz, L. J., Preece, J. R., Mote, T. L., Barrett, B. S., & Henderson, G. R. (2021). Historical trends of seasonal Greenland blocking under different blocking metrics. *International Journal of Climatology*, 41(S1), E3263–E3278. https://doi.org/10.1002/joc.6923
- Wang, H., Luo, D., Chen, Y., & Ge, Y. (2024). Spatially Heterogeneous Effects of Atmospheric Circulation on Greenland Ice Sheet Melting. Atmosphere, 15(1), Article 1. https://doi.org/10.3390/atmos15010057
- Wang, W., Zender, C. S., van As, D., Fausto, R. S., & Laffin, M. K. (2021). Greenland Surface Melt Dominated by Solar and Sensible Heating. *Geophysical Research Letters*, 48(7), e2020GL090653. https://doi.org/10.1029/2020GL090653
- Wang, W., Zender, C. S., & van As, D. (2018). Temporal Characteristics of Cloud Radiative

  Effects on the Greenland Ice Sheet: Discoveries From Multiyear Automatic Weather

  Station Measurements. *Journal of Geophysical Research: Atmospheres*, 123(20), 11,34811,361. https://doi.org/10.1029/2018JD028540
- Wazneh, H., Gachon, P., Laprise, R., de Vernal, A., & Tremblay, B. (2021). Atmospheric blocking events in the North Atlantic: Trends and links to climate anomalies and teleconnections. *Climate Dynamics*, 56(7), 2199–2221. <a href="https://doi.org/10.1007/s00382-020-05583-x">https://doi.org/10.1007/s00382-020-05583-x</a>

- Woollings, T., Barriopedro, D., Methven, J., Son, S.-W., Martius, O., Harvey, B., Sillmann, J., Lupo, A. R., & Seneviratne, S. (2018). Blocking and its Response to Climate Change.

  \*Current Climate Change Reports, 4(3), 287–300. <a href="https://doi.org/10.1007/s40641-018-0108-z">https://doi.org/10.1007/s40641-018-0108-z</a>
- Wouters, B., Bamber, J. L., van den Broeke, M. R., Lenaerts, J. T. M., & Sasgen, I. (2013).

  Limits in detecting acceleration of ice sheet mass loss due to climate variability. *Nature Geoscience*, 6(8), 613–616. https://doi.org/10.1038/ngeo1874
- Zolles, T., & Born, A. (2024). How does a change in climate variability impact the Greenland ice sheet surface mass balance? *The Cryosphere*, *18*(10), 4831–4844. https://doi.org/10.5194/tc-18-4831-2024
- Zwally, H. Jay, Giovinetto, Mario B., Beckley, Matthew A., & Saba, Jack L. (2012). *Antarctic and Greenland Drainage Systems*. GSFC Cryospheric Sciences Laboratory.

  <a href="https://earth.gsfc.nasa.gov/sites/default/files/lab\_cryo/data/polar\_ice\_altimetry/antarctic\_and\_greenland\_drainage\_systems/grndrainagesystems\_ekholm.txt">https://earth.gsfc.nasa.gov/sites/default/files/lab\_cryo/data/polar\_ice\_altimetry/antarctic\_and\_greenland\_drainage\_systems/grndrainagesystems\_ekholm.txt</a>